2001

Carbon-sulphur systematics and geochemistry of the Duvernay Formation of central Alberta.

Jing. Gao
University of Windsor

INFORMATION TO USERS

This manuscript has been reproduced from the microfilm master. UMI films the text directly from the original or copy submitted. Thus, some thesis and dissertation copies are in typewriter face, while others may be from any type of computer printer.

The quality of this reproduction is dependent upon the quality of the copy submitted. Broken or indistinct print, colored or poor quality illustrations and photographs, print bleedthrough, substandard margins, and improper alignment can adversely affect reproduction.

In the unlikely event that the author did not send UMI a complete manuscript and there are missing pages, these will be noted. Also, if unauthorized copyright material had to be removed, a note will indicate the deletion.

Oversize materials (e.g., maps, drawings, charts) are reproduced by sectioning the original, beginning at the upper left-hand corner and continuing from left to right in equal sections with small overlaps.

Photographs included in the original manuscript have been reproduced xerographically in this copy. Higher quality 6" x 9" black and white photographic prints are available for any photographs or illustrations appearing in this copy for an additional charge. Contact UMI directly to order.

ProQuest Information and Learning
300 North Zeeb Road, Ann Arbor, MI 48106-1346 USA
800-521-0600

CARBON-SULPHUR SYSTEMATICS AND GEOCHEMISTRY OF THE DUVERNAY FORMATION OF CENTRAL ALBERTA

By

Jing Gao

A Thesis submitted to
The Faculty of Graduate Studies and Research
through the Department of Earth Sciences
in Partial Fulfillment of the Requirement
for the Degree of Master of Science at the
University of Windsor

Windsor, Ontario, Canada
2001

ABSTRACT

The Upper Devonian Duvernay Formation represents one of the most important sources of conventional oil within the Western Canada Sedimentary Basin. It is an organic-rich, basinal shale and limestone sequence within the Upper Devonian Woodbend Group.

Several lithofacies from the Duvernay Formation have been identified in this study: black shale, laminated mudstone, lime mudstone, dolomitic mudstone, laminated dolomitic mudstone, grey shale, grey mudstone, wackestone, packstone and nodular limestone. This study concentrated on the shales and mudstones of the Duvernay Formation.

Total organic carbon content ranges from 1.06 to 9.83 wt % for organic-rich laminites. High quartz content was observed in samples from some wells in the north and northwest of the study area. This indicates that the terrestrial material is probably derived from the area to the north or northwest. Most of the samples from the area to the north have Type II kerogen. Most of the samples from the area to the south have mixed Type II and III kerogen or highly oxidized Type II kerogen. The degree of maturity increases from northeast to southwest. The oil generation potential decreases from northeast to southwest.

The major diagenetic processes that affected shales and mudstones lithofaices are cementation, dolomitization and pyritization. Minor processes include physical compaction, dissolution, anhydritization and fracturing. There are several observed types of calcite cement: mosaic calcite cement, sparry calcite cement, and bladed/prismatic

calcite cement. Three types of dolomite that have been identified: matrix dolomite which is subdivided into three generations, saddle dolomite and vein-associated dolomite. Pyrite occurs as framboidal pyrite, as pyrite spheres, and as cubic, pyritohedral and octahedral pyrite crystals.

Framboidal pyrite, non-ferroan calcite cement and matrix dolomite are of early diagenetic origin; ferroan mosaic and bladed calcite cement, ferroan Type II matrix dolomite, saddle dolomite, vein-associated dolomite and coarse-grained pyrite are of intermediate to deep burial origin.

Bacterial sulphate reduction is the main process of bacterial reduction. Sulphur isotopic results, TOC/S ratios, organic facies, size distribution of framboidal pyrite and lack of bioturbation all indicate that the Duvernay shales and mudstones were deposited in an anoxic, partially closed to open environment.

ACKNOWLEDGEMENTS

First and foremost, I would like to thank Drs. Ihsan S. Al-Aasm and David T.A. Symons for their encouragement, advice, and guidance throughout the years. Special thanks to Drs. Cyril G. Rodrigues, Martin Fowler and Maria T. Cioppa, Mr. Matthew Verson, Mr. John Robinson and Mrs. Ingrid Churchill for their encouragement and assistance.

Most of all, I would like to thank my husband and my parents for their love, support and encouragement through my academic years.

TABLE OF CONTENTS

LIST OF ABBREVIATIONS

AOM: amorphous organic matter

BS: black shale

BSR: bacterial sulphate reduction

C: calcite

CDT: Canyon Diable meteorite

CS: calcareous sphere

CSP: calcite spar

D: dolomite

DM: dolomitic mudstone

FBD: ferroan bladed dolomite

FC: ferroan calcite

GS: grey shale

H/C: hydrogen/carbon

HI: hydrogen index

ISM: interbedded black shale/dolomitic mudstone

LDM: laminated dolomitic mudstone

LM: laminated mudstone

LMS: lime mudstone,

LS: limestone

M: matrix

MD: matrix dolomite

O/C: oxygen/carbon

OI: oxygen index

OM: organic matter

P: pyrite

PI: production index

Q: quartz

RE: relative error

RSD: relative standard deviation

S: standard deviation

SD: saddle dolomite

T: Tasmanites

T_{max}: maximum temperature

TOC: total organic carbon

TOC/S: total organic carbon/pyrite sulphur

TSR: thermal sulphate reduction

VPDB: Vienna PeeDee Belemnite

WCSB: Western Canada Sedimentary Basin

mg HC/g : milligram hydrocarbon/gram

LIST OF FIGURES

LIST OF PLATES

CHAPTER I

INTRODUCTION

1.1 Objectives

Within the Western Canada Sedimentary Basin (WCSB), Devonian sediments contain about 55% of the recoverable and 40% of the in-place conventional oil resources (Podruski et al., 1988). Nearly all of these hydrocarbons were generated within the Duvernay Formation as the result of of subsidence associated with the Laramide orogeny (Deroo et al., 1977; Creaney and Allan, 1990; Piggot and Lines, 1991). The formation has attracted much attention from previous workers, however, little work has been done to quantify the carbon-sulphur systematics. The primary objectives of this study include:

(1) to identify the lithofacies and quantify the diagenetic modification imposed on the sediments of the Duvernay Formation.

(2) to identify the sedimentary environment of the Duvernay Formation by using geochemical methods (C/S ratios, stable isotopic compositions of C and S) and present a depositional model.

(3) to identify the source of organic matter and maturity of source rocks of the Duvernay Formation.

1.2 Previous work

1.2.1 Lithofacies

The sedimentology of the Duvernay Formation was discussed by Stoakes (1980). He suggested that this formation was accumulated as the deep basinal toes of prograding clinoforms of the Ireton Formation. The water depths were estimated from 65 m to more than 100 m in areas of poor circulation (Stoakes and Creaney, 1985). Chow et al. (1995) proposed that the depths were 40-50 m, and indicated that bottom-water anoxia was the primary control on organic matter preservation.

Generally, two principal interbedded lithofacies have been proposed: nodular to nodular-banded lime mudstones and laminated lime mudstones (Stoakes and Creaney, 1984). The former shows variable degrees of bioturbation and hence been suggested to have been formed in oxygen-reduced conditions; while the latter contains fine-grained carbonate and organic-rich layers accumulated in deep-water oxygen-starved euxinic conditions. Laminated mudstones show some of the highest values of total organic carbon (TOC) in the Duvernay Formation, generally averaging between 5 and 10 wt%, and represent accumulation in deep-water oxygen-starved conditions with low rates of sedimentation. The dark laminated rocks mark the bases of cycle of obvious increase in water depth which were the result of increases in the rate of sea level rise (Chow et al., 1995). The most organic-rich laminae are thought to form at the deep water, most condensed basinal successions with the farthest backstepped reef margins where the sediment dilution rates are lowest. However, potential source rocks with different TOC and kerogen type are also found in the shallower-water, more-bankward Duvernay laminites.

1.2.2 Organic petrology

The organic matter of the Duvernay Formation is considered to be almost entirely oil-prone and unstructured, with typical marine Type II kerogens. It is probably sourced from a planktonic origin as influences of terrestrial organic matter can be excluded largely during the Devonian time (Stoakes and Creaney, 1985; Creaney and Allan, 1990). Relatively low-reflecting, fluorescing to non-fluorescing amorphous organic matter is dominant in kerogen components in immature to overmature samples. Typically, common organic matter includes prasinophyte alginite, acanthomophic acritarchs and liptodetrinit-sized macerals. Sporinite and coccoidal alginite macerals are also contained in some samples (Li et al., 1997).

By analyzing the basin-floor laminites along the foreslope of the Redwater reef complex, Chow et al. (1995) found that normal productivity prevailed throughout the deposition of the Duvernay laminites because of the lack of algal bloom organic facies. They also indicated that the degree of near-surface water agitation is reflected by the maceral planktonic assemblages. Depositional facies and degree of bioturbation are correlated with distinct organic facies, which suggests a shared hydrodynamic control between near-surface water agitation and bottom-water oxygenation. Three main organic facies have been recognized based on the maceral assemblages:

(1) Organic facies A: the most basinward maceral assemblage; it is dominated by small (generally < 10 μm), relatively thin-walled but also minor large, Prasinophyte alginites (up to 180 μm);

(2) Organic facies B: an intermediate maceral assemblage comprising similar Prasinophyte alginites as (1), abundant acanthomorphic acritarchs, and sporinites, which may or may not be present;

(3) Organic facies C: a maceral assemblage containing the same maceral assemblage as (2) plus persistent coccoidal alginite colonies and sporinites, which formed in the shallower more-proximal foreslope settings where wave-agitated and oxygenated conditions prevailed.

Laminites with only minor bioturbation have high TOC values of > 5 wt% and correspond to organic facies A and B; moderately to extensively burrowed laminites usually correspond to TOC between 1.5 and 4.0 wt% and mainly to organic facies C with minor organic facies B; totally bioturbated lime mudstones and nodular lime mudstones correspond to organic facies C and are characterize by low TOC (generally < 0.25 wt%) due to oxidation of organic matter in shallower water.

Hydrocarbon biomarker distributions in the laminated lithofacies are taken to indicate a highly anoxic, marine palaeoenvironment of deposition (Li et al., 1997).

1.2.3 Mineralogy

Campbell and Oliver (1968) studied samples from four cored wells in central Alberta. The rocks range from pure carbonate to those with about 25% carbonate and 75 % silicates. The dominant minerals and their contents in these rocks throughout the Duvernay Formation are illite (13-39%), chlorite (3-15%), dolomite (1-32%), calcite (16-76%) and quartz (3-26%).

1.2.4 Geochemistry

The Duvernay Formation source rocks are generally rich in organic matter with TOC ranging from 2 to17 wt%. Immature samples have hydrogen indices ranging from 500-600 mg HC/g TOC (Creaney and Allan, 1990). Li et al (1997) analyzed 15 samples

over a wide maturity range. Most of the samples are from the East Shale Basin. TOC values range from 2.0 to 13.5 wt%. T_{max} values are from 415 to 450°C. A typical type II kerogen was indicated by HI to have 146-565 mg HC/g TOC values and by OI to have 6-32 mg CO_2/g TOC values.

Nine samples from the laminated, organic-rich lime mudstone lithofacies, which also span the range of maturity, were analyzed by Requejo (1994) and Requejo et al (1997). TOC values range from 1.92 to 8.79 wt%. T_{max} values are from 417 to 465°C. HI values ragne from 40 to 550 mg HC/g TOC. The whole-rock sulphur content is 1.3-2.8 wt%.

1.3 Sample Collection and Methodology

1.3.1 Sample collection

The study area is located between Townships 35 and 59, R.15, W4 and R.11,W5 (Figure 1.1). Approximately 300 samples from 13 wells were collected by Dr. Maria T. Cioppa, from which 90 thin sections were prepared. All thin sections were partly stained with a mixture of Alzarin Red-S and Potassium Ferricyanide according to the procedure described by Dickson (1965). Core descriptions combined the earlier descriptions of hand samples (M. T. Cioppa, pers, comm, 2000) and subsequent descriptions both of hand samples and thin sections.

1.3.2 Petrography

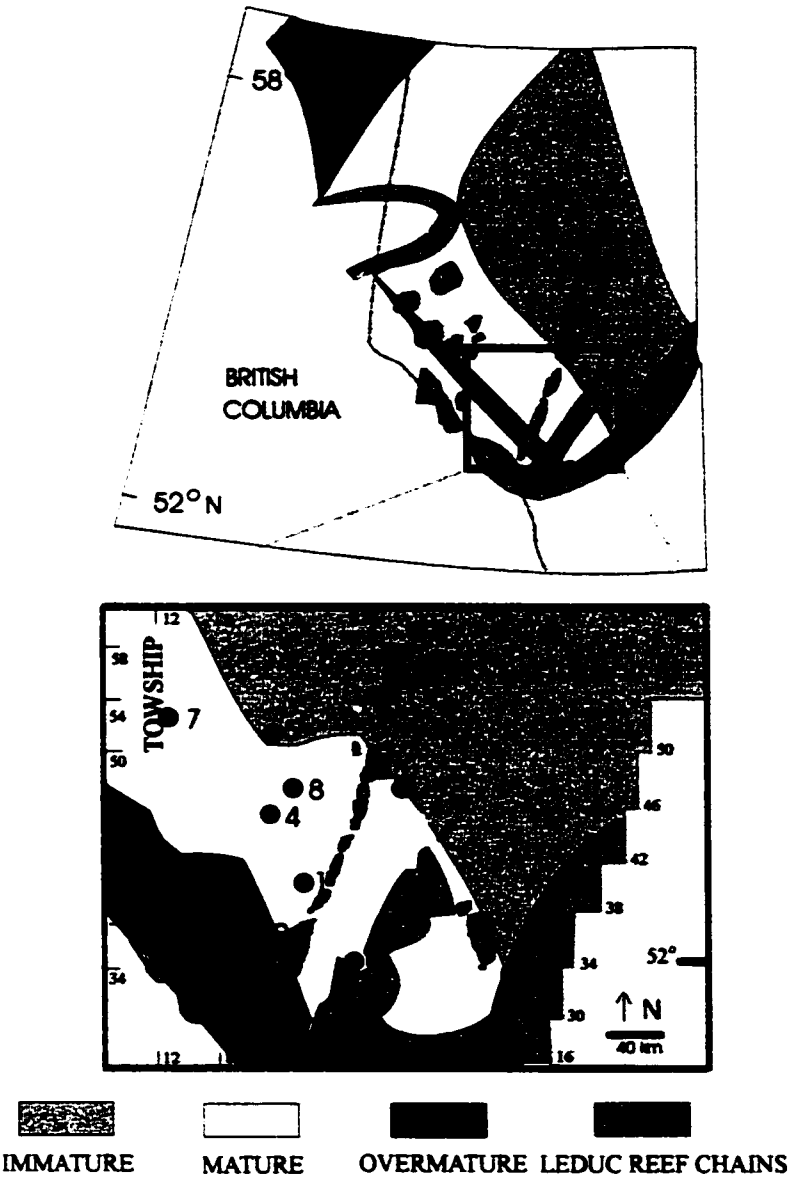

Figure 1.1 Location map of study area (modified from Stoakes and Creany,1984). The upper map shows the degree of maturation as well as the location of the reef complex. The lower map shows a close up of the sample area and the locations of sampled wells.

The thin sections were studied using a standard petrographic microscope. A Nikon EPI Fluorescence connected to a petrographic microscope was used to study the fluorescence characteristics of the organic matter as well as the carbonates. Philips 1710 X-Ray Diffraction Equipment with a Ni-filtered Cuk-alpha radiation source at a rate of 1.5° 2 Φ/min was employed to identify minerals for 12 rock samples (most of which have high TOC contents) at the University of Uppsala, Sweden. Scanning electron microscopic (SEM) studies of minerals were done using a JEOL JSM – 5800 LV Scanning Microscope at University of Windsor.

1.3.3 Oxygen and inorganic carbon isotopes

Powdered samples were reacted with 100% phosphoric acid for four hours at 25°C and 50°C for calcite and dolomite, respectively. Using the chemical separation method proposed by Al-Aasm et al. (1990), CO_2 gas was extracted from samples that contained a mixture of calcite and dolomite. A SIRA-12 mass spectrometer was then used to analyze the isotopic ratios of the CO_2 gas at the University of Ottawa. Delta (δ) values for oxygen and carbon are recorded in per mil (‰) relative to the Vienna PeeDee Belemnite (VPDB) standard. Precision was better than 0.05‰ for both $\delta^{18}O$ and $\delta^{13}C$.

1.3.4 Organic carbon isotopes

Powdered samples were reacted with 10% HCl for 12 hours to ensure that all of the CO_2 gas from the inorganic sources (e.g. calcite and dolomite) was removed. After that, the samples were rinsed with deionized water, filtered and dried. The isotopic ratios of the organic carbon of the dried samples were then analyzed by a continuous flow (CF)

elemental analyzer connected to a Delta-Plus mass spectrometer at the University of Ottawa. Precision was better than 0.05‰.

1.3.5 Sulphur isotopes

Samples were treated with kiba reagent according to the procedure outlined by Sasaki et al. (1979). The resultant SO_2 was analyzed for $\delta^{34}S$ using a SIRA-12 mass spectrometer at the University of Ottawa. Delta (δ) values for sulphur are reported in per mil (‰) relative to the Canyon Diablo Troilite (CDT) standard. Precision was better than 0.2‰.

1.3.6 Elemental analysis

Total carbon and sulphur contents were analyzed using a Carlo Erba® NA 1500 CHNS elemental analyzer. Precision was < 4 % RSD (relative standard deviation). Accuracy was < 8 % RE (relative error).

1.3.7 Rock-Eval pyrolysis

Rock-Eval pyrolysis was carried out on 40 selected samples (generally three samples from each well) using Rock-Eval VI at Geological Survey of Canada in Calgary. For details of the Rock-Eval instrumentation and the evaluation of the various parameters, see Lafargue et al. (1998) and Espitalie et al. (1985). Precision was < 0.3 % RSD.

CHAPTER II

GEOLOGICAL SETTING

2.1 Regional Stratigraphy

The WCSB is a NW-SE trending, asymmetrical, synclinal foreland basin extending from central Montana to the Northwest Territories. It is bounded by the Laramide-age Rocky Mountain overthrust belt to the west and the Precambrian Canadian Shield to the east (Porter et al., 1982). All source rocks in the basin show a progressive increase in thermal maturity from immature in the east, through mature enough to generate oil, to ultimately overmature to generate gas in western Alberta and north-eastern British Columbia (Fig 1.1).

The Upper Devonian Woodbend Group of the WCSB consists of a thick sequence of shallow-water platform and reefal carbonates of the Cooking Lake, Leduc and Grosmont formations and basin-filling shales and limestones of the Majeau Lake Member, Duvernay and Ireton formations and pre-Z marker basin fill (Stoakes and Wendte, 1987, Figs 2.1 and 2.2). The Upper Devonian Rimbey-Meadowbrook Leduc reef trend in central Alberta separates the basin into two parts: the East Shale Basin and the West Shale Basin. The Duvernay Formation formed at the same time as Leduc reef growth during the Frasnian and is absent where the Leduc Formation exists. In the East Shale Basin, the Duvernay Formation overlies the carbonate build-up of the Cooking Lake Formation. In the West Shale Basin, where the Cooking Lake Formation is absent, the unit conformably overlies the sediments of similar basinal aspect referred to as the

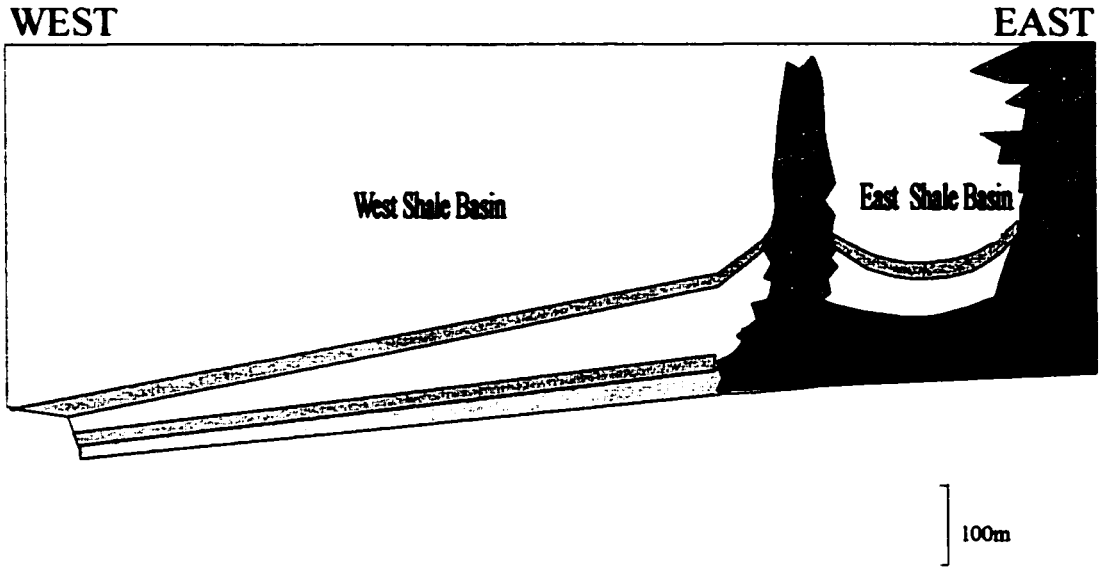

Figure 2.1 Composite schematic cross-section across the Alberta Basin of the Woodbend Succession (After Chow et al., 1995).

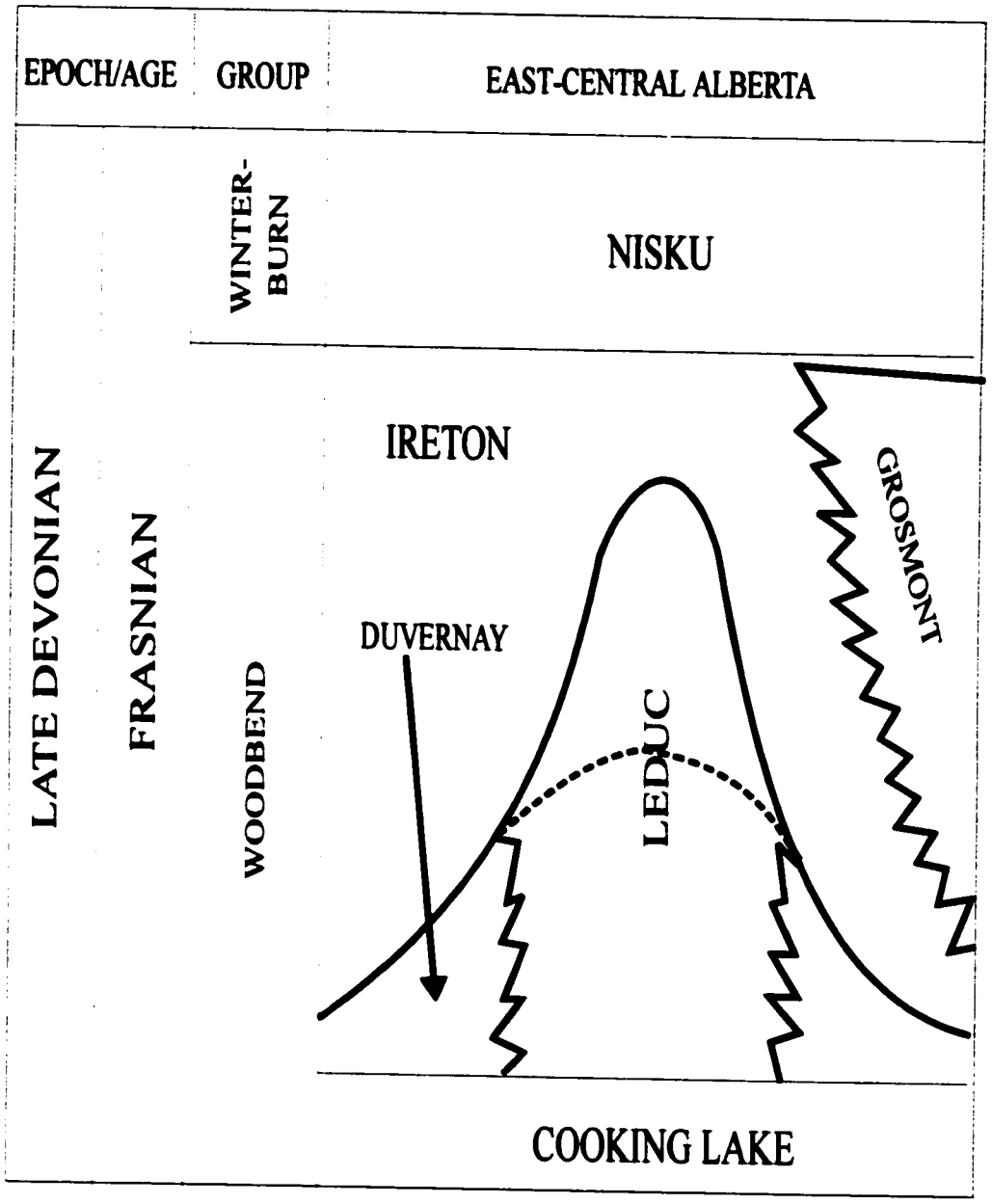

Figure 2.2 Generalized stratigraphic column of east central Alberta (After Chow et al., 1995).

Majeau Lake Member. The Majeau Lake Member is the basinal equivalent of the Cooking Lake platform and is lithologically identical to the Duvernay Formation. The Ireton Formation conformably overlies the Duvernay Formation and eventually surrounds and covers the Leduc Formation (Stoakes, 1980; Stoakes and Creaney, 1985). The highest occurrence of brown or brown-black shales in the Woodbend Group marks the upper boundary of the Duvernay Formation (Andrichuk, 1958).

2.2 Duvernay Formation in the Study Area

The Upper Devonian Duvernay Formation represents one of the most important sources of conventional oil within the WCSB. It is an organic-rich, basinal carbonate succession that generated most of the oil in the Leduc reefs of central Alberta (Stoakes and Creaney, 1984). Although immature over much of its occurrence, there is a band of progressive oil-window maturation occuring in the deep, western part of the basin adjacent to the overthrust belt (Creaney and Allan, 1990).

The thickness of the Duvernay Formation is variable, ranging up to greater than 60 m near the marginal reef complex in the east and southeast and toward the Grosmont reef in the north, and it is thinnest on the east side of the Rimbey- Meadowbrook reef chain (Andrichuk, 1958; McCrossan, 1961).

Generally, the Duvernay Formation consists of interbedded limestones that are locally dolomitized, calcareous brown and brown-black shales, and green and gray shales. The formation is divided into three units (Andrichuk, 1961). The lowest unit ranges from 0.3 m to 20 m and averages 6 m thick. It consists of tan, brown and gray

argillaceous limestone with thin interbeds of gray, green-gray and brown calcareous shales. Brachiopods, ostracods and crinoids are present.

The middle unit (5 m – 21 m) consists of cream to tan bioclastic limestone with reef-derived skeletal debris from brachiopods, crinoids, stromatoporoids, amphiporids and corals. The debris is interpreted to have been partly derived from erosion of the early Leduc reef.

The upper unit ranges from 5 m to 60 m thick and consists of brown to black shale, tan to brown dense limestone, gray to brown argillaceous limestone, and gray and brown-gray shale. Tentaculites, spines, crinoid and smooth linguloid brachiopods are present in this unit.

Based on the information gathered in this study, most of the samples probably represent the upper unit of the Duvernay Formation.

In the West Shale Basin, the Duvernay Formation comprises two main organic-rich laminites separated by an organic-lean lime mudstone that thins to the west. These strata dip slightly to the west. The two organic-rich intervals merge to the north of the Peace River Arch where they are referred to as the Muskwa Formation. In these study, most of the wells are located in the West Shale Basin (Fig 1.1). In the East Shale Basin, the upper organic-rich laminite intertongues with shallow-water carbonates of the Leduc reefs and platform carbonates of the Grosmont reefs (Stoakes, 1980, 1992; Cutler, 1983; Switzer et al.,1994).

An obvious increase in the rate of subsidence of the depositional interface, shown by the change from biostromal to biohermal reef growth on certain shoals, happened at the end of Cooking Lake time. To survive, the reefs grew mainly upward from their original

base or foundation (Link, 1950). During earlier Duvernay time, the reef shoals did not have enough topographic relief to form a restricted water environment so that brown to black shales are relatively absent. Newland (1954) suggested that the upward increase in black shale content was caused by increasing water stagnation that resulted from progressive reef growth.

From the study of regional resistivity maps, McCrossan (1961) thought there may have been a southeasterly moving current as least locally which derived from the reefs spread throughout the basin during Duvernay and Ireton time. He also showed petrographic evidence that suggested that the calcite in Duvernay rocks is of clastic origin and that part of the finer calcite was reef-derived.

CHAPTER III

SEDIMENTOLOGY OF THE DUVERNAY FORMATION

3.1 Introduction

The sedimentology of the Duvernay Formation will be described and discussed using the concept of facies analysis. This concept involves considerations of vertical sequences of facies changes to identify large scale depositional processes and environments, as well as the examination of individual facies (Tucker, 1996).

A facies is a body of rock defined by various attributes such as lithology, color, texture, sedimentary structures, and nature and preservation of fossils (Tucker, 1996). A combination of core analysis and petrographic studies is used to identify the facies of the Duvernay Formation. The limestone classification is employed for the carbonate section according to Embry and Klovan (1971), which was modified from the schemes of Dunham (1962).

Several lithofacies have been identified: (1) black shale/laminated mudstone; (2) carbonate-rich mudstone; (3) grey shale/grey mudstone; and (4) laminated dolomitic mudstone. In this thesis, the main focus is on the shale/mudstone lithofacies. The carbonate sections have been investigated by Adam (2000). Nodular limestone, wackestone and packstone are not discussed in this study; descriptions of these rocks are

according to Adam's (2000) descriptions. They are all referred to as limestone in core descriptions (Appendix II).

3.2 Lithofacies and mineralogy

3.2.1 Black shale/Laminated mudstone

In hand samples, rocks of black shale and laminated mudstone are dark grey to black in color. The laminations range in thickness from < 1mm to 2 cm (Plate A-1). The lithofacies ranges from 0.47 to 4.32 m thick (the thickness of rocks described in this study may not provide complete record due to drilling conditions from cores sampled) and occurs at depths from 1008 m in the East Shale Basin to 3650 m in the West Shale Basin. This facies is interbedded with mudstone, wackestone and packestone in wells 1, 4, 5, 8, 9, 12 and occasionally appeared in wells 3 and 10. The laminations are parallel to wavy. Bivalve, brachiopods, gastropods, ostracods, pelecypods, and tentaculites were occasionally found. Three kinds of calcareous spheres were found in wells 3, 4, 5, 8, 9, 10, and 12.

(1) **Calcareous spheres with radial structure.** Spheres of this type were found in wells 5, 9 and are locally abundant in well 12 (Plate B-1 and B-2). These spheres range from 150 μm to 200 μm in diameter and have a spherical chamber with a calcitic wall. The wall consists of radially oriented spines or prisms that may extend inward from the outer edge into the chamber to variable extent. According to Stanton (1963), these calcispheres are probably related to Radiosphaera that are abundant in Leduc reef complex.

(2) **Calcareous spheres with an outer rim.** These spheres with outer rims were found in wells 3, 4, 5, 9, 10 and 12 (Plate B-3). They range from 100 μm to 300 μm in diameter. The widths of the rims range from 5 μm to 20 μm. The origin of these spheres is not clear. Both organic and inorganic origins are possible.

(3) **Calcareous spheres without structures.** Most of the calcareous spheres found in the Duvernay Formation have no clear structure. They range from 50 μm to 400 μm and are found in all wells (Plate B-4 and B-5). In the black shale/laminated mudstone facies, the spheres are mainly found in wells 3, 4, 5, 9, 10 and 12. Because no original structures remained, they also could be either organic and inorganic in origin.

The main maceral components of the organic matter in this facies include:

(1) Amorphous organic matter: it is from non-fluorescent to light brown, to brown and finally to dark brown fluorescent.

(2) Thick-walled Tasmanites: they are only found in wells 5 and 10 and very rare in this facies. The Tasmanites are 15 μm to 60 μm in thickness and 100 μm to 300 μm in length (Plates B-4 and B-5).

(3) Thin-walled Prasinophyte alginates: they are only found in wells 3, 5 and 10 and are also rare in this facies.

Carbonates in this facies usually display yellow to green fluorescence. This indicates that there is residual organic matter remaining in the grains (e.g. Jeffrey and Donald, 1985).

The dominant minerals in this facies (Appendix III) are calcite (15 to 80%), quartz (5 to 55%) and dolomite (< 5 to 10%). Feldspars, mica, clay and Fe-Ti oxides account for

PLATE A

Facies

Photo 1. Core photograph of the interbedded limestone/black shale facies. Grey limestone facies gradually change into black shale facies from the left to the right. Laminations are < 1 millimetres to 2 millimetres. Laminations are parallel to the depositional surface. Location: well 9 (6-14-37-7w5), 3649.66 metres. Core is 8 centimetres wide. In all core photographs, top of the core piece is to right.

Photo 2. Core photograph of the lime mudstone facies. Location: well 5 (16-18-52-5w5), 2340.65 metres. Core is 8 centimetres wide.

Photo 3. Core photograph of the dolomitic mudstone facies. Location: well 7 (3-1-52-11w5), 2638.45 metres. Core is 8 centimetres wide.

Photo 4. Core photograph of the interbedded black shale/dolomitic mudstone facies. Black shale is interbedded with very thin grey dolomitic mudstone. Laminations are parallel to the depositional surface and range from < 1 millimeter to 1 millimeter. Location: well 8 (2-6-47-4w5), 2645.1055 metres. Core is 8 centimetres wide.

Photo 5. Photograph of the interbedded black shale/dolomitic mudstone facies under plane polarized light. Laminations are parallel to the depositional surface. Location: well 5 (16-18-52-5w5), 2338 metres. Field of view is 2 millimetres.

Photo 6. Core photograph of the laminated dolomitic mudstone facies. Thinner black organic-rich part is wavily laminated with thicker grey organic-lean part. Laminations are usually 0.1 to 3 millimetres, but also can reach 1centimetres thick. Location: well 11(5-19-54-25w4), 1629.334 metres. Core is 8 centimetres wide.

PLATE B

Calcareous Spheres and Prasinophyte Alginates

Photo 1. Photograph of calcisphere under plane polarized light. Both the outer wall and inner wall are clear. Radial spines extend inward from the outer edge into the chamber in some parts. The chamber and the outer wall are filled with calcite cement. Later ferroan cement replaced the center of the chamber. Location: well 5 (16-18-52-5w5), 2340.72 metres. Field of view is 0.2 millimetres. Alzarin Red-S and Potassium Stained (hereafter referred to as stained).

Photo 2. Photograph of calcispheres under plane polarized light. The inner wall is clear but the boundary of the outer call has been destroyed by later cementation of brighter crystals. Radial spines extend inward until the center of the chamber. Location: well 12 (11-26-58-23w4), 1288.212 metres. Field of view is 0.5 millimetres. Stained.

Photo 3. Photograph of calcareous sphere with an outer rim under plane polarized light. The outer rim is relatively thick comparing to the rims of other spheres and is composed of non-ferroan calcite. Ferroan calcite cement fills in the spheres. Location: well 4 (4-22-45-5w5), 2883.56 metres. Field of view is 0.5 millimetres. Stained.

Photo 4. Photograph of non-structure calcareous sphere and thick-walled Tasmanites (arrow) under plane polarized light. Non-ferroan mosaic calcite cement fills in the calcareous sphere. Location: well 10 (14-18-54-25w4), 1621.18 metres. Field of view is 0.5 millimetres. Stained.

Photo 5. Photograph of non-structure calcareous sphere and thick-walled Tasmanites (T) under blue-violet illumination (the same field as above). Amorphous organic matter (AOM) is greenish brown. The calcareous sphere (CS) shows dark green color. Location: well 10 (14-18-54-25w4), 1621.18 metres. Field of view is 0.5 millimetres. Stained.

Photo 6. Photograph of thick-walled Tasmanites (T) and thin-walled Prasinophyte alginates (arrow) under blue-violet illumination. Amorphous organic matter (AOM) is yellowish brown. Green crystals are dolomite (D). Location: well 11 (5-19-54-25w4), 1625.27 metres. Field of view is 1 millimetres.

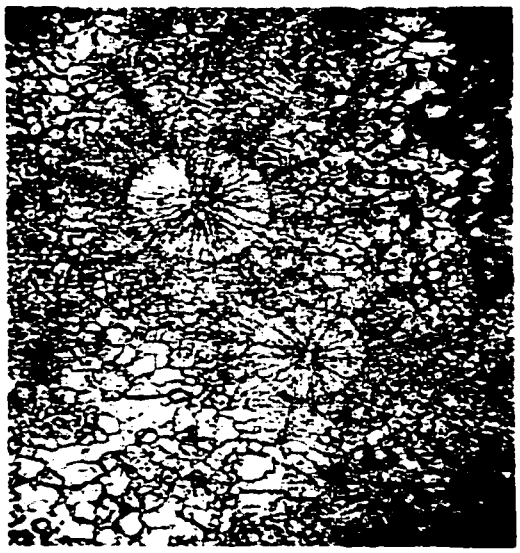

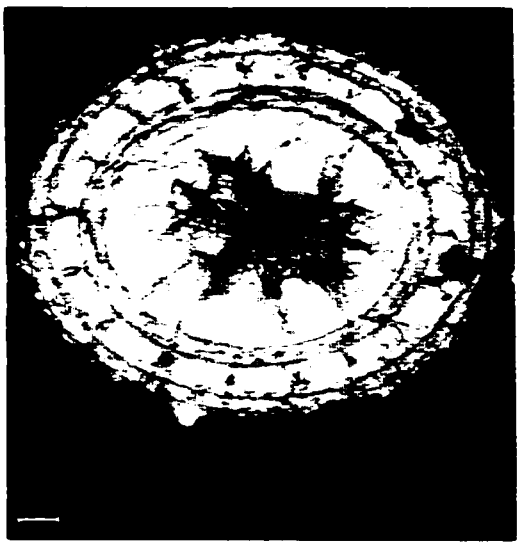

5% or less each.

3.2.2 Carbonate-rich mudstone

In hand specimens, rocks from the carbonate-rich mudstone have various colors, including light brown, grey, brownish grey, dark grey and black. Lime mudstones occur in wells 4, 5, and 8 and dolomitic mudstones in wells 5, 7 and 8.

Lime mudstone (Plate A-2) is 0.24 m to 5.16 m thick and occurs at depths ranging from 2340.65 to 2884.78 m. Brachiopods, ostracods, tentaculites, and all three kinds of calcareous spheres exist in this facies. Amorphous organic matter is non-fluorescent to dark brown fluorescent. Few thin-walled Prasinophyte alginates are found in well 5. Carbonate components fluoresce yellow to green.

Dolomitic mudstone occurs mainly in well 7 (Plate A-3) and reaches a maximum thickness of 13.26 m. This facies also appears in wells 5 and 8 where it is mm-scaled and interbedded with black shale (Plate A-4 and A-5). It occurs at depths ranging from 2334.3 to 2925.8 m. The facies is identified by its Type II matrix dolomite (see Chapter IV). Bivalves, brachiopods, ostracods, tentaculites and little calcareous spheres are found in dolomitic mudstones. Amorphous organic matter is non-fluorescent to dark brown fluorescent. Few thick-walled Prasinophyte alginate (Tasmanite) is found in well 5. The dolomite displays both yellow and green colors under blue-violet illumination (Plate D-2).

3.2.3 Laminated dolomitic mudstone

In hand samples, the laminated dolomitic mudstone display fairly wavy laminations of thinner, black organic-rich laminae interbedded with thicker, grey organic-lean laminae (Plate A-6 and D-3). The laminations commonly range from 0.1 mm to 3 mm and occasionally reach 1.0 cm. This facies is 0.84 to 6.35 m thick and occurs mainly in wells 10 and 11, which are mostly near the reef complex, and occurs at depths ranging from 1622.43 to 1631.47 m. The facies is characterized by its Type III matrix dolomite (see Chapter IV) that accounts for 20 to 40% of the whole rock. Quartz content is also high at 50 to 60%. Calcite, feldspars, mica and Fe-Ti oxides are relatively less abundant, each accounting for 5% or less. Clay is absent.

The only identifiable fossil in this facies was a gastropod. However, this facies contains numerous thick-walled Tasmanites as well as thin-walled Prasinophyte alginates (Plate B-6). The Tasmanites range from 50 μm to 150 μm in length and, because they are invariably compacted, the thickness of the wall is hard to estimate. Thin-walled Prasinophyte alginates are usually less than 15 μm in length. Amorphous organic matter is brown under blue-violet illumination. Carbonate components show green fluorescence, the same as in other facies.

3.2.4 Grey shale/Grey mudstone

In hand samples, the grey shale and grey mudstone are light grey in color and very soft. They occur mainly in well 13 from 891.18 to 896.77 m and one same sample from well 3 occurs at 1009.36 m. Shales are fissile and occur at the upper part of well 13 where they are 5.6 m thick. Mudstones occur in the lower part of the core and are 2.6 m thick. Nearly no fossils can be found in this facies and only minor thin-walled Prasinophyte

alginates are present. The rocks are composed mainly of calcite, dolomite, quartz and feldspar. Concentrations of mica and Fe-Ti oxides are low. Clay is absent.

CHAPTER IV

DIAGENESIS OF THE DUVERNAY FORMATION

4.1 Introduction

Diagenesis is defined as all processes that occur in and affect sediments from immediately after deposition and continuing until the onset of metamorphism at elevated temperatures and / or pressures (Boggs, 1992). In carbonates, diagenetic processes may include modifications to texture, mineralogy, chemistry and physical properties. Processes that produce such changes are widespread and include mechanical and chemical compaction, cementation, dissolution, dolomitization and recrystallization.

The sediments of the Duvernay Formation have undergone a complex diagenetic history. The major processes affecting shales and mudstones are dolomitization, pyritization and calcite cementation. Minor processes include physical compaction, dissolution, anhydritization and fracturing. Most of the diagenetic processes are facies controlled.

Descriptions of diagenetic modifications were made primarily from a combination of SEM, XRD, petrographic and blue-violet fluorescence microscopic observations.

4.2 Compaction

During progressive burial of the Duvernay Formation, the increase in pressure led to a reduction in sediment thickness. Compactional textures are observed in the samples.

PLATE C

Mechanical Compaction, Cementation and Dolomite

Photo 1. Photograph of thin laminae which display mechanical compaction under plane polarized light. Location: well 12 (11-26-58-23w4), 1284.529 metres. Field of view is 2 millimetres. Stained.

Photo 2. Photograph of ferroan mosaic calcite cement filling in an ostracod under polarized light. Crystals around the ostracod are Type II Matrix dolomite (MD) (blue crystals in the upper left part of the photograph is ferroan dolomite (arrow)). Location: well 7 (3-1-52-11W5), 2643.403 metres. Field of view is 0.5 millimetres. Stained.

Photo 3. Photograph of calcite cement filling in a tentaculite under polarized light. Ferroan calcite (FC, blue) postdates non-ferroan calcite (C). Calcite spar (CSP, brownish red) fills in the fossil later. Matrix dolomite (MD) replaces calcite spar at last. Location: well 8 (2-6-47-4W5), 2633.218 metres. Field of view is 2 millimetres. Stained.

Photo 4. Photograph of mosaic calcite cement filling in a tentaculite under polarized light (left part of the fossil in Plate C-3). Ferroan calcite cement (blue) postdates non-ferroan calcite cement. Location: well 8 (2-6-47-4W5), 2633.218 metres. Field of view is 0.5 millimetres. Stained.

Photo 5. Photograph of bladed/prismatic cement filling a vein under polarized light. Crystals in upper right is ferroan (arrow). Location: well 9 (6-14-27-7w5), 3642.13 metres. Field of view is 2 millimetres. Stained.

Photo 6. Photograph of Matrix dolomite I (arrow) under polarized light. Matrix dolomite replaces mud matrix here. Location: well 1 (7-1-4-3w5), 2804.51 metres. Field of view is 0.5 millimetres. Stained.

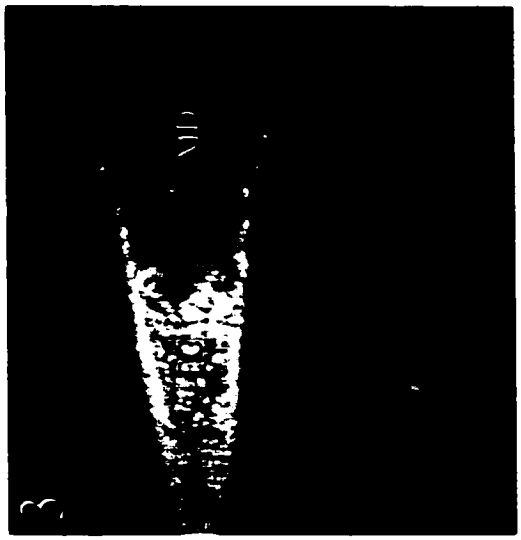

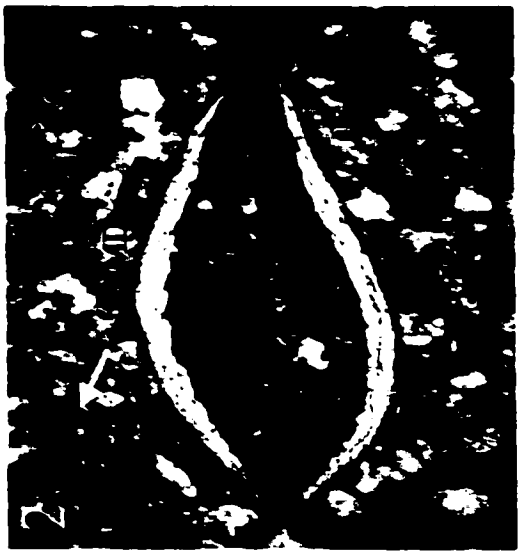

PLATE D

Dolomite

Photo 1. Photograph of Matrix dolomite I (MD) in a fossil under polarized light. Matrix dolomite I replaced calcite cement here. Location: well 5 (16-18-52-3w5), 2340.72 metres. Field of view is 0.5 millimetres. Stained.

Photo 2. Photograph of Matrix dolomite II under blue-violet illumination. These dolomite crystals are yellow and green and show zoning which cannot be identified under polarized light. Amorphous organic matter (AOM) is non-fluorescent. Location: well 8 (2-6-47-4w5), 2636.977 metres. Field of view is 0.5 millimetres.

Photo 3. Photograph of Laminated dolomitic mudstone and Matrix dolomite III (MD) under crossed Nichols. The upper part is organic-lean, whereas the lower part contains much organic matter. Location: well 11 (5-19-54-25w4), 1627.327 metres. Field of view is 1 millimetres. Stained.

Photo 4. Photograph of Saddle dolomite (SD) cement filling in a vein under polarized light. Saddle dolomite is filling in the center of the vein (right part). To its left is ferroan bladed dolomite cement (FBD). Location: well 8 (2-6-47-4w5), 2641.168 metres. Field of view is 2 millimetres. Stained.

Photo 5. Photograph of Saddle dolomite and Vein-associated dolomite (arrow) under polarized light. Saddle dolomite (SD) at the lower part is partially ferroan. Planar-e dolomite replaces calcite cement. Location: well 9 (6-14-37-7w5), 3642.13 metres. Field of view is 2 millimetres. Stained.

Photo 6. Photograph of vein-associated dolomite and pyrite under polarized light. Planar-e dolomite replaces calcite cement. Cubic and irregular pyrite crystals replace calcite cement along the boundary of the vein. Location: well 9 (6-14-37-7w5), 3642.13 metres. Field of view is 2 millimetres. Stained.

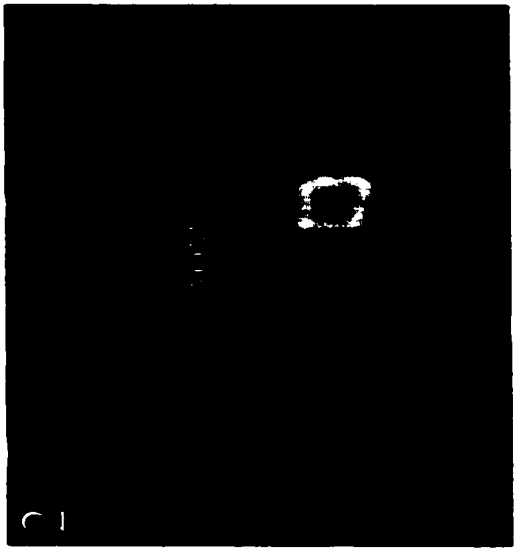

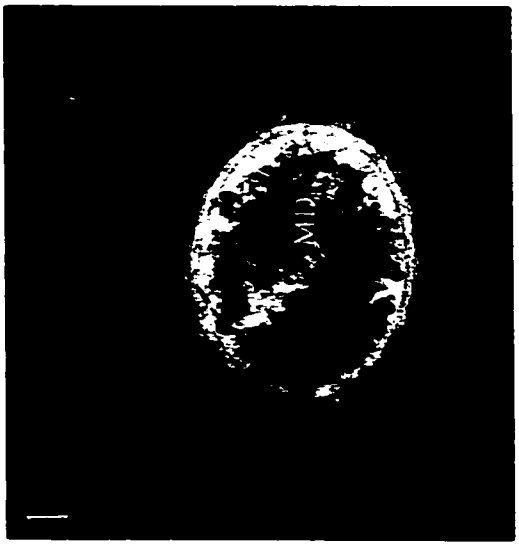

There are two types of compaction: mechanical (physical) compaction and chemical (pressure-solution) compaction (Boggs, 1992). Only mechanical compactional features were observed in the shales and mudstones.

Mechanical compaction causes reductions in porosity, permeability and sediment thickness, deformation of organic matter, re-orientation, flattening and breakage of allochems, dewatering and fracturing, and closer packing of grains (Shinn and Robbin, 1983; Choquette and James, 1987; Boggs, 1992).

In the Duvernay Formation, mechanical compaction occurs mainly in black shales, laminated mudstones, lime mudstones and laminated dolomitic mudstones. Thick-walled Prasinophyte alginates (Tasmanites) were invariably flattened (Plate B-6) in the laminated dolomitic mudstones. Most of the fossils show crushed fragments in all facies. In the laminated mudstone in well 12, thin laminae drape around the geopetal fabrics and display some flattening (Plate C-1). Fractures exist mainly in black shales and lime mudstones, probably resulting from the mechanical compaction. The grey shales/grey mudstones facies lacks evidence of mechanical compaction, probably most due to its fine-grained nature that prevents structures from being identified.

4.3 Calcite cementation

Calcite cementation, both ferroan and non-ferroan, was a significant diagenetic process in the Duvernay Formation. The major types of cement are mosaic calcite cement and sparry calcite cement. Bladed/prismatic calcite cement is a minor constituent.

4.3.1 Mosaic Calcite Cement

Mosaic calcite cements occur both as ferroan (Plate C-2) and non-ferroan types (Plate B-4). They fill in most of the fossils, calcareous spheres and veins. Cementation occurs in almost all of the facies except for the laminated dolomitic mudstone facies. The crystal sizes of the cement range from 10 to 700 μm. Ferroan cement occurs mainly in wells 4, 5, 7, 8 and 12. It postdates non-ferroan cement (Plate C-4) and thus represents a later stage of diagenesis.

4.3.2 Sparry Calcite Cement

This is the dominant form of cementation in rocks of the Duvernay Formation. Its crystals range in size from 15 μm to 40 μm and are non-ferroan. In a tentaculite in well 8 (Plate C-3), blue ferroan mosaic cement postdates non-ferroan mosaic cement and, subsequently, sparry calcite fills in the fossil. Matrix dolomite replaces sparry calcite cement at last. The shell of the tentaculite is perhaps composed of low-magnesian calcite, thus resistant to either dissolution or replacement.

4.3.3 Bladed/Prismatic Calcite Cement

Bladed cements are not common but do occur in veins and in geopetal fabric in the black shales and laminated mudstones. Both ferroan and non-ferroan cements are present (Plate C-5 and D-4). Non-ferroan cement gradually changes into ferroan cement. This is, perhaps, because of the change in the chemistry of the precipitating diagenetic fluids. Lengths of the crystals range from 150 μm to 3 mm and widths from 70-600 μm.

4.4 Dolomitization

PLATE E

Dolomite, Pyrite and Quartz

Photo 1. SEM view of matrix dolomite I (D) and framboidal pyrite (P). Location: well 9 (6-14-37-7w5), 3642.13 metres.

Photo 2. SEM view of Matrix dolomite III. Location: well 11 (5-19-54-25w4), 1626.413 metres.

Photo 3. SEM view of matrix dolomite III. Dissolution is obvious on the top of the dolomite. Location: well 11 (5-19-54-25w4), 1626.413 metres.

Photo 4. SEM view of framboidal pyrite. Location: well 10 (14-18-54-25w4), 1624.178 metres.

Photo 5. SEM view of pyrite spheres, cubic and octahedral pyrite crystals. Location: well 5 (16-18-52-5w5), 2336.02 metres.

Photo 6. SEM view of quartz of detrital origin (Q). Location: well 11 (5-19-54-25w4), 1626.413 metres.

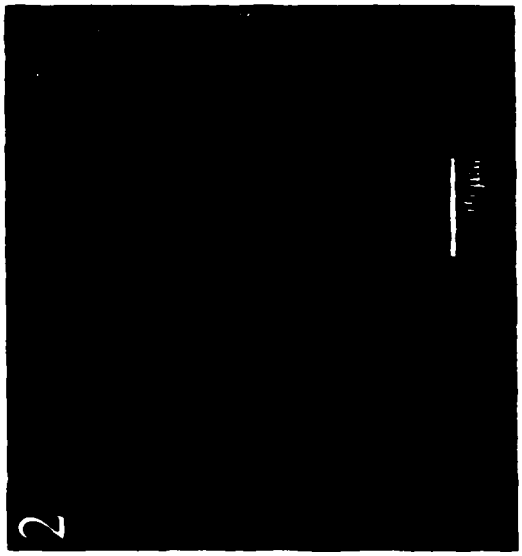

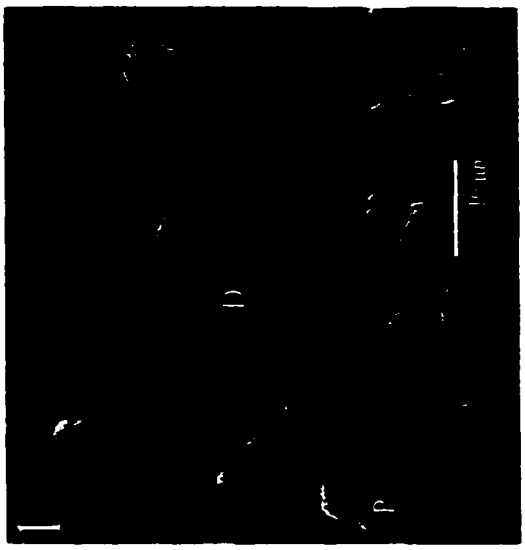

Dolomitization is the most important diagenetic process that affected the carbonates of the Duvernay Formation, occuring in all facies and dominating in the dolomitic mudstone and laminated dolomitic mudstone. Three types of dolomite are recognized: matrix dolomite, saddle dolomite and vein-associated dolomite.

4.4.1 Matrix Dolomite

Matrix dolomite accounts for more than 90% of the dolomite and 5 to 35% of the rock in this study. Three types have been found in different lithofacies.

4.4.1.1 Matrix Dolomite I

Matrix dolomite I consists of 5-20 μm crystals with most between 5 to 10 μm. They have a non-planar to planar-s texture (Plate C-6 and E-1). Matrix dolomite I is widespread in the black shales, laminated mudstones, lime mudstones, grey shales and grey mudstones. The dolomite pervasively replaces the mud matrix, however, it only selectively replaces fossil fragments (Plate D-1) to various degrees.

4.4.1.2 Matrix Dolomite II

Matrix dolomite II occurs only in dolomitic mudstones. It ranges from 10 μm to 40 μm in size with an average size of 20 μm, and has a planar-e texture. Both ferroan and non-ferroan crystals are found (Plate C-2). They are green or yellow under blue-violet illumination and some of them show zoning that cannot be seen under polarized light (Plate D-2). Zoning is not common.

4.4.1.3 Matrix Dolomite III

Matrix dolomite III is only found in laminated dolomitic mudstones. It has a non-planar to planar-s texture and accounts for 20-40% of the whole rock (Plate D-3, E-2 and E-3). The dolomite is non-ferroan and its crystals range from 10-200 μm.

4.4.2 Saddle Dolomite

Saddle dolomite is not common and occurs primarily as a fracture and void-filling cement (Plate D-4 and D-5). It is identified by its curved crystal faces, cleavage and sweeping extinction in cross-polarized light. The crystals range from 200 μm to 2 mm and are found mainly in black shales, carbonate-rich mudstones and laminated mudstones.

4.4.3 Vein-associated Dolomite

Vein-associated dolomite is found only in one sample from laminated mudstones. Two sizes of planar-e dolomite, which replace calcite cement, were found in two veins. The smaller dolomite crystals range from 60 to 80 μm (Plate D-5) and the larger ones range from 100 to 500 μm (Plate D-6).

4.5 Pyritization

Pyritization is also an important process in the Duvernay Formation occuring in all other facies except for the carbonate-rich mudstone facies. Pyrite occurs mainly as framboids (Plate E-4), cubic, pyritohedral and octahedral crystals, and pyrite spheres

PLATE F

Pyrite, Anhydrite and Quartz

Photo 1. Photograph of pyrite crystals under polarized light. Cubic pyrite crystals replace dolomitic matrix. Overgrowth and erosion of the crystals can be seen. Location: well 10 (14-18-54-25w4), 1622.425 metres. Field of view is 2 millimetres. Stained.

Photo 2. Photograph of pyrite under polarized light. Pyrite replaces a big dolomite crystal along its edge (arrow). In the middle left part of the photograph, small cubic pyrite crystals replace the matrix. Black pyrite dots replace both the matrix and the cement in the Tentaculite. Location: well 9 (6-14-37-7w5), 3642.13 metres. Field of view is 0.5 millimetres. Stained.

Photo 3. Photograph of pyrite under polarized light. A rectangular pyrite crystal replaces the center of a dolomite crystal (arrow). Cubic pyrite crystals in the lower part show etched boundaries. Black pyrite dots replace the matrix. Location: well 5 (16-18-52-5w5), 2333.75 metres. Field of view is 0.5 millimetres. Stained.

Photo 4. Photograph of pyrite under polarized light. Pyrite replaces fossils. Location: well 9 (6-14-37-7w5), 3643.72 metres. Field of view is 2 millimetres.

Photo 5. Photograph of vein anhydrite under crossed Nichols. Anhydrite vein is separated with the laminated dolomitic mudstone by a dissolution seam. The vein is > 3 centimetres wide. Location: well 10 (14-18-54-25w4), 1622.45 metres. Field of view is 2 millimetres.

Photo 6. SEM view of calcite (C) and authigenic quartz (Q). Location: well 8 (2-6-47-4w5), 2639.314 metres.


3


2

(Plate E-5). Framboids have diameters ranging from 2 to 10 μm but most are < 5 μm. They are composed of cubic microcrystals that range from 0.2 to 1 μm. Pyrite crystals range from 2 μm to 2 mm but most of them are fine-grained (2 - 10 μm). Pyrite selectively replaces calcite cement, fossils, dolomite crystals and matrix. Replacement occurs mainly as the following types:

(1) Cubic and irregular pyrite crystals occur along the boundaries of veins and replace calcite cement as well as vein-associated dolomite crystals (Plate D-6).

(2) Pyrite replaces matrix (Plate F-1, F-2 and F-3). Overgrowths and corrosion of the crystals can be seen in some samples.

(3) Pyrite replaces dolomite crystals both along their edge (Plate F-2) and in their centers (Plate F-3). The pyrite crystals show etched boundaries.

(4) Pyrite replaces fossils (Plate F-4).

4.6 Anhydritization

Secondary anhydrite occurs as cement in veins cutting laminated dolomitic mudstone (Plate F-5). Different crystal sizes are found. Although the veins occur within dolomitic mudstone, they show no dolomitization.

4.7 Quartz

Quartz appears in all the facies and accounts for more than 50% of the content in some black shales and laminated dolomited mudstones. The fine-grained fragments of

quartz are always angular and range from 5-30 μm. Some of the quartz grains are authigenic (Plate F-6), while others are detrital in origin and show various degrees of dissolution (Plate E-6). Because a high quartz content is found in samples from wells 4, 5, 8, 10 and 11, the clasts are probably derived from the area to the northwest or north.

4.8 Clay

Clay minerals found in this study are kaolinite and chlorite. They occur mainly in black shales and laminated dolomitic mudstones. Both detrital and authigenic clay crystals exist.

4.9 Dissolution

Dissolution is defined as the process involving removal of previously existing minerals in solution, leaving void spaces in the rocks (Boggs, 1992). In the Duvernay Formation, dissolution is manifested in the following forms:

(1) Fossils, which were originally composed of metastable aragonite and high-Mg calcite, were dissolved and the resulting void was filled with calcite cement (Plate C-2).

(2) Etching of crystals of matrix dolomite (Plate E-3), saddle dolomite and cubic pyrite (Plate F-1) indicates minor dissolution after precipitation.

4.10 Fracturing

Fractures were found in black shales, laminated mudstones, carbonate-rich mudstones and laminated dolomitic mudstones of the Duvernay Formation. At least three generations were identified.

The first generation are randomly oriented thin veins (40 μm to 200 μm) that are filled by non-ferroan calcite cement.

The second generation is also randomly oriented and includes thin to thick veins (100 μm to 1cm) filled by both ferroan and non-ferroan calcite cements. Ferroan calcite cement replaces non-ferroan calcite cement and subsequently, dolomite replaces ferroan calcite cement. Pyrite crystals replace some of these veins along their boundaries.

The third generation is always perpendicular to the depositional surface. These veins are thin to thick (200 μm to 1cm) and filled by anhydrite.

CHAPTER V

GEOCHEMISTRY OF THE DUVERNAY FORMATION

5.1 Rock-Eval pyrolysis

5.1.1 Introduction

Kerogen is an organic constituent of sedimentary rocks that is insoluble in both aqueous alkaline solvents and common organic solvents (Breger, 1961). Three types of kerogen are classified (Tissot and Welte, 1984):

Type I is defined as kerogen with a high initial H/C atomic and a low initial O/C ratio. This kind of kerogen is composed mostly of lipid material. It has high potential for yielding both oil and gas and is thought to be preserved in anoxic/suboxic conditions. Most Type I oil-prone kerogens were deposited in lacustrine settings.

Type II refers to kerogen with relatively high H/C and low O/C ratios. It is often derived from bacterially-altered marine organic matter with a minor component of terrigenous organic matter. This kerogen has a medium to high sulphur content and is thought to be preserved in anoxic/suboxic conditions.

Type III kerogen has a relatively low initial H/C ratio and a high initial O/C atomic ratio. It is derived mainly from terrestrial higher plants. This kerogen has only a moderate oil potential but may generate abundant gas at greater depths. It can accumulate under oxic and upper dysoxic conditions.

Rock-Eval pyrolysis is a method that is used to characterize the various types of kerogen, based on the relative content of hydrocarbons and carbon dioxide generated

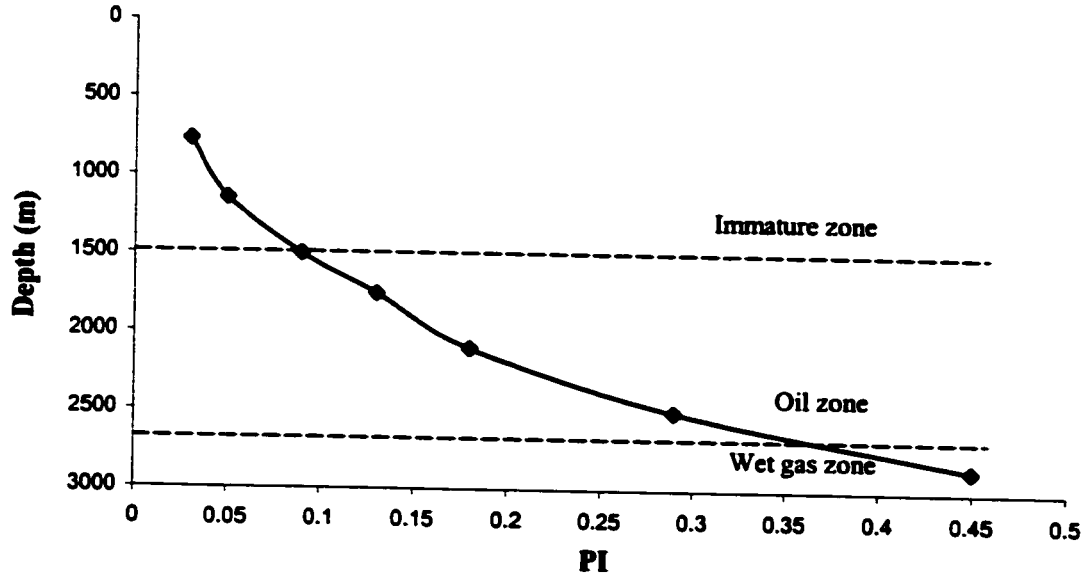

Figure 5.1 Characterization of source rock maturity by PI (Espitalie et al., 1977)

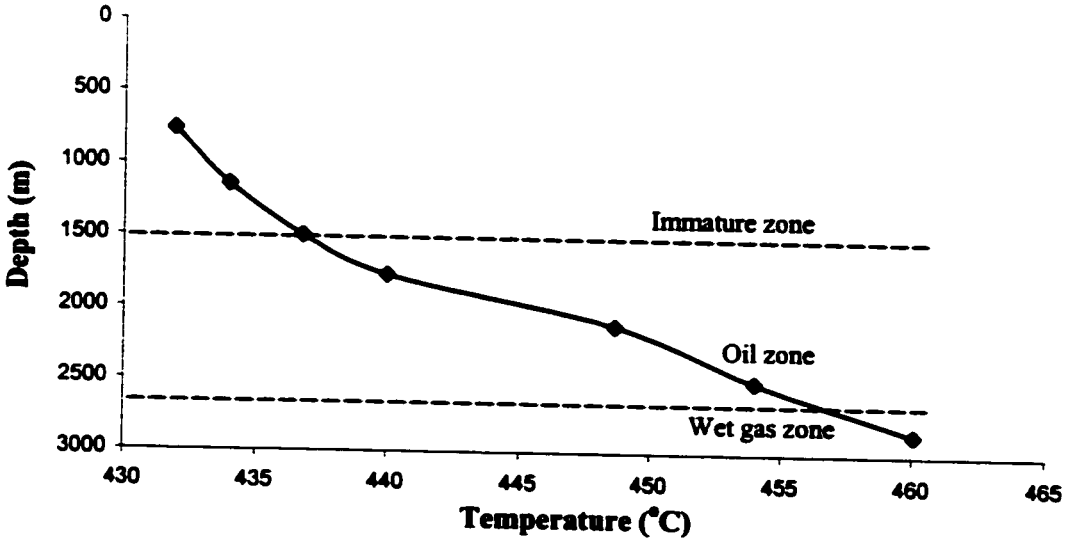

Figure 5.2 Characterization of source rock maturity by T_{max} (Espitalie et al., 1977)

during pyrolysis. Total Organic Carbon (TOC), T_{max}, S_1, S_2, and S_3 are the parametres that are obtained from Rock-Eval pyrolysis.

S_1 is hydrocarbon released from source rocks measured at 300°C; S_2 is hydrocarbons and hydrocarbon-like compounds generated from source rocks measured at temperatures between 300°C-850°C; and, S_3 refers to oxygen-containing volatiles and water (Tissot and Welte, 1984).

Kerogen type is determined from two indices (Espitalie et al., 1977, Fig 5.7): hydrogen index (HI) and oxygen index (OI). HI is defined as S_2 / TOC and OI as S_3 / TOC, respectively. Although they are independent of the content of organic matter, these indices strongly correlate to the elemental composition of kerogen. Type III kerogen usually has HI values < 100 mg HC/g TOC whereas Type II kerogen has HI values from 250-550 mg HC / g TOC. Mixing of terrestrial material and well-preserved algal organic matter (HI > 550) in various proportions will lead to HI values between these end-member values. Values of HI < 150 mg HC/g TOC might indicate either highly oxidized organic matter of planktonic origin or mostly terrestrial material derived from higher plants (Arthur and Sageman, 1994).

T_{max} and production index (PI) are two indices of thermal maturation. T_{max} is the temperature measured at the maximum of hydrocarbon generation during pyrolysis. PI (S_1 / (S_1 + S_2)) is the ratio of free hydrocarbons to those generated by pyrolysis of the sample. Both T_{max} and PI increase with depth (Figs 5.1 and 5.2). PI is independent of the type of organic matter during catagenesis and metagenesis, whereas T_{max} is affected by the type of the organic matter during the diagenetic stage and the beginning of catagenesis. T_{max} is higher in types I and II kerogen and lower in types III kerogen.

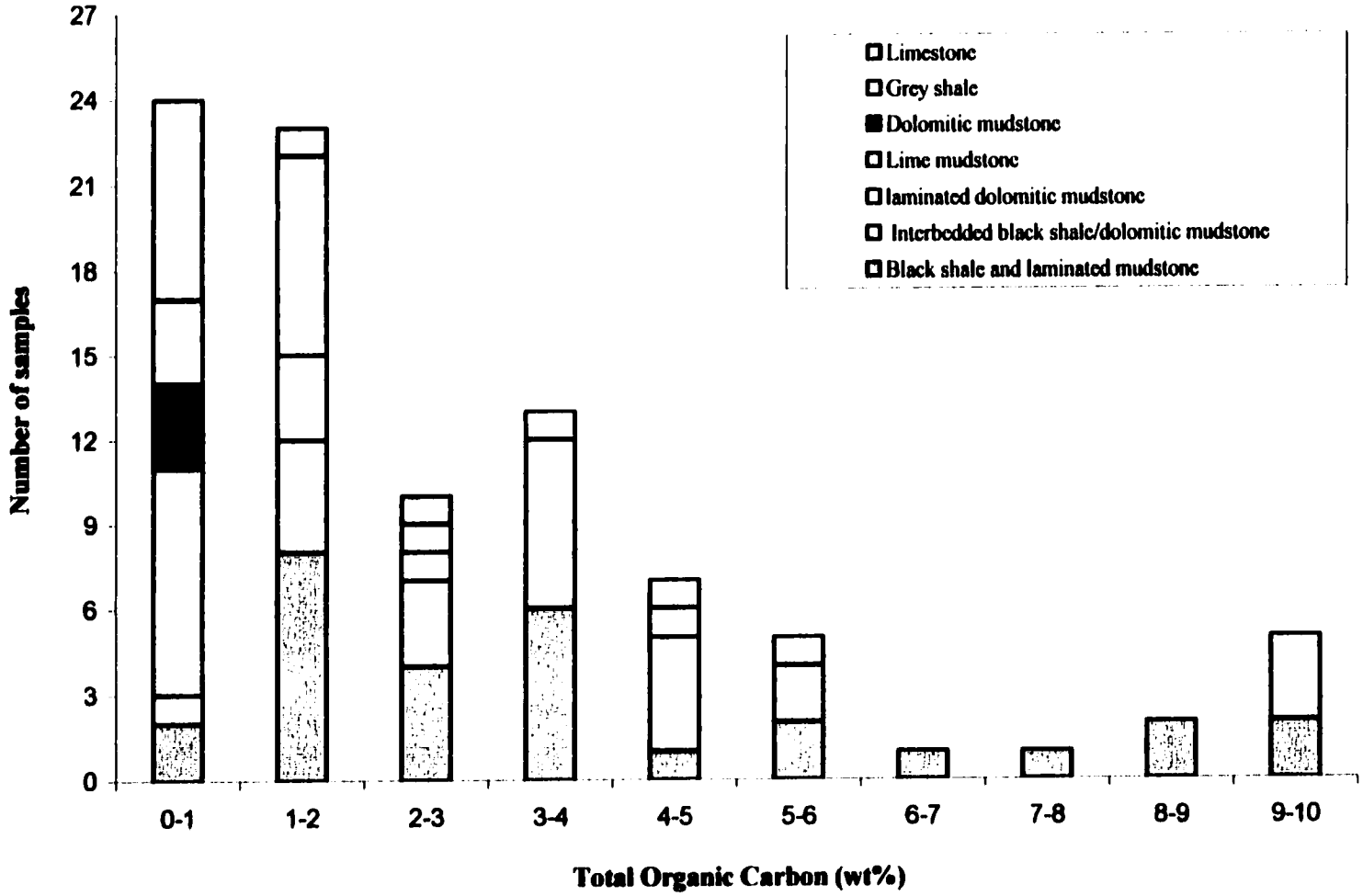

Figure 5.3 Histogram of TOC distribution for different facies

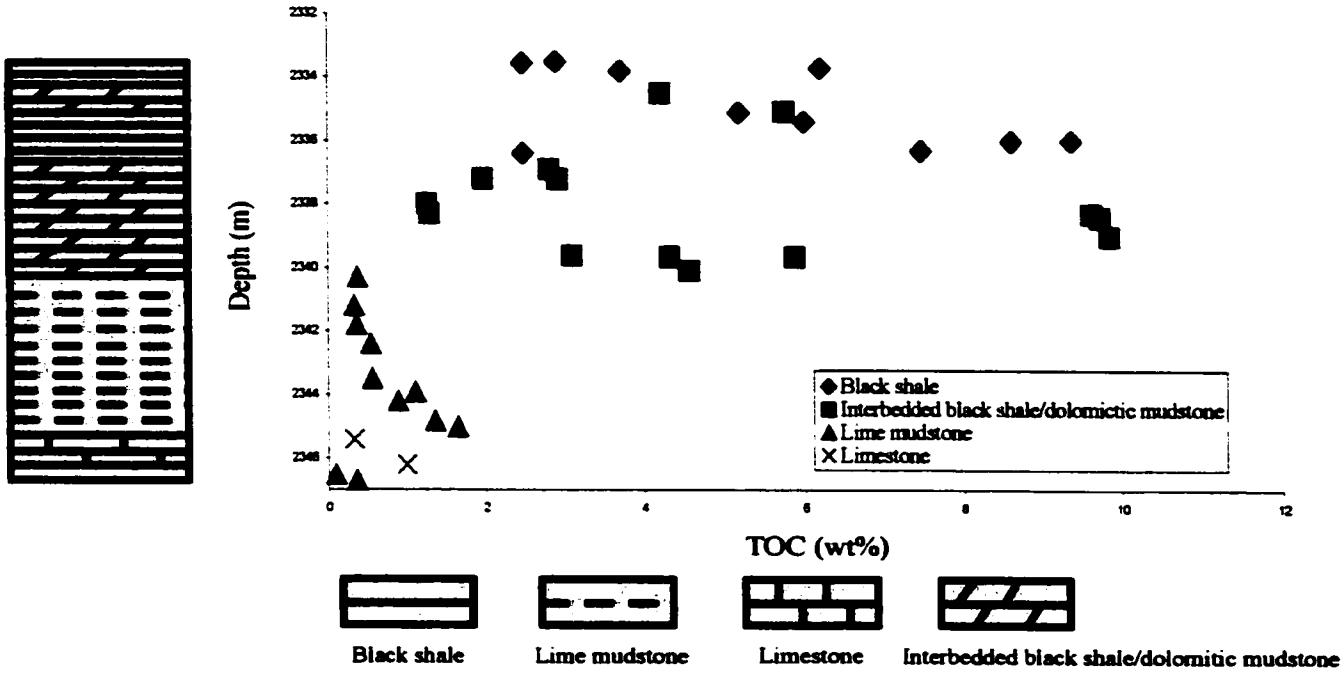

Fig 5.4 TOC distribution in well 5 (16-18-52-5w5)

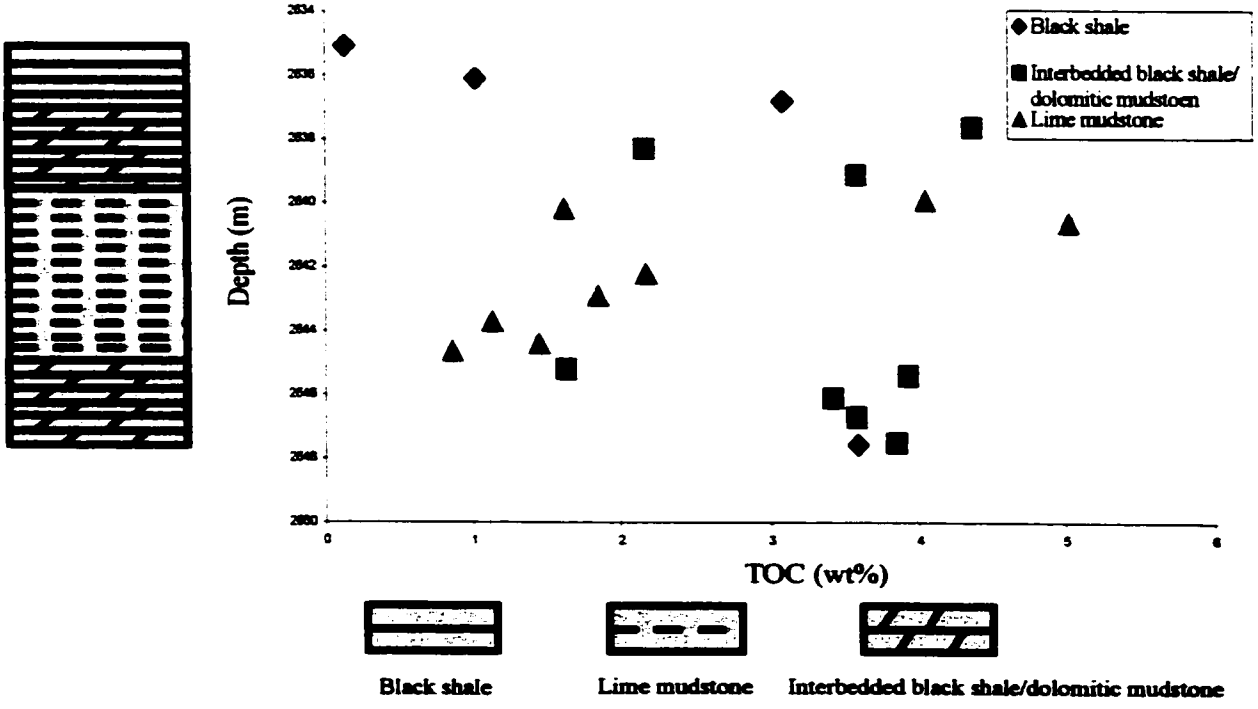

Fig 5.5 TOC distribution in well 8 (2-6-47-4w5)

However, in the peak zone of oil generation and in the gas zone, T_{max} values are almost equivalent for the different types of kerogen (Espitalie et al., 1977). Generally, PI values of 0.1 and 0.4, and T_{max} values of 435 to 445°C and 470°C indicate the threshold of the top oil window and bottom oil window, respectively (Peters, 1986).

5.1.2 Results of Rock-Eval pyrolysis

The results of Rock-Eval pyrolysis are listed in Appendix IV.

5.1.2.1 Results of Total Organic Carbon

The results of TOC are illustrated in Figure 5.3.

For black shales and laminated mudstones, the TOC values vary substantially between different wells. The values are relatively low in wells 1 and 4, ranging from 1.06 to 2.09 wt%. However, in well 12 the values of TOC are as high as from 4.67 to 9.42 wt%, whereas in wells 3 and 9, they range from 1.25 to 3.61 wt%.

For dolomitic mudstones in well 7, The TOC values are very low with the range from 0.14 to 0.18 wt%.

In well 5, four facies exist (Fig 5.4). The black shale facies has TOC values ranging from 2.47 to 9.36 wt%. Similarly, the interbedded black shales/dolomitic mudstones facies has the values from 1.25 to 9.83 wt%, probably because black shale is dominant whereas the dolomitic mudstone interbeds are very thin. The lime mudstones facies has relatively low TOC values in this well, ranging from 0.09 to 1.64 wt%. The values of limestones are also low, ranging from 0.32 to 0.99 wt%.

There are three facies identified in well 8 (Fig 5.5). The black shale facies has the TOC values ranging from 0.13 to 3.58 wt% and the interbedded black shales/dolomitic

mudstone facies from 1.63 to 4.36 wt% because the laminations of dolomitic mudstones are also thin in this well. Unlike the brownish lime mudstones in well 5, the dark-greyish lime mudstones in well 8 have higher TOC values ranging from 0.86 to 5.02 wt%.

All samples measured in wells 10 and 11 are laminated dolomitic mudstones. The black organic-rich layers in these two wells are thinner than the greyish organic-lean layers, resulting in the combined TOC values ranging from 0.43 to 4.58 wt% (Fig 5.6).

The TOC values in grey shales are very low with a range from 0.09 to 0.13 wt%, indicating this facies is not oil-prone.

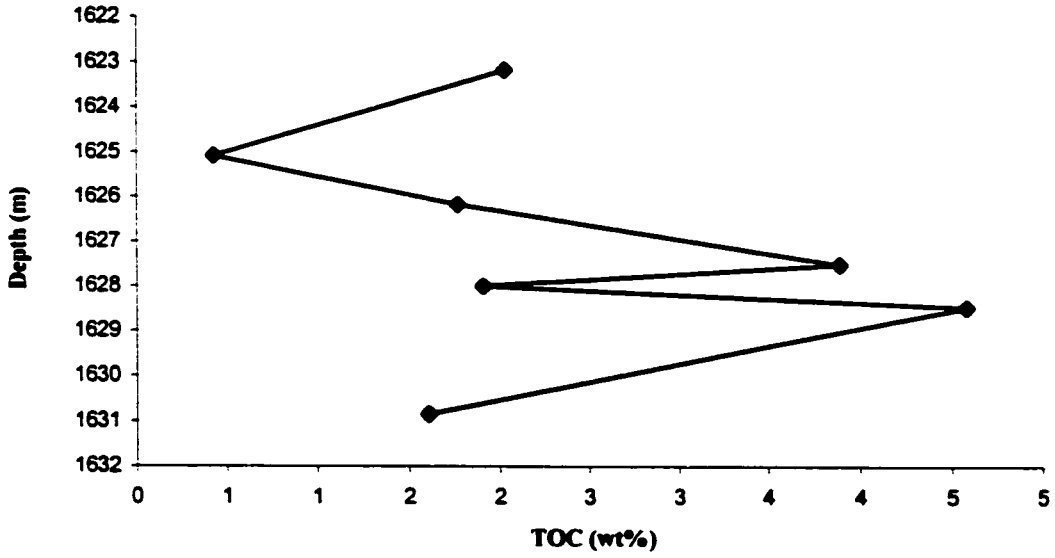

Figure 5.6 TOC for Laminated dolomitic mudstone in well 10 (14-18-54-25w4) and well 11 (5-19-54-25w4)

5.1.2.2 Results of hydrogen index and oxygen index

All three types of kerogen were found in the black shales, laminated mudstones and interbedded black shales/dolomitic mudstones (Fig 5.7). Type I kerogen was indicated in

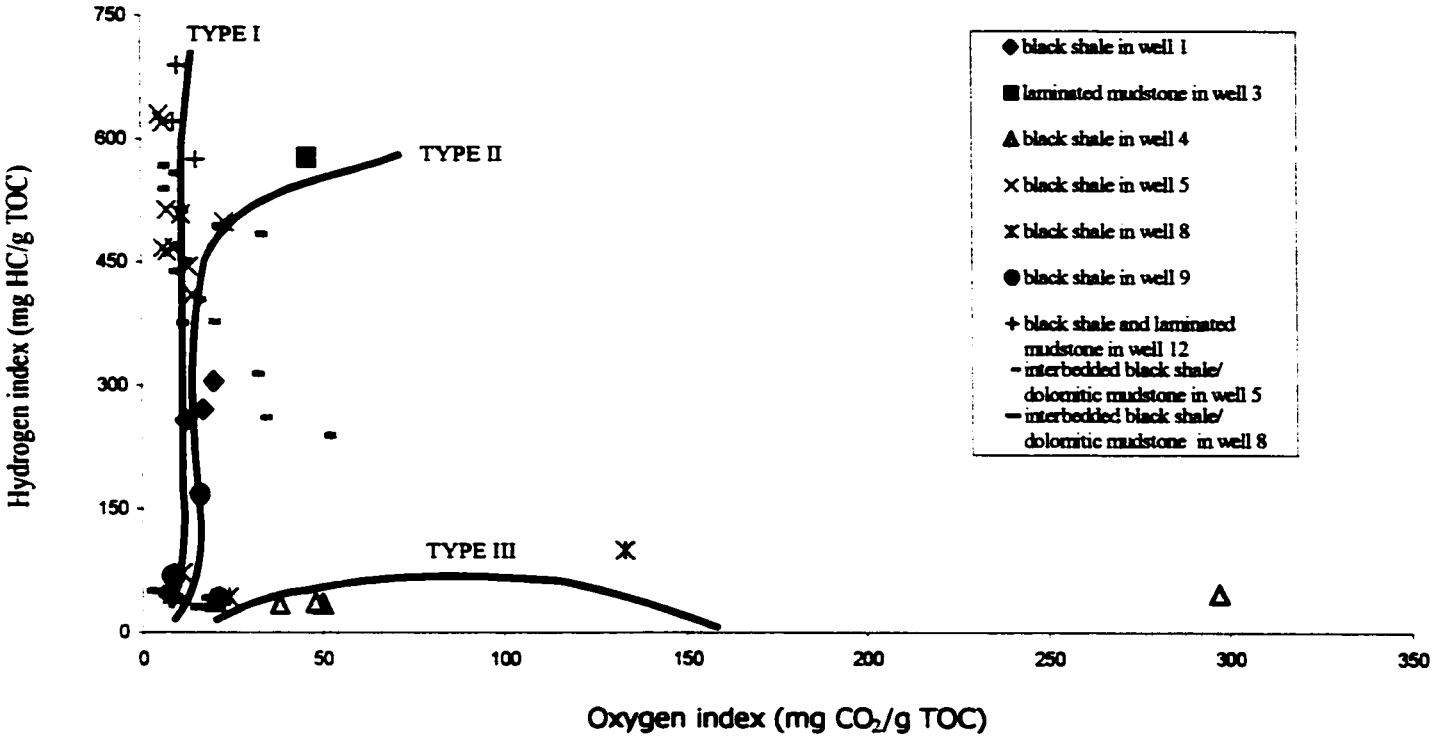

Figure 5.7 Plot of hydrogen index versus oxygen index for black shales, laminated mudstones and interbedded black shale/dolomitic mudstones. The three lines are after Tissot and Welte, 1984.

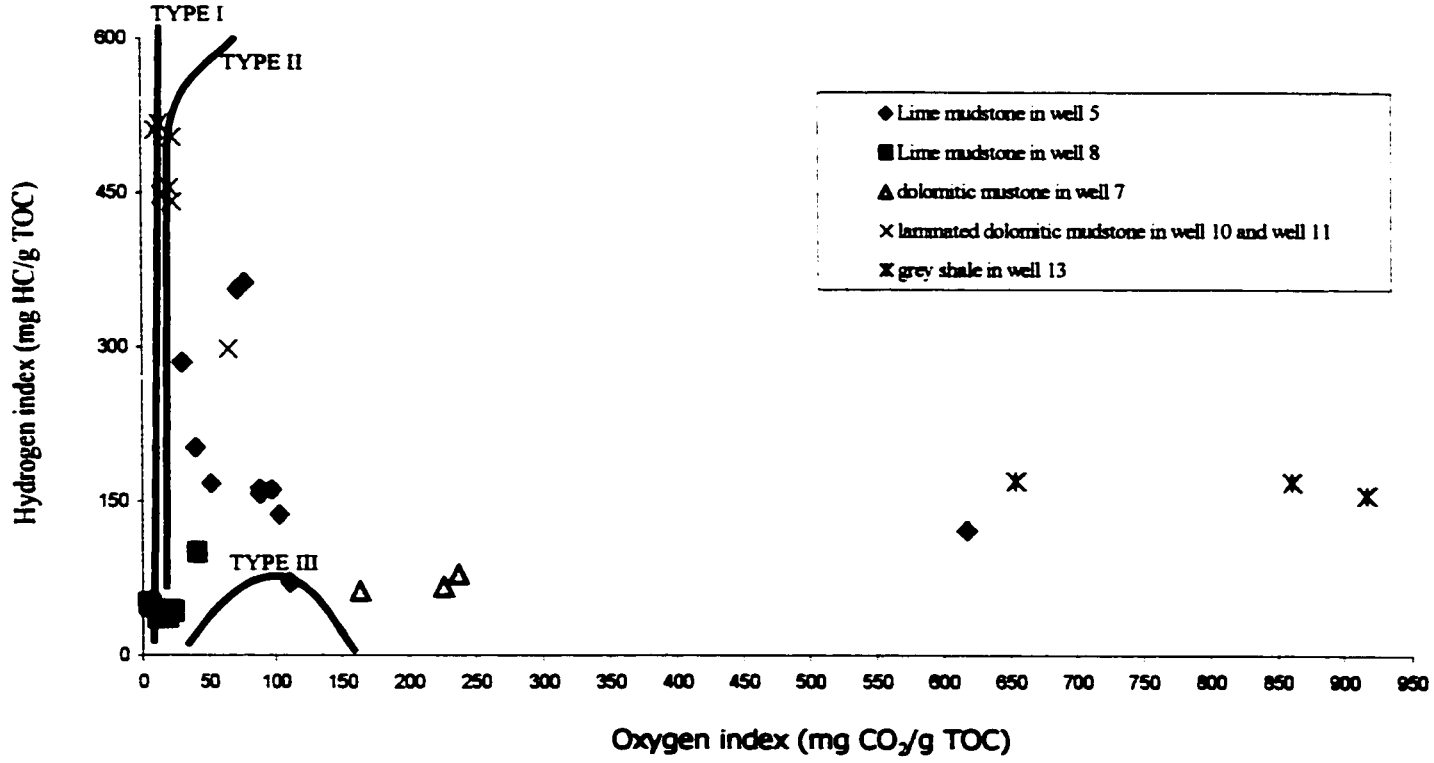

Figure 5.8 Plot of hydrogen index versus oxygen index for lime mudstones, dolomitic mudstones, laminated dolomitic mudstones and grey shales. The three lines are after Tissot and Welte, 1984.

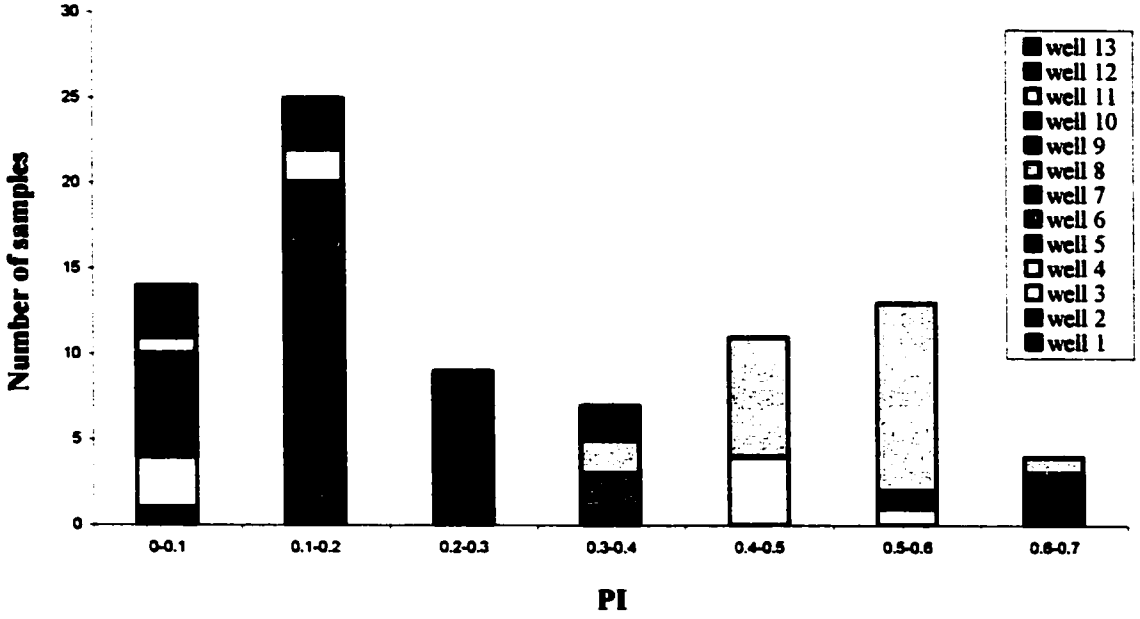

Figure 5.9 Histogram of PI distribution in different wells

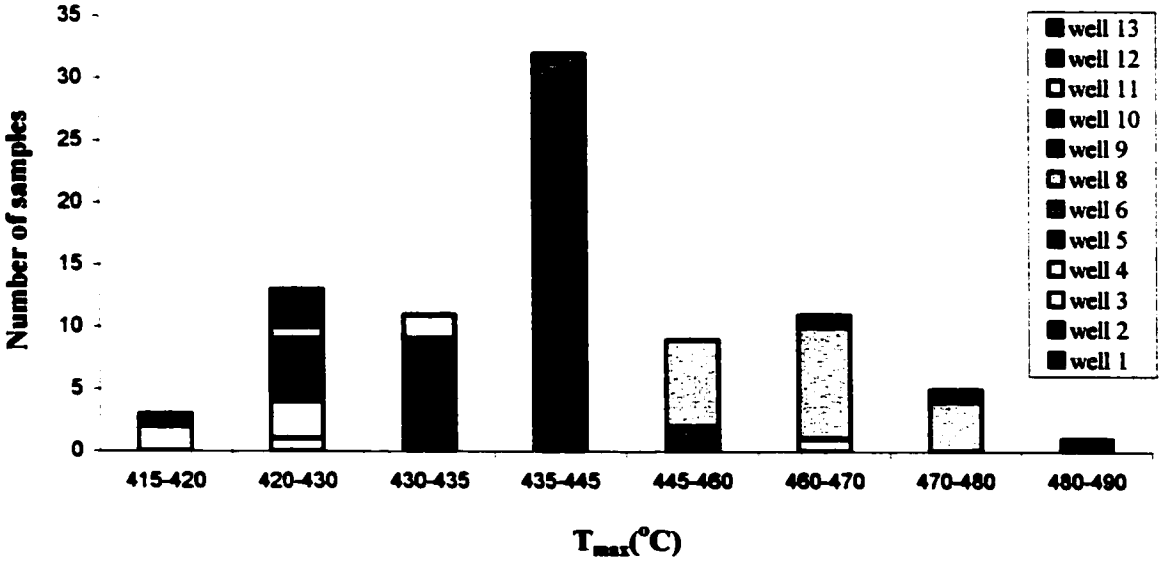

Figure 5.10 Histogram of T_{max} distribution in different wells

samples from well 12 and some samples from well 5. Type II kerogen was found in wells 1, 3 and 5. All the samples measured from wells 4, 8 and 9 contained Type III kerogen.

Type III kerogen was found in grey shales, dolomitic mudstones and lime mudstones (Fig 5.8). However, some lime mudstones in well 5 also contain Type II kerogen. Type II kerogen was also found in laminated dolomitic mudstones.

Generally, Type I kerogen was found only in the black shales and laminated mudstones in wells 5 and 12. Type II kerogen was found in almost all the facies except grey shales and dolomitic mudstones. Type III kerogen was also found in almost all the facies except laminated dolomitic mudstones.

5.1.2.3 Results of production index

PI values are not facies controlled in this study (Fig 5.9). Samples from wells 3 and 12 have values of less than 0.1 and thus are immature. Samples from wells 6, 9 and 13 show mature values ranging from 0.125 to 0.4. Samples from wells 1, 7, 10 and 11 have immature to mature values ranging from 0.06 to 0.2. Samples from well 4 show overmature values ranging from 0.42 to 0.59. Samples from wells 2 and 8 are mature to overmature, showing values from 0.23 to 0.64. Well 5 has samples that are from immature to overmature, showing values from 0.08 to 0.66.

5.1.2.4 Results of T_{max}

Like the PI values, the T_{max} results are area-controlled rather than facies-controlled (Fig 5.10). Samples from wells 3, 10, 11, 12 and 13 show immature values of less than 435°C. Samples from wells 2 and 5 have values ranging from 429 to 444 °C that are from

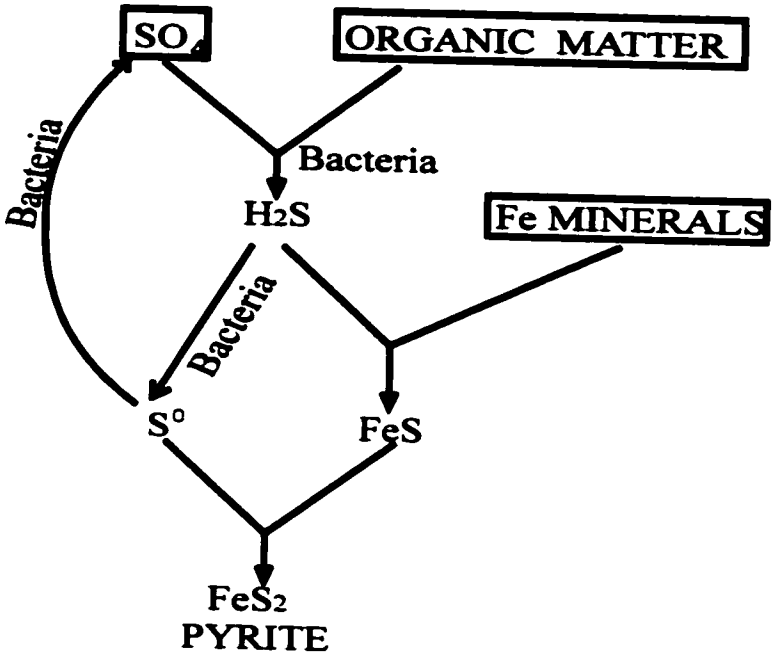

Figure 5.11 Diagramatic representation of the overall process of sedimentary pyrite formation. (After Berner, 1984)

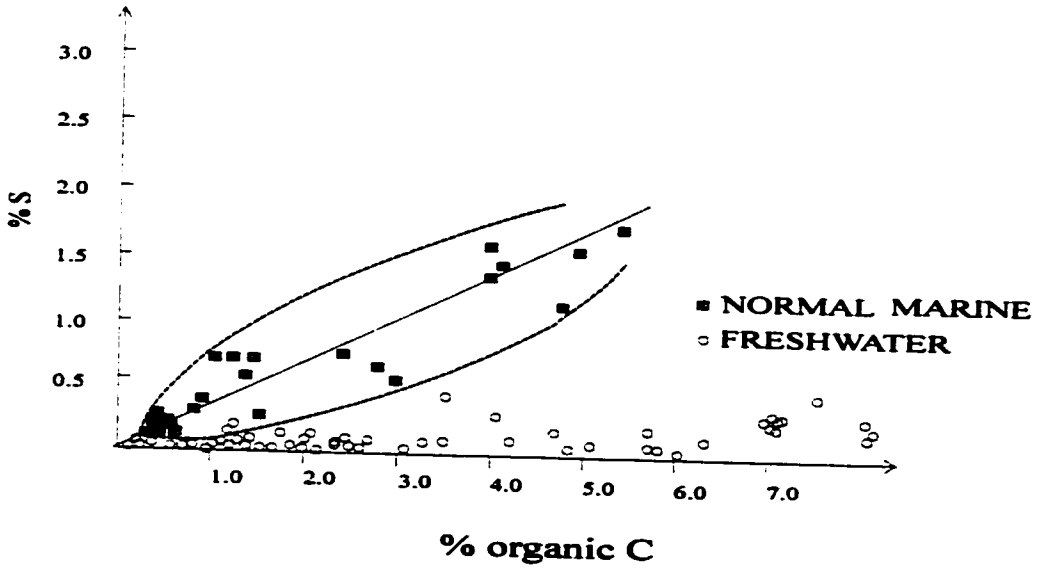

Figure 5.12 Plot of weight percent organic carbon versus weight percent reduced sulfur for modern freshwater lake sediments and normal marine (non-euxinic) sediments. Dashed line encloses many additional points (after Berner and Raiswell, 1983).

immature to mature. Samples from wells 1 and 6 show mature values from 435 to 460°C. Samples from well 9 have mature to overmature values greater than 460°C. The T_{max} values of samples in well 8 range from 435 to 480°C, which indicate that the samples are mature to overmature. There are 5 samples measured in well 4. Four of them have values from 420 to 430°C and thus are immature. One sample has mature value of 465°C.

5.2 Elemental analysis

5.2.1 Introduction

It has been demonstrated that total organic carbon/pyrite sulphur (TOC/S) ratios can be used to distinguish a marine environment from a freshwater environment (Berner and Raiswell, 1983; Berner, 1984). The differences in TOC/S ratios between different environments are caused by the process of sedimentary pyrite formation (Fig 5.11). First, H_2S is produced by bacterial sulphate reduction in the porewater and this can only happen in anoxic conditions (0 ml/l O_2). In this step, the supply of dissolved sulphate and organic matter are two important factors that control the process. Second, the resulting H_2S reacts with detrital iron minerals to form iron monosulphides (FeS). In this step, the amount and reactivity of detrital iron minerals play an important role in pyrite formation, especially in the case of highly calcareous sediments, as in this study, where iron is insufficient. Also, the amount of reactive iron limits pyrite formation in euxinic and semi-euxinic system where H_2S exceeds the availability of iron (Raiswell and Berner, 1985). Lastly, the monosulphides react with elemental sulphur to produce pyrite (FeS_2) during early diagenesis.

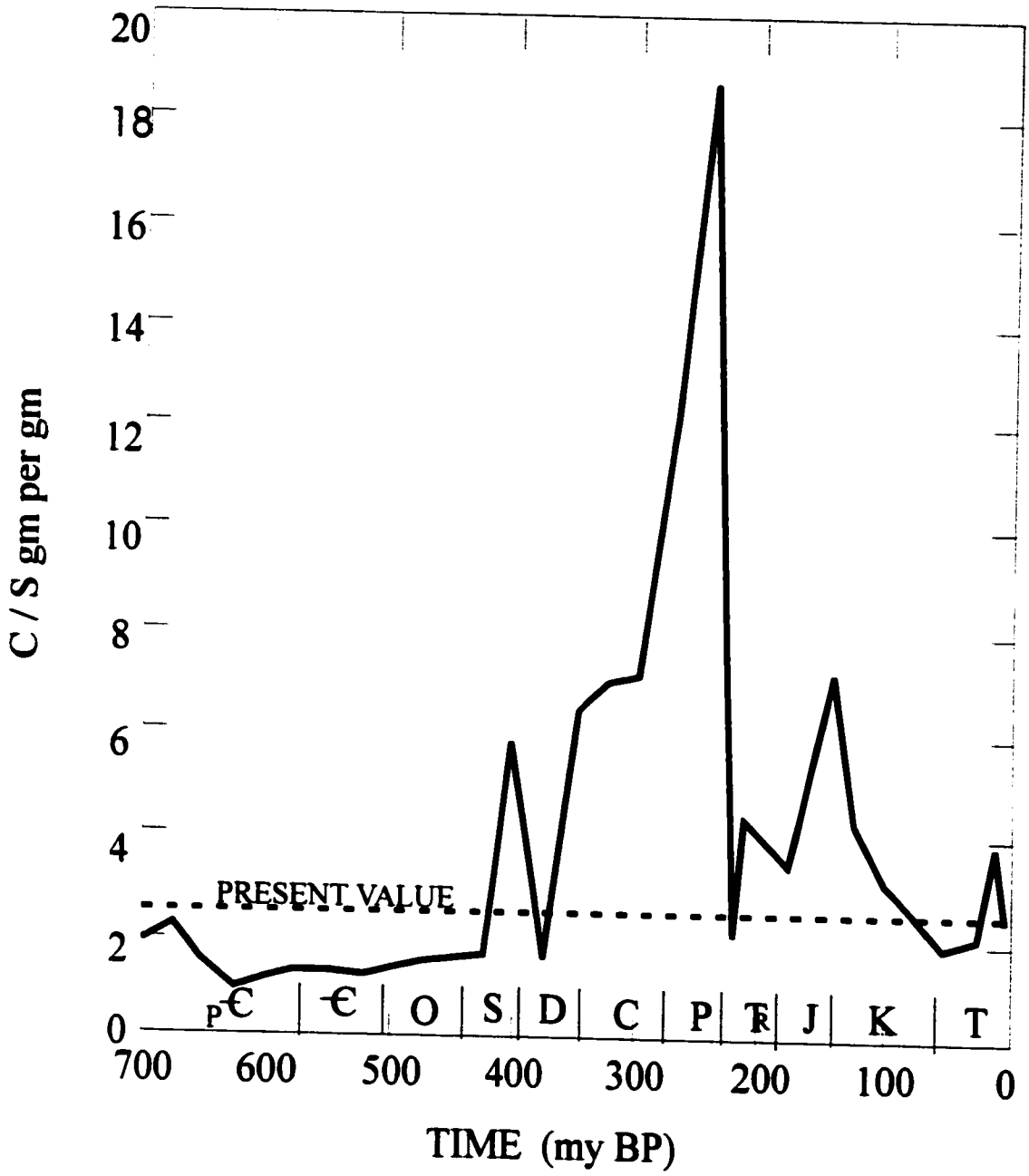

Figure 5.13 Weight ratio of organic carbon to pyrite sulfur (C/S) buried in sediments over Phanerozoic time. (After Berner and Raiswell, 1983)

The relationship between pyrite sulphur and TOC is shown in Figure 5.12. The positive slope and zero intercept of the line representing a normal marine environment indicate that pyrite formation is dependent on the amount of metabolized organic matter. This positive relationship is obtained by assuming that an approximately constant proportion of originally deposited organic matter is used to form pyrite.

In freshwater sediments, because the concentration of sulphate is very low, all sulphate has been consumed by sulfate reduction resulting in little pyrite and much organic matter. Hence, a high TOC/S ratio of 10 or more can be found relative to that found in the marine sediments.

In normal marine environments with oxygenated rather than anoxic bottom water conditions, the TOC/S ratios of modern oceans average 2.8 (Raiswell and Berner, 1986). The dashed line in Figure 5.12 encloses many additional points that are summarized by Leventhal (1983). During the Upper Devonian, the TOC/S ratio was higher than that in modern time (Berner and Raiswell, 1983, Fig 5.13).

Under euxinic marine conditions, sediments are deposited in anoxic saline bottom waters containing dissolved H_2S. Bacterial sulphate reduction happens in both the water column and the sediments; however, in normal marine environments, bacterial sulphate reduction only occurs near the sediment-water interface. As a result, more organic matter is used up during sulphate reduction in an euxinic environment than in a normal marine environment. Thus the TOC/S ratios under euxinic marine conditions are lower than in normal marine conditions. In this case, there is sufficient H_2S so that the abundance of iron minerals becomes the main factor in controlling pyrite formation. For the same reason, a low sedimentation rate can result in a high production of pyrite even with the

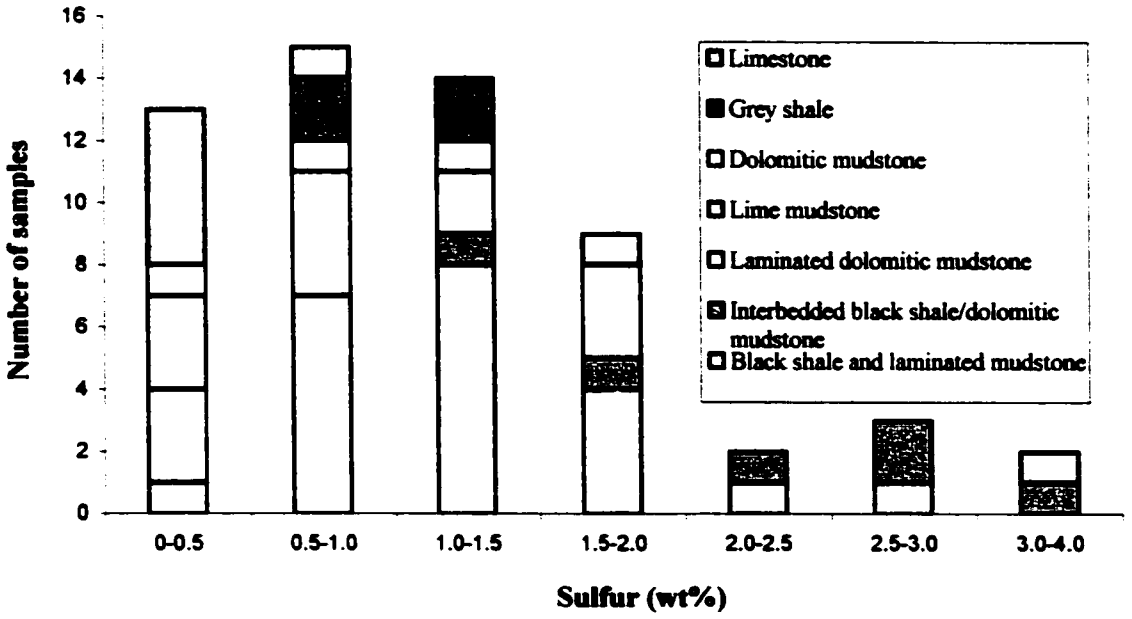

Figure 5. 14 Histogram of Sulfur distribution for different facies

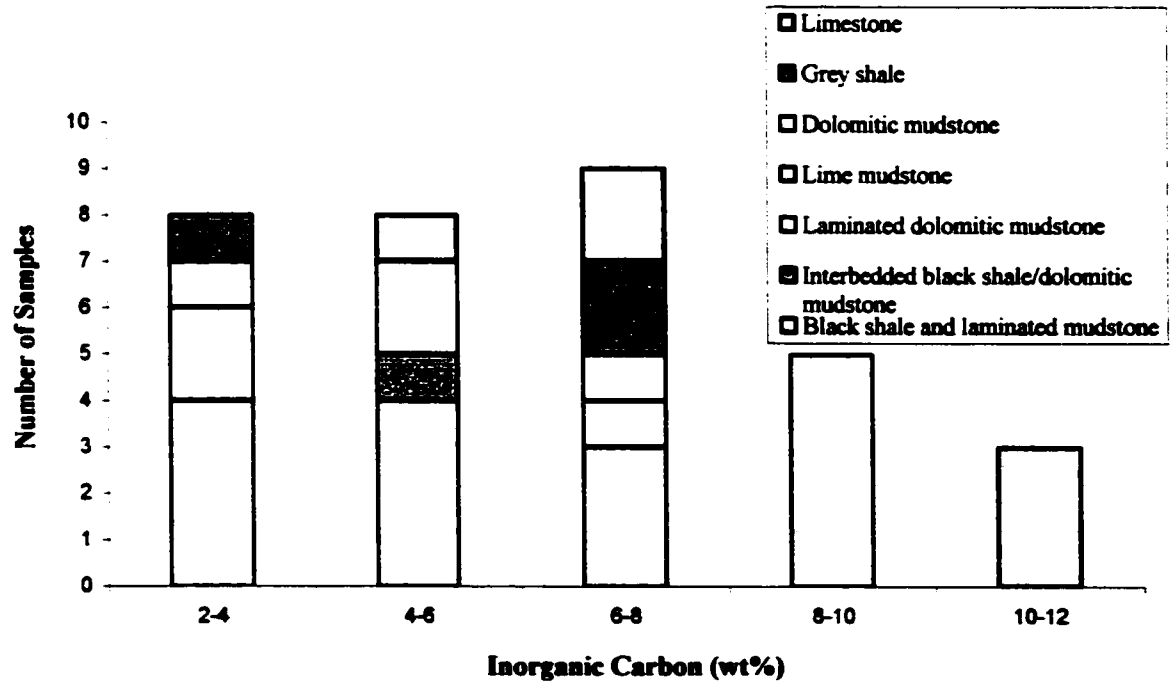

Figure 5. 15 Histogram of inorganic carbon distribution for different facies

locally low concentrations of organic matter. A linear regression of total organic carbon-sulphur data generally shows an positive intercept in this environment (Raiswell and Berner, 1985). However, the positive intercept is probably not a palaeoenvironmental indicator in iron-poor environments because most of the sulphur forms as organic sulphur (Bein et al., 1990). In such envionments, the slope of the regression line may distinguish a restricted to euxinic environment (slope < 0.2) from a restricted (0.2-2.0 ml/l O_2) to aerobic (>= 2.0 ml/l O_2) environment (slope > 0.2) (Minister et al., 1992).

5.2.2 Elemental analytical results

The results of sulphur and carbon analysis are listed in Appendix V.

5.2.2.1 Results of sulphur

The results of sulphur content of the whole rock samples are illustrated in Figure 5.14.

Only two dolomitic mudstone samples were measured. They exhibit very low sulphur values of 0 and 0.56 wt%. The sulphur content for lime mudstone (n = 4) is also low, ranging from 0 to 1.49 wt% with an average of 0.49 wt%. Although most of the limestones have low values of sulphur, two samples from well 3 have values as high as 1.93 and 4.03 wt%. The latter sample is a wackestone that contains a pyrite vein. The sulphur content of grey shales (n = 4) ranges from 0.6 to 1.16 wt%, and its average is 0.94 wt%. Higher sulphur values were obtained for laminated dolomitic mudstones (n = 12), ranging from 0.34 to 1.85 wt% with an average of 1.0 wt%.

Black shales and laminated mudstones (n = 22) have a wide range of sulphur content from 0.34 to 2.67 wt% with an average of 1.28 wt%. Values are relatively low in wells 1 and 4 compared to values in wells 5, 8, 9 and 12.

Samples of interbedded black shale/dolomitic mudstone (n = 6) have values of sulphur ranging from 1.19 to 3.09 wt% with the highest average value of 2.28 wt%.

Disregarding facies, samples from wells 3, 5, 8 and 9 have relatively high sulphur content.

5.2.2.2 Results of inorganic carbon

Results for the inorganic carbon content of whole rock samples are illustrated in Figure 5.15.

Iorganic carbon content does not differ significantly between different facies or between different wells within the basin. Limestones (n = 6) have the highest values, ranging from 4.4 to 11.8 wt% with an average of 8.8 wt%. Laminated dolomitic mudstones (n = 5) have the lowest values ranging from 2.1 to 7.2 wt% with an average of 4.3 wt% because of the low calcite content (5%). Only one value each is available for the dolomitic mudstone and the interbedded black shale/dolomitic mudstone; they are 6.36 wt% and 4.02 wt%, repectively. Two values of lime mudstones are 3.8 wt% and 10.06 wt%. Values of inorganic carbon for grey shales (n = 3) range from 3.39 to 7.78 wt% with an average of 5.91 wt%.

The concentration of inorganic carbon in samples from black shales and laminated mudstones (n = 16) have a large range from 2.6 to 10.7 wt% with an average of 6.29 wt%. The values are relatively high in wells 9 and 12 and relatively low in wells 4 and 8.

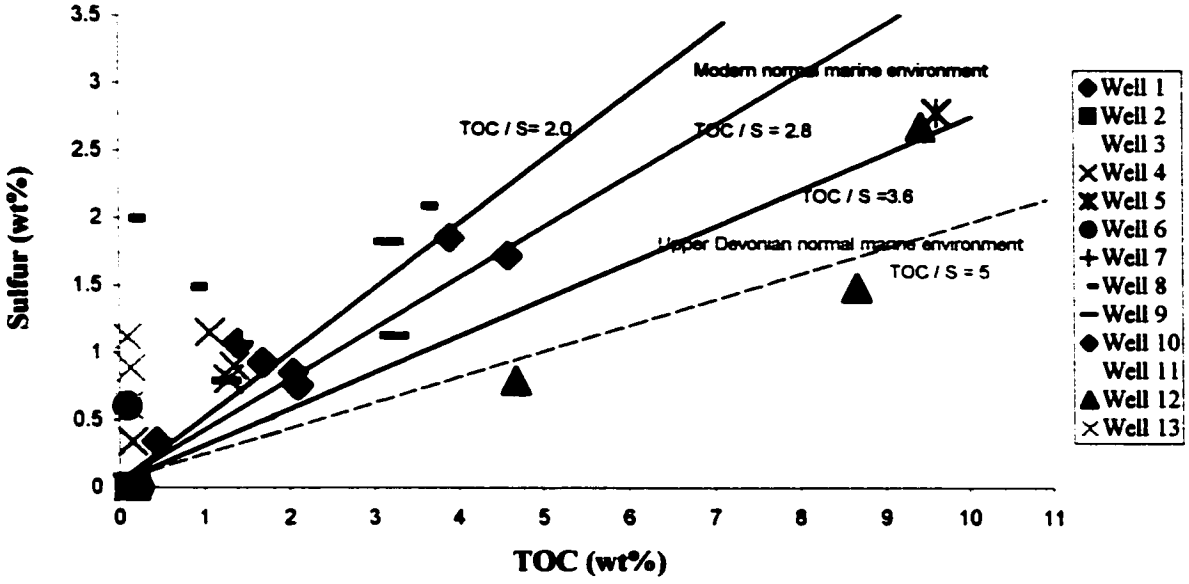

Figure 5.16 Plot of sulfur versus TOC in different wells(the three black lines are after Berner, 1982; the red line is after Berner and Raiswell, 1983.)

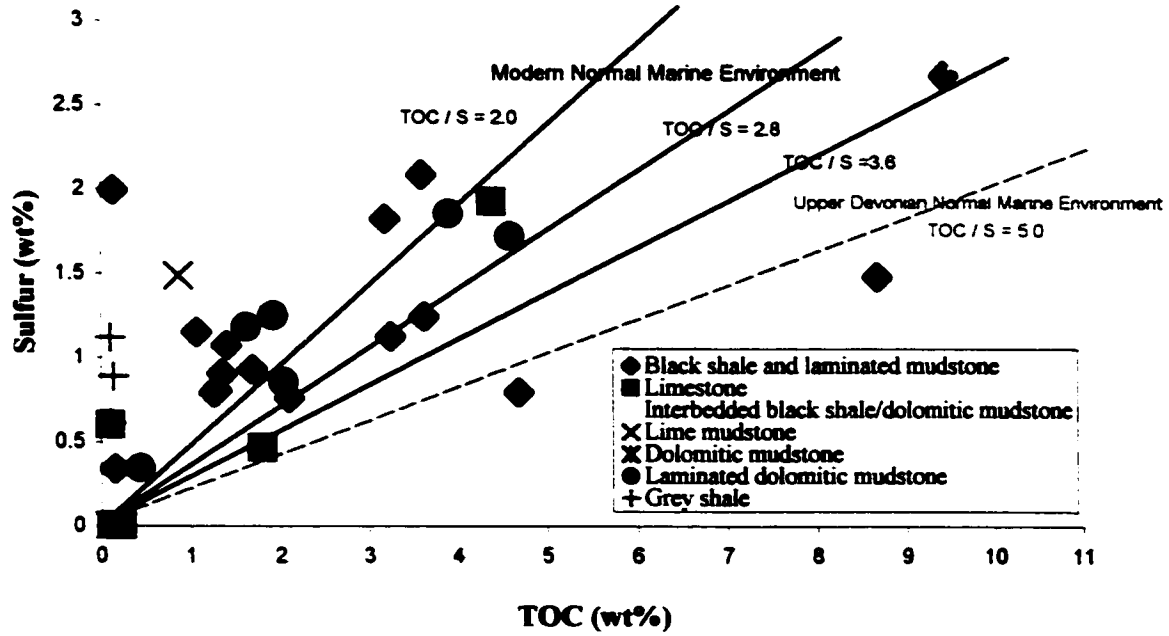

Figure 5.17 Plot of Sulfur versus TOC in Different Facies (the three black lines are after Berner, 1982; the red line is after Berner and Raiswell, 1983.)

5.2.2.3 Results of TOC/S ratio

In this study, the total content of pyrite sulphur was not measured. However, petrographic and SEM observations, as well as the light $\delta^{34}S$ values of the samples suggest that the sulphur in the rocks is mainly in pyrite. Thus, the value of sulphur in the whole rock is deemed to be the value of pyrite sulphur. The TOC/S ratios are illustrated in Figures 5.16 and 5.17 with respect of wells and facies. Using the secular curve from Berner and Raiswell (1983, Fig 5.13), a TOC/S value of 5 is considered to characterize the Upper Devonian normal marine environment.

Three samples from limestone, one sample from dolomitic mudstone and one sample from lime mudstone show negligble sulphur values. Because these values are too low, they will not be discussed here.

Two samples of black shale and laminated mudstone from well 12 have values that fall under the Upper Devonian line, with TOC/S values of 5.86 and 5.89, respectively.

Five samples have TOC/S values greater than 2.8 and less than 5. They include two black shales from wells 9 and 12, one limestone from well 3, one laminated mudstone from well 3 and one interbedded black shale/dolomitic mudstone from well 5.

Apart from the 12 samples mentioned above, the remaining 23 samples all have TOC/S values of less than 2.8.

5.3 Carbon and oxygen isotopes

5.3.1 Inorganic carbon and oxygen isotopes

5.3.1.1 Introduction

Isotopes of an element have the same number of protons but different numbers of neutrons. Thus, atoms of a particular element may have different masses. This difference in physical characteristics results in isotopic fractionation during phase transformation, mineral precipitation and diagenetic reactions (Hoefs, 1987).

Carbon has two stable isotopes: ^{12}C (98.89%) and ^{13}C (1.11%). Oxygen has three stable isotopes: ^{16}O (99.763%), ^{17}O (0.0375%) and ^{18}O (0.1905%). In practice, the relative abundances of ^{16}O and ^{18}O are usually measured. The isotopic composition of a mineral is expressed as the difference in the isotopic ratio relative to a standard substance (Anderson and Arthur, 1983). For example, $\delta^{18}O$ for a sample is determined by:

$$\delta^{18}O = \{[(^{18}O/^{16}O)_{sample} - (^{18}O/^{16}O)_{standard})] / (^{18}O/^{16}O)_{standard}\} \times 1000\ ‰$$

For carbonate minerals, oxygen and carbon are reported relative to the Vienna PeeDee Belemnite (VPDB) standard.

The major carbon isotope fractionation occurs as a result of the kinetic isotope effect during generation of organic matter. Newly formed organic matter becomes enriched in ^{12}C during incorporation of inorganic carbon into living matter via photosynthesis. However, little fractionation of carbon isotopes occurs during precipitation of carbonate minerals and their carbon isotopic composition is considered to reflect that of the precipitating water. With a constant terrestrial input of inorganic carbon, two processes can preferentially extract ^{12}C from the sea water and make it isotopically heavier: (1) increased rate of organic matter preservation in the sea; and, (2) increases in the rate of photosynthetic organic carbon production in the sea (Friedman and Chakraborty, 1997).

Internal recrystallization during diagenesis will result in little change in the abundance of ^{13}C. Degradation of organic matter during diagenesis releases CO_2 enriched

in ^{12}C and thus make the carbonates that precipitate in the pore water much lighter in isotopic compositon (Friedman and Schultz, 1994). On the other hand, bacterial fermentation of organic matter releases CO_2 enriched in ^{13}C making the precipitates from the pore water isotopically heavier (Friedman and Chakraborty, 1997). Because meteoric waters pass through soil that has ^{12}C-enriched CO_2 generated from oxidation of organic matter within the soil, carbonate sediments that recrystallize in near-surface meteoric waters tend to have depleted $\delta^{13}C$ values (Allen and Matthews, 1977).

Carbonate minerals are enriched in ^{18}O compared to the precipitating water and the degree of enrichment depends on the temperature of precipitation. Lower temperatures lead to increased enrichment (Friedman and Chakraborty, 1997). Oxygen isotopic composition of carbonates becomes progressively more depleted in ^{18}O with increasing depth during diagenesis because of recrystallization of minerals in elevated temperatures. Recrystallization of minerals in meteoric waters also results in ^{18}O depletion.

The $\delta^{13}C$ composition of a diagenetic dolomite is largely influenced by the composition of the original carbonate phase (Tucker and Wright, 1990) because of the relative insolubility of CO_2 in water (Land, 1980). Depleted $\delta^{13}C$ values are usually found in near-surface meteoric environments because of input from decaying organic matter on the Earth's surface (James and Choquette, 1984) and because of sulphate reduction at shallow burial depths (Machel, 1987; Hendry, 1993). Enriched values of $\delta^{13}C$ can be obtained at high temperatures by the fermentation of organic matter during methanogenesis (Irwin et al., 1977).

The $\delta^{18}O$ composition of dolomite is controlled mainly by temperature, the composition of the carbonate minerals being replaced, and the isotopic composition of

the precipitating water (Land, 1980; Tucker and Wright, 1990). This is especially true for diagenetic reactions with low water/rock ratios and during recrystallization. Depleted oxygen isotope values in diagenetic dolomites, usually interpreted to result from meteoric or heated water, can also result from sulphate reduction (Sass et al., 1991; Machel et al., 1995). The equilibrium $\delta^{18}O$ value for primary dolomite that is co-precipitated with calcite is 3 ± 1‰ at 25°C as proposed by Land (1980), however, it may range from 1‰ to 7‰ according to Tucker and Wright (1990).

For Upper Devonian marine calcite, a $\delta^{18}O$ composition ranging from -4‰ to -6‰ and a $\delta^{13}C$ composition ranging from 1.5‰ to 3.5‰ were suggested by Hurley & Lohmann (1989). Using $^{18}O_{dolomite\text{-}calcite} = 3 \pm 1‰$ (cf. Land, 1980), the oxygen isotopic composition of Upper Devonian marine dolomite is expected to be -1‰ to -3‰. Since equilibrium fractionation of ^{13}C between calcite and dolomite is negligible, both minerals will have nearly identical $\delta^{13}C$ compositions.

5.3.1.2 Inorganic carbon and oxygen isotopic results

The inorganic carbon and oxygen isotopic results for calcite and dolomite from whole rock samples are listed in Appendix VI and shown in Figures 5.18 and 5.19.

Since no values of specific phases of calcite and dolomite were measured, the results are discussed with respect to facies.

1. Black shales and laminated mudstones

(1) Calcite: Calcite in these facies is dominantly in the form of matrix, non-ferroan mosaic cement, sparry calcite cement and minor ferroan cements. Except for one sample from well 4 that contains numerous calcareous spheres filled by ferroan

calcite cement and shows rather depleted values for both $\delta^{13}C$ (-2.13‰) and $\delta^{18}O$ (-11.73‰), all others fall in the range from -7.4 to -5.71‰ for $\delta^{18}O$ with an mean of -6.41‰ ± 0.54‰ (standard deviation - S) and from -0.08 to 3.47‰ for $\delta^{13}C$ with an mean of 1.61‰ ± 1.25‰. If the value of the sample from well 4 is included, the S for $\delta^{18}O$ is 1.51‰, which is anomalous being about three times the standard deviation of 0.54‰. Two samples from well 9 show relatively depleted values for $\delta^{18}O$, whereas one sample from well 5 and three samples from well 12 that contain a small amount of ferroan cement show relatively depleted values for $\delta^{13}C$. The rest of the samples show values close to the postulated values for carbonates deposited during Upper Devonian.

(2) Dolomite: Dolomite in this facies is mainly Type I matrix dolomite as well as some saddle dolomite and vein-associated dolomite. All the samples show depleted $\delta^{18}O$ values ranging from -6.55 to -9.67‰ with a mean of -7.64‰ ± 1.1‰. Five samples from wells 1 and 9 show $\delta^{13}C$ values consistent with the Upper Devonian dolomite while those from wells 4, 5, 9 and 12 show depleted $\delta^{13}C$ values ranging from - 0.95 to 1.12‰. The mean of the $\delta^{13}C$ is 1.34‰ ± 1.4 ‰.

2. Lime mudstone

Only one sample from lime mudstone from well 4 was measured for calcite. It contains both ferroan and non-ferroan calcite cements. The sample has depleted $\delta^{13}C$ value of -0.08‰ and $\delta^{18}O$ value of -7.67‰.

3. Dolomitic mudstone

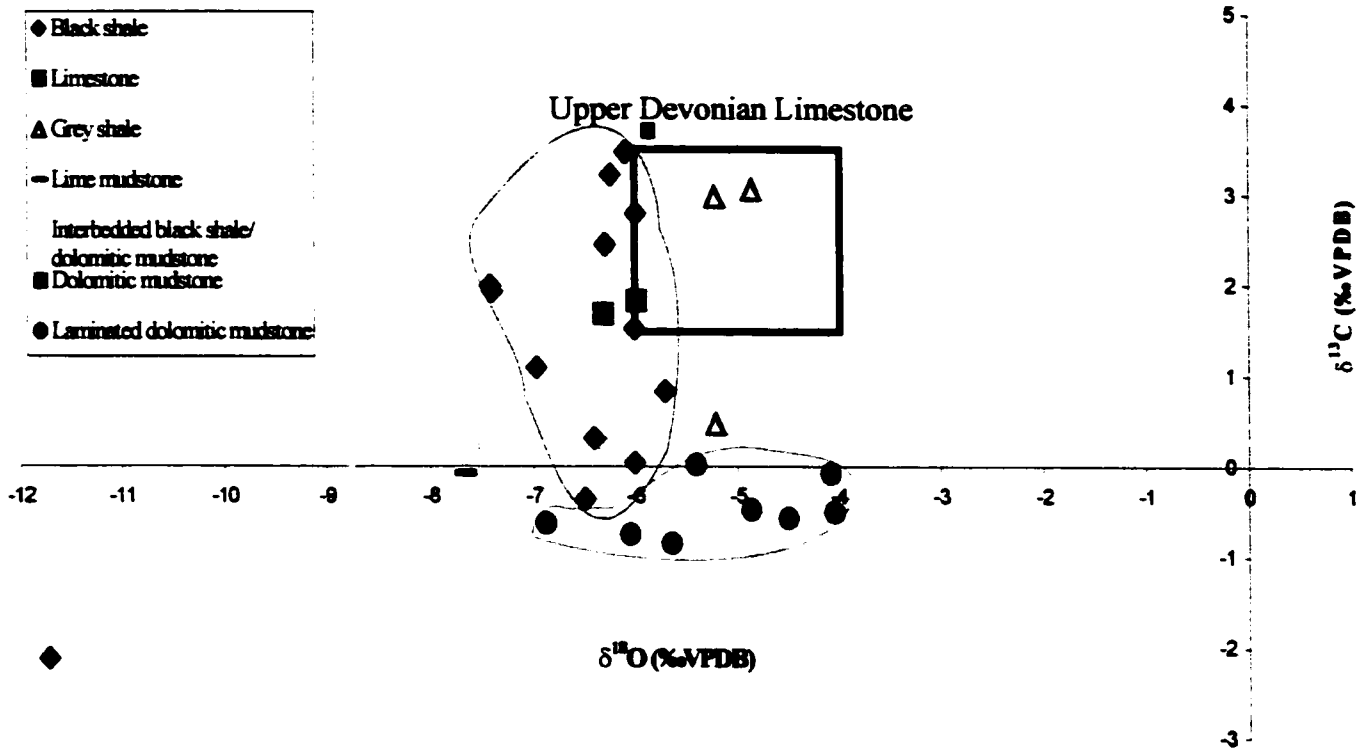

Figure 5.18 Plot of $\delta^{13}C$ versus $\delta^{18}O$ for calcite

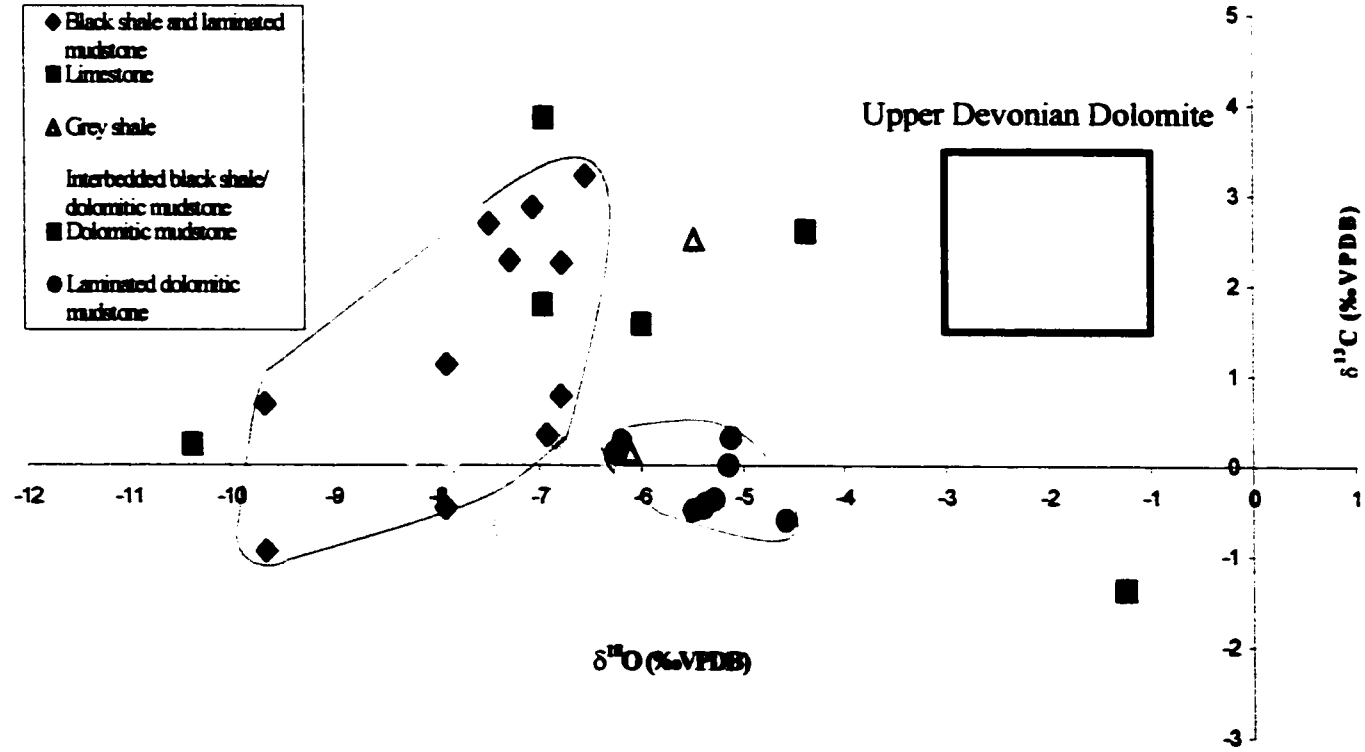

Figure 5.19 Plot of $\delta^{13}C$ versus $\delta^{18}O$ for dolomite

(1) Calcite: Both ferroan and non-ferroan mosaic calcite cement and sparry calcite cement are found in this facies. However, only one sample was measured and it showed slightly enriched $\delta^{13}C$ values of 3.71‰. Its $\delta^{18}O$ value falls within the Upper Devonian seawater range.

(2) Dolomite: Type II matrix dolomite is characteristic of this facies and two samples were measured. One sample shows lightly depleted $\delta^{18}O$ value of -4.37‰ with the $\delta^{13}C$ value (2.6‰) falling in the Upper Devonian dolomite compositional range. The other sample shows a fairly depleted $\delta^{18}O$ value of -10.39‰ and a $\delta^{13}C$ value of 0.23‰.

4. Interbedded black shale/dolomitic mudstone

(1) Calcite: This facies has almost all types of calcite cement, both non-ferroan and ferroan. The isotopic results of whole rock analysis yield the most depleted values of all of the facies. The $\delta^{18}O$ values range from -9.06‰ to -6.29‰ with a mean of -7.79‰ ± 1.0‰ and $\delta^{13}C$ values range from -0.91‰ to 0.2‰ with a mean of -0.12‰ ± 0.48‰.

(2) Dolomite: This facies contains both Type I and Type II matrix dolomite as well as saddle dolomite. Values of $\delta^{18}O$ and $\delta^{13}C$ are strongly depleted compared to the values of Upper Devonian dolomite. The $\delta^{18}O$ values range from -8.25‰ to -6.35‰ with a mean of -7.5‰ ± 0.8‰ and the $\delta^{13}C$ values range from -0.67‰ to 0.23‰ with a mean of -0.18‰ ± 0.34‰.

5. Laminated dolomitic mudstone

(1) Calcite: Calcite in this facies only accounts for 5% of the whole rock and exists as matrix. Most of the samples show $\delta^{18}O$ values that match the Upper Devonian

seawater composition except for one that has a depleted value of -6.88‰. The mean is -5.19‰ ± 1.0‰. However, their $\delta^{13}C$ gives depleted values ranging from -0.85‰ to 0.02‰ with a mean of -0.48‰ ± 0.3‰.

(2) Dolomite: Type III matrix dolomite characterizes this facies. The values of $\delta^{18}O$ and $\delta^{13}C$ are depleted. The $\delta^{18}O$ values range from -6.27‰ to -4.58‰ with a mean of -5.43‰ ± 0.53‰ and the $\delta^{13}C$ values range from -0.6‰ to 0.31‰ with a mean of -0.18‰ ± 0.36‰.

6. Grey shale

(1) Calcite: Calcite in this facies includes very fine-grained calcite in the matrix and little ferroan and non-ferroan calcite cement in the fossils. Two samples from well 13 have values falling in the Upper Devonian limestone composition whereas the third sample from well 3 has a slightly depleted $\delta^{13}C$ value of 0.47‰.

(2) Dolomite: Dolomite in this facies is too fine-grained to be classified. It accounts for 15% of the whole rock. Only two samples were measured. The sample from well 13 has a depleted $\delta^{18}O$ value of -5.48‰ whereas the sample from well 3 has depleted values for both $\delta^{18}O$ of -6.11‰ and $\delta^{13}C$ of 0.15‰.

5.3.2 Organic carbon isotopes

5.3.2.1 Introduction

In the modern environment, carbon in terrestrial plants is depleted in ^{13}C compared in marine plants (Wickman, 1952; Craig, 1953). Marine plants have $\delta^{13}C$ values of around -13 to -17‰ whereas terrestrial plants have values around -24 to -26‰. The explanation of Park and Epstein (1960) is that terrestrial plants utilize more CO_2 from the

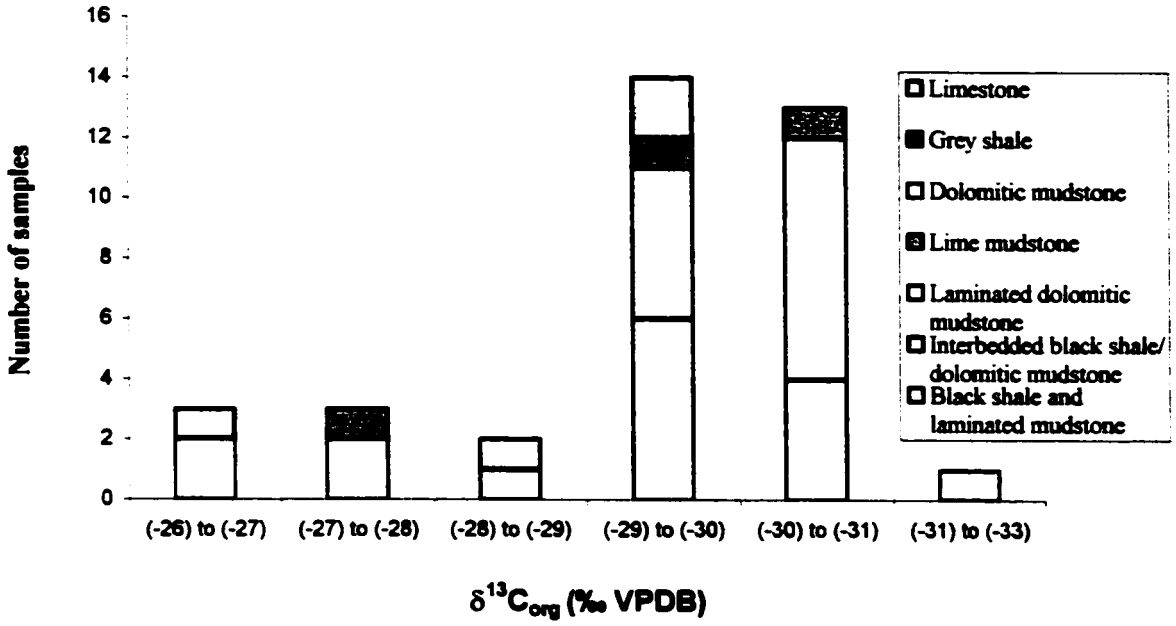

Figure 5.20 Histogram of organic carbon isotopes distribution for different facies

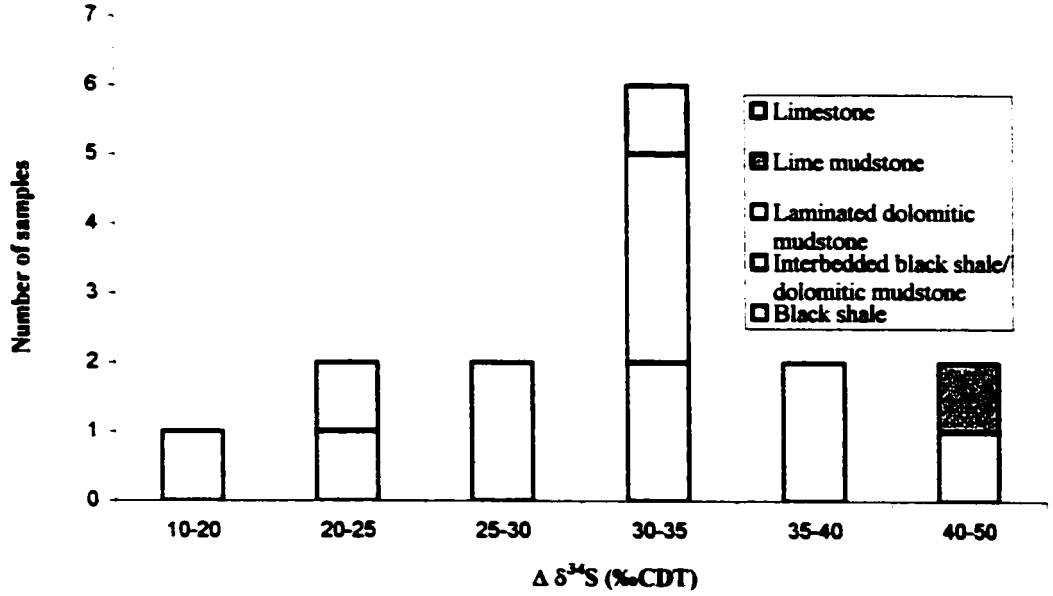

Figure 5. 21 Histogram of $\Delta\ \delta^{34}S$ ($\delta^{34}S_{sulfate}$-$\delta^{34}S_{pyrite}$) distribution for different facies. The $\delta^{34}S_{sulfate}$ vaule for Upper Devonian is adapted after Machel, 1986.

atmosphere that is leaner in ^{13}C than the bicarbonate of sea water utilized by marine plants. A kinetic effect causes a slight depletion of ^{13}C in plants that obtain their carbon from the atmosphere compared to plants that obtain ^{13}C from seawater. Deuser and Degens (1967) have shown that plants growing in river and lake waters with slightly acid pH utilize dissolved CO_2 with a $\delta^{13}C$ of -7‰, whereas plants growing in sea water with a basic pH are utilizing HCO_3^- with a $\delta^{13}C$ of 0‰.

The above theory is supported by numerous studies. For example, Tan and Vilks (1987) studied sediments in Groswater Bay and Goose Bay in southeastern Labrador. The $\delta^{13}C$ values of the terrestrial organic carbon range from -28.4‰ to -26.9‰ and for marine muds are -21.4‰. A study by Sackett and Thompson (1963) found that $\delta^{13}C$ values of organic carbon in some river sediments ranged from –24.3 to –28.3‰ with an average of –26.2‰ while in an open marine depositional environment they ranged from -19 to -21‰. However, other factors can also affect the organic carbon isotopes in marine organic matter. They include water temperatures (Fontugne et al., 1991), organic matter type (Peters et al.,1978), diagenesis (McArthur et al., 1992), redox conditions (Jasper and Hates, 1994) and surface water productivity (Aravena et al., 1992).

5.3.2.2 Organic carbon isotopic results

The values of $\delta^{13}C_{org}$ in this study are very negative. They are listed in Appendix VII and illustrated in Figure 5.20.

Dolomitic mudstones show the least depleted values of -26.49‰ and -26.71‰. Interbedded black shale/dolomitic mudstones show $\delta^{13}C_{org}$ values ranging from -29.99 to -28.72‰ with an average of -29.46‰. The black shale values cover a wide range

between -30.91‰ and -27.85‰ with an average of -29.56‰. Only one sample was measured for lime mudstone and its value is -30.54‰. Two values were measured for grey shales. The value for the sample in well 3 is -29.68‰ and for the sample in well 13 is -27.66‰. Laminated dolomitic mudstones have the lowest values ranging from -32.54‰ to -30.45‰ with an average of -31‰.

5.4 Sulphur isotopes

5.4.1 Introduction

Sulphur in sediments can exist as sulphides, sulphates, elemental sulphur (S^0, which usually occurs only in trace amounts) and organic sulphur (Westgate and Anderson, 1982). Isotopes of sulphur differ in their chemical properties and are fractionated in biological and geological processes (Thode et al., 1953). Sulphur has four stable isotopes: ^{32}S (95.02%), ^{33}S (0.75%), ^{34}S (4.21%) and ^{36}S (0.02%) (Hoefs, 1987). Most sulphur isotope studies utilize variations in the ratio of the two more abundant isotopes: ^{32}S and ^{34}S. The δ value of $^{34}S/^{32}S$ ratio is calculated relative to the sulphur occurring as troilite in the Canyon Diablo meteorite (CDT) by the following formula:

$$\delta^{34}S = [^{34}S/^{32}S_{(sample)} - {}^{34}S/^{32}S_{(standard)}]/[^{34}S/^{32}S_{(standard)}] \times 1000‰$$

Sulphate reduction can occur through two processes: bacterial sulphate reduction (BSR) and thermochemical sulphate reduction (TSR). BSR usually takes place with the mediation of microbes in low-temperature diagenetic environments ($0 < T < 60\text{-}80°C$), whereas TSR takes place by inorganic (abiological) mediation in high-temperature diagenetic environments ($80\text{-}100 < T < 150\text{-}200°C$) (Machel et al., 1995).

In an anoxic environment sulphate is reduced to sulphide by bacteria that discriminates against the heavy sulphur isotope. Thus, the formed sulphides are enriched in ^{32}S relative to seawater sulphate. The process is illustrated schematically below:

$$^{34}SO_4^{2-} + \text{bacteria} \rightarrow H_2{}^{32}S + \text{metal} \rightarrow \text{metallic sulphide}$$

The sulphur isotope fractionation between pyrite and H_2S is insignificant and usually < 10‰ (Fry et al., 1986; 1988; Schwarcz and Burnie, 1973; Rees, 1973). The isotopic ratios of pyrite or H_2S that originate from BSR can be - 45 ± 20 ‰ lighter than source sulphate at < 25°C. Above this temperature, the values are unclear because most sulphur isotopic results have been obtained from modern shallow-burial environments. Shallow-burial BSR occurs in the top few metres below the sediment-water interface whereas deep-burial BSR occurs within the sediment at temperatures up to 80°C and depths up to 3 km (Painter et al., 1999).

The kinetic sulphur isotope fractionation during TSR is predicted to decrease from ~ 20‰ at 100°C to ~10‰ at 200°C, and to further decrease with increasing temperature (Harrison and Thode, 1957; Husain, 1967; Husain and Krouse, 1978; Kiyosu, 1980; Kiyosu and Krouse, 1990). In real systems, the fractionation factors vary between -10 to 0‰ (Ohmoto et al., 1990). The major conditions that have to be met for TSR to occur are: (1) wet gas in the system; (2) presence of dissolved sulphate; and, (3) temperatures > 100-135°C (Orr, 1977; Machel, 1989).

Two major environmental factors control the degree of fractionation of sulphur isotopes during sulphate reduction. They are: (1) "open system" or "closed system"; and, (2) "anoxic system" or "oxic system" (Kajiwara et al., 1997).

In an open system, the sulphate reservoir is infinite and the rate of sulphate supply largely exceeds the sulphate-reduction rate. The isotopic composition of the sulphate stays unchanged and thus the extent of isotopic fractionation in pyrite with respect to the sulphate is expected to remain constant.

In partially or completely closed environments, progressive reduction will cause a systematic increase in the $\delta^{34}S$ value of the remaining sulphate. Accordingly, H_2S and pyrite formed during progressive reduction of sulphate will become progressively enriched in ^{34}S. In a closed system, little or no isotope fractionation between initial sulphate and pyrite may occur for both BSR and TSR (Nakai and Jensen, 1964; Rees, 1973). In this case, BSR and TSR could not be distinguished by measuring the sulphur isotopic ratios.

In an anoxic system, where no aerobic sulphur-oxidizing bacteria survive, the extent of isotope fractionation of pyrite with respect to the initial source sulphate remains constant if the system is open. However, the extent of fractionation can be zero if the system is closed.

In an oxic system, where aerobic bacteria is active, the initial or prior pyrite that formed as the result of initial sulfate reduction is almost always unexceptionably reoxidized at or near the sediment-water interface to secondary sulphate with a similar isotopic composition as the initial pyrite. The secondary sulphate is then used in a subsequent sulphate reduction and the resultant secondary pyrite will have a more depleted isotope composition than initial pyrite with respect to the initial sulphate (Kajiwara et al., 1997).

5.4.2 Sulphur isotope results

The results of the sulphur isotopic analysis of the rock samples are listed in Appendix VIII, and the $\Delta\ \delta^{34}S$ ($\delta^{34}S_{\text{contemporaneous seawater sulphate}} - \delta^{34}S_{\text{sulphide}}$) values are illustrated in Figure 5.21. The value for $\delta^{34}S$ of sulphates in Upper Devonian oceans was estimated as 25‰ (Machel, 1986).

Three samples were measured for laminated dolomitic mudstones. The $\Delta\ \delta^{34}S$ values range from 30.1‰ to 32.7‰. One lime mudstone has a $\Delta\ \delta^{34}S$ value of 40.8‰.

The black shale facies has a wide range of $\Delta\ \delta^{34}S$ values from 12.7‰ to 47.8‰ with most of them > 25‰. The lowest value appears in well 1 and the highest value is from well 8. Only one sample was measured for the interbedded black shale/dolomitic mudstone facies and its $\Delta\ \delta^{34}S$ value is 23.4‰.

CHAPTER VI

DISCUSSION AND INTERPRETATION

6.1 Diagenesis

Interpretation of the diagenetic history of the Duvernay Formation is based on the preceding stratigraphic, petrographic and geochemical results. The products and timing of the diagenetic events are illustrated in Figure 6.1.

6.1.1 Calcite Cementation

6.1.1.1 Inferences from inorganic carbon and oxygen isotopic results

As illustrated in Figure 5.18, samples from dolomitic mudstones, limestones, some black shales, laminated mudstones, and grey shales have carbon isotopes similar to that of Upper Devonian seawater. Depleted $\delta^{13}C$ values are found in samples from interbedded black shale/dolomitic mudstones, lime mudstones, laminated dolomitic mudstones and some samples from black shales and grey shales.

Calcite in laminated dolomitic mudstones is non-ferroan, only accounts for 5% of the whole rock, and is too fine-grained to be identified. The depleted $\delta^{13}C$ values indicate that the calcite is precipitated from ^{12}C-enriched water. However, the $\delta^{18}O$ values of samples from this facies are consistent with the Upper Devonian seawater. This excludes the possibility that the calcite was precipitated from the meteoric water that is both ^{12}C and ^{16}O-enriched. The origin of the light water is not clear, but it is probably pore water enriched in ^{12}C resulted from degradation of organic matter.

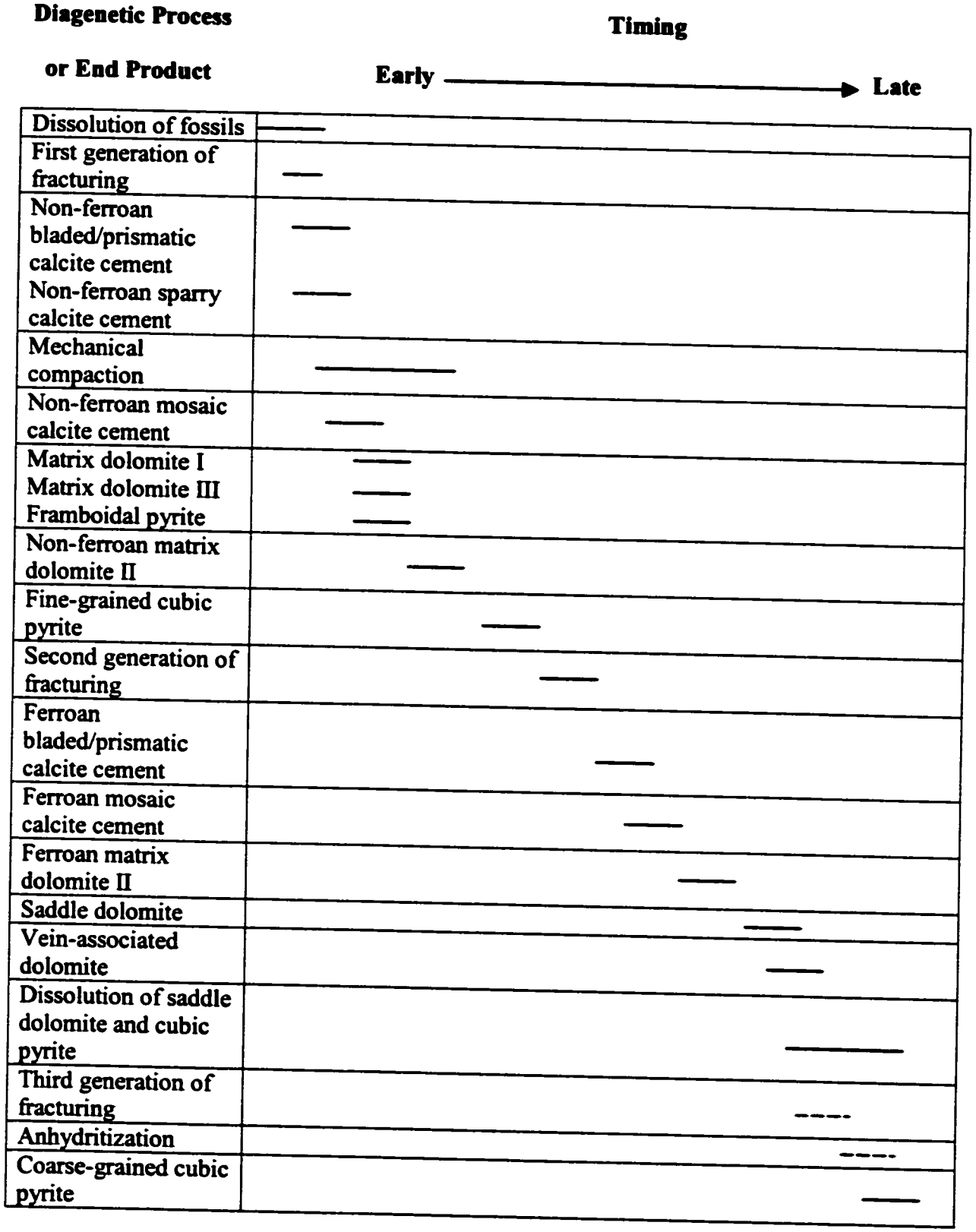

Fig 6.1 Paragenetic sequence of the Duvernay Formation

The depleted $\delta^{13}C$ values of all of the other facies are accompanied by the occurence of ferroan calcite cement except for laminated dolomitic mudstone. Increased content of ferroan calcite cement in the rocks correlates with more depleted $\delta^{13}C$ values. The black shales and laminated mudstones have some samples that only contain non-ferroan calcite cement and some samples that contain both non-ferroan calcite cement and ferroan calcite cement. Larger standard deviation of 1.25‰ of $\delta^{13}C$ values for black shale and laminated mudstones facies compared to other facies demontrates the carbon isotope fractionation between non-ferroan calcite cement and ferroan calcite cement. This may indicate that the ferroan calcite cement was precipitated from both ^{12}C and iron-enriched fluids.

Some samples from black shales, laminated mudstones, lime mudstones and interbedded black shale/dolomitic mudstones show depleted $\delta^{18}O$ values when compared to the oxygen isotopes of Upper Devonian seawater. As in the case of $\delta^{13}C$, increased content of ferroan calcite cement in the rocks correlates with more depleted $\delta^{18}O$ values. This may indicate that ferroan calcite cement was also precipitated from ^{16}O-enriched fluids. Conventionally, these light $\delta^{18}O$ values have been explained as being caused by carbonate formation at elevated temperature and / or involving meteoric water. However, restricted circulation of ground water is indicated by the well preserved organic matter in the subsurface. This restriction is probably due to the low permeability of the organic-rich rocks. Moreover, the samples with the lightest $\delta^{18}O$ values and those with the heaviest values have the same degree of thermal maturity, and hence formed in similar temperatures. Low $\delta^{18}O$ values caused by elevated temperature can thus be excluded. Sass et al. (1991) suggested that a light oxygen composition of diagenetic calcite can

result from the decomposition of organic matter in the bacterial sulphate-reducing zone. Therefore, the depleted $\delta^{18}O$ values of the calcite could result from precipitation in ^{12}C, ^{16}O and iron enriched fluids, precipitation in bacterial sulphate-reducing zone, or a combination of both factors.

6.1.1.2 Mosaic Calcite Cement

Ferroan mosaic calcite cement postdates the non-ferroan mosaic calcite cement according to both the petrographic (Plate C-4) and isotopic evidence described above. The volumetrically minor ferroan calcite cement in black shale compared to that in interbedded black shale/dolomitic mudstone, results in the black shale facies having a higher $\delta^{18}O$ values than the interbedded black shale/dolomitic mudstone facies. The most depleted $\delta^{18}O$ value is exhibited by a black shale sample from well 4 and its depletion is caused by large numbers of calcareous spheres that are filled with ferroan calcite cement. The similarity in the isotopic composition of non-ferroan mosaic calcite cement with that of Upper Devonian seawater indicates that this cement precipitated relatively early in the diagenetic sequence. The ferroan cement precipitated from a later iron-enriched fluid and was probably formed in an intermediate to deep burial environment.

6.1.1.3 Sparry Calcite Cement

In the laminated dolomitic mudstone and grey shale facies, the main form of calcite cement is sparry calcite cement. The least depleted $\delta^{18}O$ values were obtained in samples from these two facies, indicating that they were not affected by the later iron-enriched

fluids. Thus this kind of cement predates the ferroan calcite cement and represents an early diagenetic event.

6.1.1.4 Bladed/Prismatic Calcite Cement

Bladed/prismatic cement is rare in the samples used in this study, and thus isotopic evidence is hard to obtain from the results of whole rock samples. According to Adam (2000), fairly depleted $\delta^{18}O$ values of non-ferroan cement (-9.48 to -9.43‰) and ferroan cement (-10.53‰) were measured for this kind of calcite cement. Petrographic observations suggest that the non-ferroan cement is one of the earliest phases that precipitated in the Duvernay Formation. Non-ferroan cement was probably formed in the bacterial sulphate-reducing zone. Ferroan cements were affected by later iron-enriched fluids and thus represent an intermediate to deep burial diagenetic event.

6.1.2 Dolomitization

6.1.2.1 Matrix Dolomite I

Type I matrix dolomite is found mainly in black shales, laminated mudstones, lime mudstones, interbedded black shale/dolomitic mudstones and grey shales. It represents a relatively early diagenetic event compared to other dolomites. The fact that matrix dolomite I replaces both sparry calcite cement (Plate C-6) and mosaic calcite cement (Plate D-1) in fossils indicates that this dolomite postdates both of these calcite cement. Because most of the facies mentioned above do not contain only Type I matrix dolomite, the isotopic values of these samples are not indicators of any specific dolomite. However, some samples show sightly depleted $\delta^{18}O$ values and $\delta^{13}C$ values, and fall in the Upper

Devonian dolomite composition range (Fig 5.19). For example, one sample from the dolomitic mudstone shows isotopic values of - 4.37‰ for $\delta^{18}O$ and 2.6‰ for $\delta^{13}C$. Unlike other dolomitic mudstones that are dominated by Matrix II dolomite, this sample from the top of well 7 has only non-ferroan dolomite. The average grain size of the dolomite is slightly bigger than Type I matrix dolomite found in the other facies and may be considered to be a transition from Type I matrix dolomite to Type II matrix dolomite.

The fine-grained nature of Type I matrix dolomite and its occurrence in organic-rich sediments indicate that it is probably organogenic. Organogenic dolomite has a significant proportion of its carbon derived from the degradation of organic matter during bacterial sulphate reduction and from the dissolution of calcite (Compton, 1988). Differing amounts of carbon are incorporated into the dolomite from the different bacterial zones of organodiagenesis, from seawater bicarbonate, and from dissolution of precursor carbonates, resulting in a wide range for $\delta^{13}C$ values for organogenic dolomites. Sulphate-reduction dolomites are always depleted in $\delta^{13}C$ to varying degrees relative to that of ambient seawater because of the addition to pore fluids of ^{12}C-enriched CO_2, derived mainly from bacterially-degraded organic matter (Mazzullo, 2000). In the Duvernay Formation, this kind of dolomite has a very similar $\delta^{13}C$ distribution to that of the precursor calcite and the range of $\delta^{13}C$ values of the dolomite is only approximately 0.5‰ lower than the calcite, particularly in black shales and laminated mudstones (Figs 5.18 and 5.19). This may indicate that the carbon that they retain is mainly from the precursor calcite dissolution. The 0.5‰ depletion may indicate that some ^{12}C-enriched CO_2, derived from bacterially degraded organic matter, was incorporated into the dolomite.

The $\delta^{18}O$ values of the samples that contain Type I matrix dolomite are depleted relative to their precursor calcite. As mentioned before, slight $\delta^{18}O$ depletions are expected in authigenic carbonates formed as byproducts of sulphate reduction (Sass et al,1991). Moreover, such depletions are significant only if the system is closed during sulphate reduction (Machel et al, 1995). From the sulphur isotopic results discussed later, the Duvernay Formation was formed in partially-closed to open environments. Therefore, the light oxygen isotopes of Type I matrix dolomite are probably the result of sulphate reduction.

6.1.2.2 Matrix Dolomite II

Type II matrix dolomite exists mainly in dolomitic mudstones and interbedded black shale/dolomitic mudstones. Because it is the only dolomite that exists in dolomitic mudstone, the isotopic values can be used to indicate its diagenetic character. However, only one sample was measured and this sample was dominated by ferroan dolomite. This sample has rather depleted values of -10.39‰ for $\delta^{18}O$ and 0.23‰ for $\delta^{13}C$ compared to the values of its precursor calcite, which are -5.87‰ for $\delta^{18}O$ and 3.71‰ for $\delta^{13}C$. This indicates that the ferroan Type II dolomite was precipitated in a light carbon and oxygen water that was enriched in iron or formed at elevated temperatures. Thus it may represent an intermediate to deep burial diagenetic origin. Petrographic observation shows that ferroan Type II dolomite postdates non-ferroan Type II matrix dolomite (Plate C-2).

6.1.2.3 Matrix Dolomite III

Type III matrix dolomite occurs only in laminated dolomitic mudstones. It has a very similar isotopic composition to the calcite that accompanies it. This may indicate that the carbon that the dolomite used during its precipitation came from dissolution of the calcite. The average oxygen isotopic value of this kind of dolomite is the highest of all of the dolomites in the Duvernay Formation. This excludes the possibility that Type III matrix dolomite formed at an elevated temperature, which would make its oxygen isotopic value lighter. Thus, type III matrix dolomite probably formed during early diagenesis.

6.1.2.4 Saddle Dolomite

There are three types of dolomite in the black shales and laminated mudstones facies: Type I matrix dolomite, saddle dolomite and vein-associated dolomite. The large standard deviation of 1.4‰ of $\delta^{13}C$ values indicates carbon isotope fractionation among these dolomite. As mentioned above, Type I matrix dolomite has only slightly depleted isotopic values. Therefore, the substantially depleted isotopic values for some black shale samples may be the result of the existence of saddle dolomite and vein-associated dolomite. The depleted values are probably the result of elevated temperatures in deep burial environments. In thin section, saddle dolomite fills the middle of veins and replaces non-ferroan as well as ferroan calcite cements. Thus, a deep burial origin is proposed for the saddle dolomite.

6.1.2.5 Vein-associated Dolomite

Vein-asssociated dolomite replaces saddle dolomite along crystal boundaries and, therefore, postdates saddle dolomite. It is thus inferred to be of deep burial origin also.

6.1.3 Pyritization

In the Duvernay Formation, both framboidal pyrite and crystalline pyrite exist. They selectively replace calcite cements as well as matrix. In sedimentary rocks, framboidal pyrites are generally considered syngenetic (e.g. Degens et al., 1972) or early diagenetic products (e.g. Love and Amstuzt, 1966). Fine-grained pyrite spheres are not common but do occur in almost all the facies. Fine-grained cubic pyrite has diameters ranging from 2 to 10 μm and some of them are dissolved along the edge. Pyrite spheres and fine-grained cubic pyrite are probably formed at a later diagenetic stage than framboidal pyrite. Coarse-grained cubic pyrite is rare. It replaces both calcite cement and vein-associated dololmite in veins, as well as in the matrix. It is of deep burial origin.

6.1.4 Anhydritization

Vein anhydrite is the final fracture-filling event, following the calcite veining events as shown by cross-cutting relationships (Adam, 2000). This anhydrite precipitated after Type III matrix dolomite and represents a deep diagenetic event.

6.1.5 Dissolution

Dissolution of metastable fossil shells, possibly affected by the infiltration of meteoric water, leaves the voids for later mosaic calcite cementation (Plate C-2). Since

the earliest calcite cement is of early diagenetic origin, this kind of dissolution accordingly represents an early diagenetic event.

On the other hand, dissolution of dolomite (Plate E-3), pyrite (Plate F-1) and quartz (Plate F-6) may occur as the result of interaction with diagenetic fluids. It is of deep burial diagenetic origin.

6.2 Thermal maturity

As illustrated in Figures 5.9 and 5.10, samples from wells 3, 10, 11, 12 and 13 are immature with T_{max} values of less than 435°C and PI values of less than 0.13. Several samples from wells 10, 11 and 13 have PI values that are greater than 0.1. This may indicate that these samples have just become mature. Samples from wells 1 and 7 have T_{max} values ranging from 440 to 445°C and PI values ranging from 0.07 to 0.14. This indicates that the samples just reached the top oil window. Samples from well 6 are mature with T_{max} values ranging from 442 to 456°C and PI values ranging from 0.13 to 0.40. Samples from wells 8 and 9 are mature to overmature with T_{max} values between 445 to 490°C and PI data between 0.2 and 0.7. The T_{max} values and PI values for wells 2, 4 and 5 do not match each other, because their PI values always indicate higher degrees of maturity than T_{max} values. Assuming that the T_{max} values are affected by the type of organic matter, the PI values are chosen to be the index for the samples in these wells. Samples from well 2 have PI values ranging from 0.23 to 0.67, which indicate that they are mature to overmature. Samples from well 5 have values ranging from 0.09 to 0.66 and thus are immature to overmature. Overmature samples appear at the bottom of this

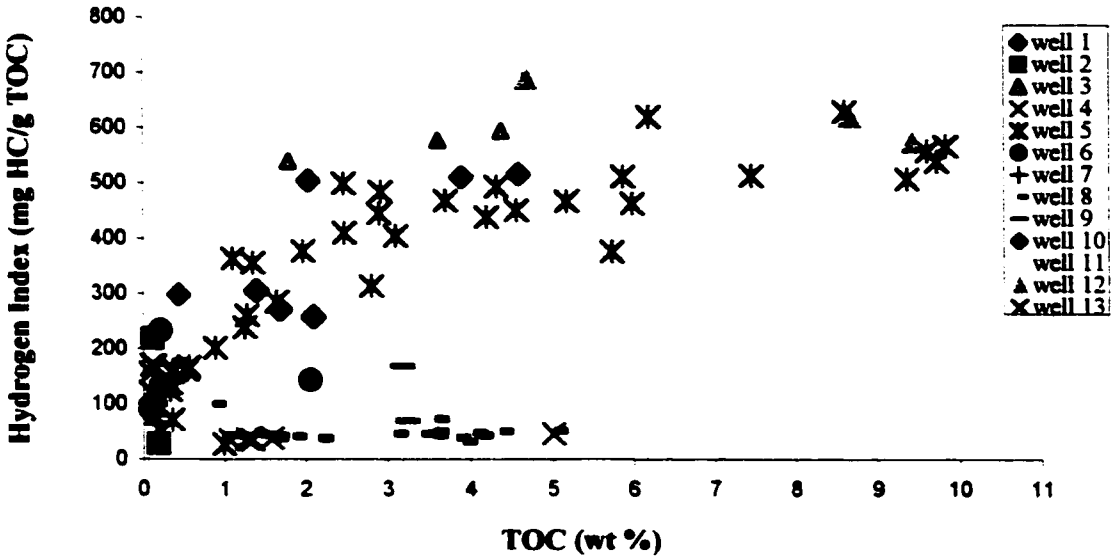

Figure 6. 2 Hydrogen Index versus TOC in different wells

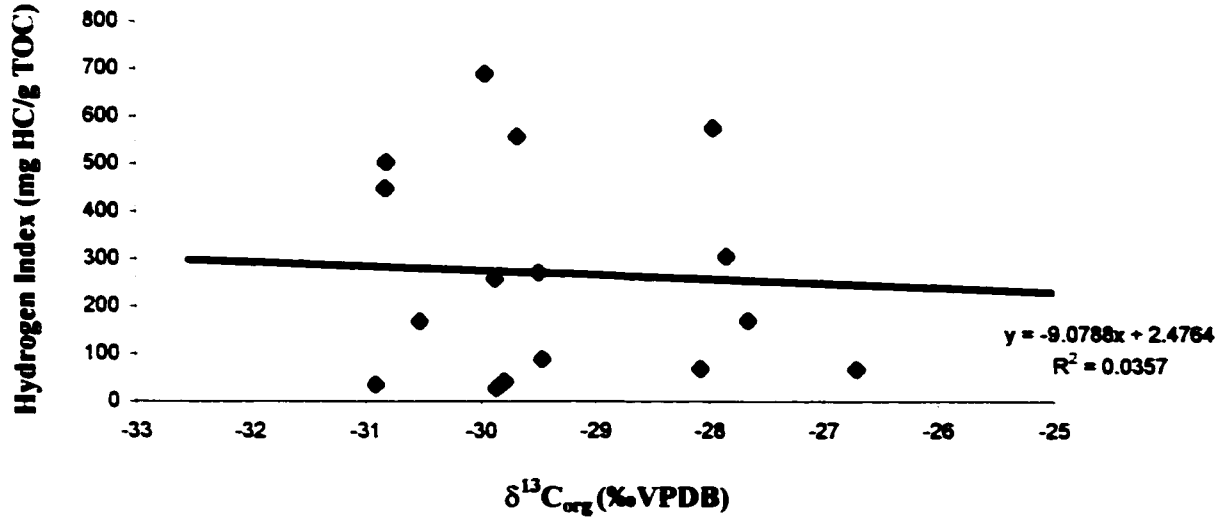

Figure 6.3 Plot of Hydrogen Index versus organic carbon isotope

well. A range of PI values from 0.41 to 0.5 for samples from well 4 indicates that they are overmature.

Wells 2, 4, 5, 8 and 9 show maturation different from the previous works by Stoakes and Creaney (1984) as shown in Fig 1.1. On the original map, samples from well 5 are immature; from well 2 are immature to mature; from wells 4 and 8 are mature; from well 9 are overmature. However, from the results in my study, samples from well 5 are immature to overmature, from wells 2, 4, 8 and 9 are mature to overmature. Generally, the degree of maturity increases from northeast to southwest in the study area.

6.3 Sources of organic matter and source rock generative potential

6.3.1 Sources of organic matter

The results of Rock-Eval pyrolysis (Figs 5.7 and 5.8) show that the source of organic matter in the Duvernay Formation is spatially controlled rather than facies controlled. Type I kerogen is found in some samples from wells 5 and 12 with HI values ranging from 550 to 689 mg HC/g TOC. Type II kerogen is found in samples from wells 1, 3, 5, 10, 11, and 12 with their HI values ranging from 250 to 550 mg HC/g TOC. Light brown to dark brown fluorescent amorphous organic matter and abundant Tasmanites in these samples also indicates they are of marine origin. Figure 6.2 shows the relationship between HI and TOC. HI gradually increases with increasing TOC for samples from wells 1, 3, 5, 10, 11 and 12. This indicates that the organic matter becomes more lipid-rich as the amount of organic matter increases (Dean et al., 1986). This proves that the organic matter comes from a marine source.

In Figure 6.2, above 5 wt% of TOC, increases in TOC are not accompanied by proportional increases in HI for black shales. Two explanations may account for this observation. First, a relatively constant amount of terrestrial or oxidized marine organic matter was mixed with a variable amount of hydrogen-rich (marine) organic matter. Alternatively or additionally, oxidative degradation of marine organic matter results in a proportionally greater hydrogen loss than carbon loss. Also, increasing the supply of organic matter results in more reducing conditions, leading to the preferential preservation of organic matter during early diagenesis (Dean et al., 1986).

Some samples from wells 5, 9 and 13 have HI values ranging from 100 to 250 mg HC/g TOC that may indicate mixing of terrestrial material and marine material. Organic matter from wells 4, 5, 7, 8 and 9 has HI values of < 100 mg HC/g TOC that may indicate type III kerogen of terrestrial origin. However, because the low HI values may result from oxidation of organic matter, they may not be indicators of a terrestrial origin. Moreover, some samples from wells 4, 5, 7, 8 and 9 are thermally mature to overmature as discussed above. Thermal maturity can also decrease the HI values of the source rocks.

In the case of well 5, the samples with HI values lower than 250 mg HC/g TOC are found in samples from the lime mudstone facies. These samples occur at the lower part of the core and have relative low TOC values of less than 2 wt% when compared to the black shales that occur in the upper part of the well (Figure 5.4). Most samples of the lime mudstones have HI values higher than 150 mg HC/g TOC that are positive related to TOC (Fig 6.2). This probably indicates that, although organic matter in these samples has low HI values, it is still of marine origin.

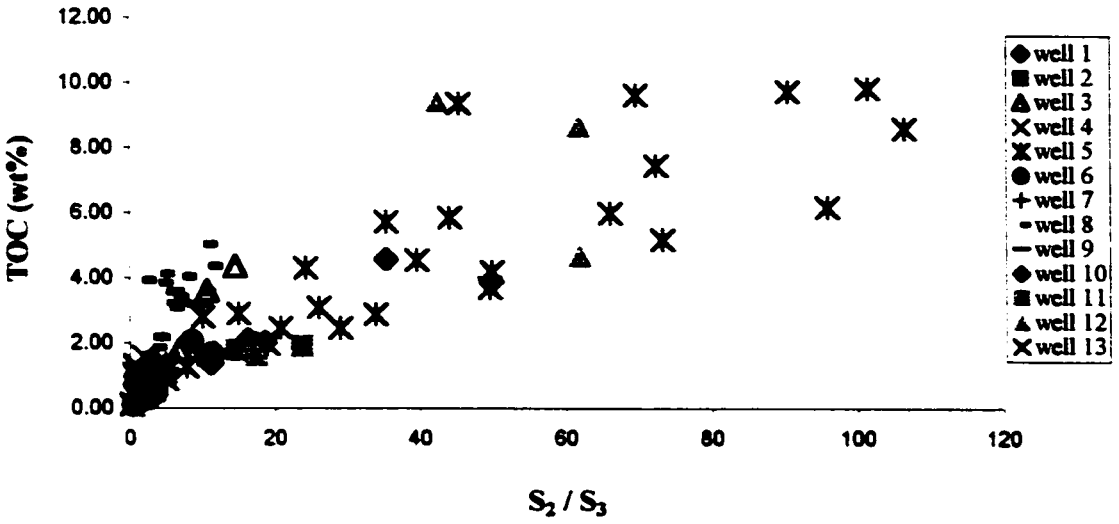

Figure 6.4 Plot of TOC versus the ratio S_2 / S_3

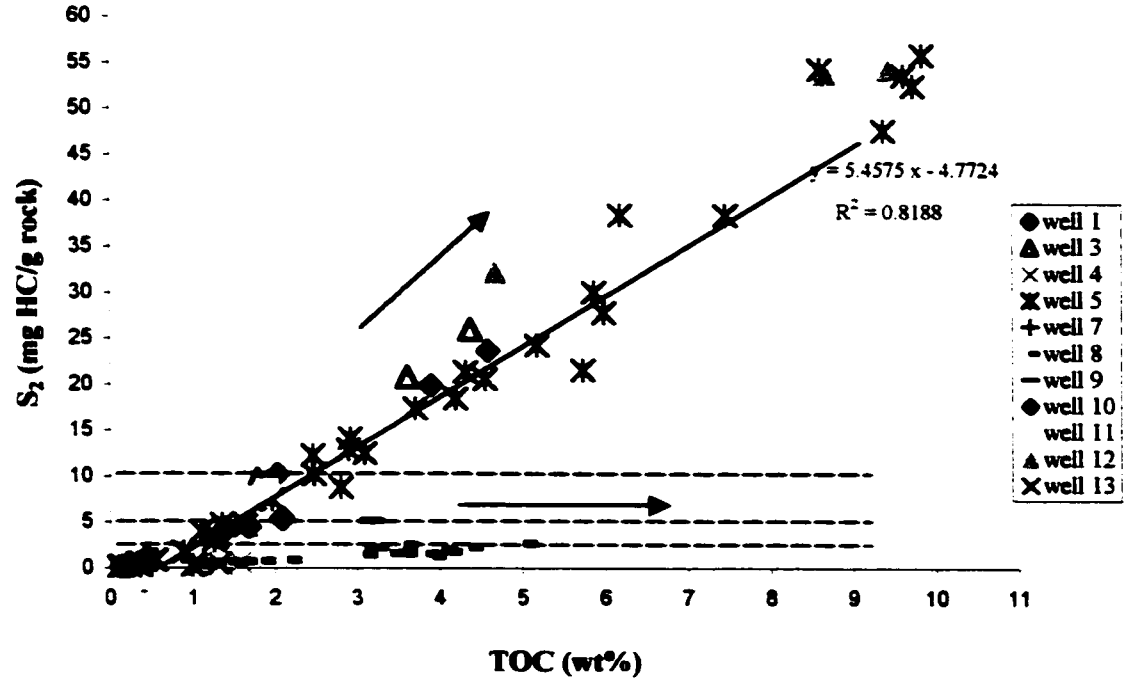

Figure 6.5 S_2 versus TOC

The samples from wells 4 and 8 have HI values < 100 mg HC/g TOC and high quartz content of between 35% and 55%. The organic matter in these wells is probably of terrestrial origin.

The origin of organic matter in wells 7, 9 and 13 is not clear. In Figure 6.2, HI values of the samples from these wells do not have a positive correlation with the TOC values. The amorphous organic matter in most of these samples is non-fluorescent. Therefore, the source of the organic matter in these wells could be either mixing of Type II and Type III kerogen or highly-oxidized Type II kerogen.

6.3.2 Organic carbon isotope values as indicators of organic matter source

The carbon isotopic composition of modern marine organic matter ranges from -16 to -23‰ between 40°N and 40°S (Rau et al., 1982). The values of the organic matter from the Duvernay Formation range from -26.49 to -32.54 ‰ with an average of -29.64‰. In modern environments, the organic carbon isotopic composition is an indicator of the source of organic matter. In this study, however, the data do not comply with the rule of "terrestrial-lighter-than-marine" found in modern environments. As illustrated in Figure 5.20, Type III kerogen in well 7 has the heaviest organic carbon isotopic values and Type II kerogen in wells 10 and 11 has the lightest values. Further, the $\delta^{13}C_{organic}$ values of the samples from wells dominated by Type II kerogen are not different from the values of the samples from wells dominated by Type III kerogen. There is at least a 6‰ difference for $\delta^{13}C_{organic}$ values between marine organic matter from Duvernay Formation and modern marine organic matter. If the HI is used as an index of the relative contribution of marine organic matter and if this marine organic

matter has heavier isotopic values than terrestrial organic matter, then the HI values should have a positive correlation with $\delta^{13}C_{organic}$. However, scatterd data show no correlation in this study (Fig 6.3). From previous studies noted below, several other factors have been cited that could also affect organic carbon isotopic values.

During diagenesis, the organic matter was enriched in lipids by the preferential removal of other components during anaerobic degradation by bacteria. Lipid-rich tissues have relatively light $\delta^{13}C$ isotopes (Barghoorn et al., 1977) and thus their preferential preservation would produce lighter kerogens. Decarboxylation reactions, which would remove ^{13}C-enriched groups from the organic material, result in ^{13}C depletion in the residual material (Deines, 1980). Arthur et al. (1992) found a 0.3 to 2.5‰ shift to lighter $\delta^{13}C_{organic}$ values from oxic to nitrate-reducing zones during early diagenesis in recent turbidites of Madeira and they attributed this change to oxidation of organic matter. Thermal maturation of organic matter results in a loss of ^{13}C-depleted hydrocarbons and thus the remaining kerogen is enriched in ^{13}C.

In the Duvernay Formation, the evidence for a shift of $\delta^{13}C_{organic}$ to lighter values during diagenesis is inconclusive. No difference for $\delta^{13}C_{organic}$ values is found between mature and immature samples. In individual wells, the isotopic compositional changes are neither positive nor negative with increasing depth. Therefore, diagenesis does not seem to be an important factor in controlling the $\delta^{13}C_{organic}$ values in the Duvernay Formation.

Productivity blooms scavenge CO_2 from the upper part of the water column (cf. Deuser, 1970), leading to reduced pCO_2 and depleted ^{12}C in the remaining CO_2 (McKenzie, 1985). Thus, continued productivity increases lead to the burial of organic

carbon that is progressively enriched in $\delta^{13}C_{organic}$ (Aravena et al., 1992). Increases in carbon burial rate can also make organic carbon isotopically heavier (Joachimski, 1997). Figure 6.4 show the relationship between TOC and the ratio of S_2 / S_3. The linear relationship indicates a common "preservability trend" for the sediments. The high TOC and S_2 / S_3 values of some samples from wells 5 and 12, relative to values of samples from other wells, are thought to imply enhanced organic productivity in these two wells. If enhanced productivity leads to enriched $\delta^{13}C_{organic}$ values as mentioned above, the $\delta^{13}C_{organic}$ values of samples in these wells should be heavier than the values of samples from other wells. However, the values of the samples from these two wells are neither higher nor lower than the values of the samples from other wells. Therefore, productivity blooms cannot also be solely responsible for the light organic carbon isotopic composition in the Duvernay Formation.

Wenger et al. (1987) also found very light $\delta^{13}C$ values of marine organic matter in two Pennysylvanian cyclothemic sequence cores in the cental United States. They explained that these values are derived from organisms that utilized a dissolved CO_2-source that was influenced by isotopically light "recycled" CO_2 derived from the decomposition of organic matter. Therefore, using "recycled" CO_2 derived from the decomposition of organic matter by marine organisms may account for the light $\delta^{13}C$ values of marine organic matter in this study.

Atmospheric pCO_2 levels were up to 10 times higher than modern values during the Devonian (Berner, 1994). A higher atmospheric pCO_2 would lead to a higher pCO_2 level of surface water (Rau et al., 1989, 1991) and concomitantly lighter $\delta^{13}C_{organic}$ values of marine organic matter compared with the values of terrestrial plant (Denies, 1980). As

previously mentioned, the organic carbon isotopic composition of marine organic matter is at least 6‰ lighter than that formed in the modern environment. Because diagenesis does not produce a significant decrease in $\delta^{13}C_{organic}$ in Holocene to Miocene sediments (Cronin and Morris, 1982), there is no evidence that diagenesis alone could make such large difference. The higher atmospheric pCO_2 level during Devonian time, or use of "recycled" CO_2 derived from the decomposition of organic matter by marine organisms, therefore, are probably the causes of the extremely light $\delta^{13}C_{organic}$ values found in the Duvernay Formation. The differences of $\delta^{13}C_{organic}$ values between different wells or between different facies are not clear, and requires further study.

6.3.3 Source rock generative potential

TOC is the first index used in evaluating source rock potential in all studies. In the Duvernay Formation, grey shales, grey mudstones and dolomitic mudstones have very low TOC values of less than 0.18 wt% and, therefore, have no oil potential. Samples from the other facies have variable ranges of TOC values and those that have TOC values of greater than 1 wt% could be thought to have good generative potential. However, further study of the hydrocarbons generated by Rock-Eval pyrolysis show that some samples, even those having high TOC values, do not have generative potential.

Figures 6.5 shows the relationship between S_2 and TOC. The slope of the regression line shows that the organic material in these samples has 54.6% pyrolizable hydrocarbons (the percentage of pyrolizable hydrocarbons in TOC is calculated as 10 times the slope given in the equation in caption of Fig 6.5, Langford and Valleron, 1990). The positive x–intercept (0.87 wt% TOC) showed in Fig 6.5 implies that the rock matrix adsorbs some

of the hydrocarbons liberated by pyrolysis. This value represents the amount of organic material with a given HI that should be present before hydrocarbons can be liberated from the rock by pyrolysis (Langford and Valleron, 1990).

According to Peters (1986), source rock that has S_2 values of more than 2.5, 5 and

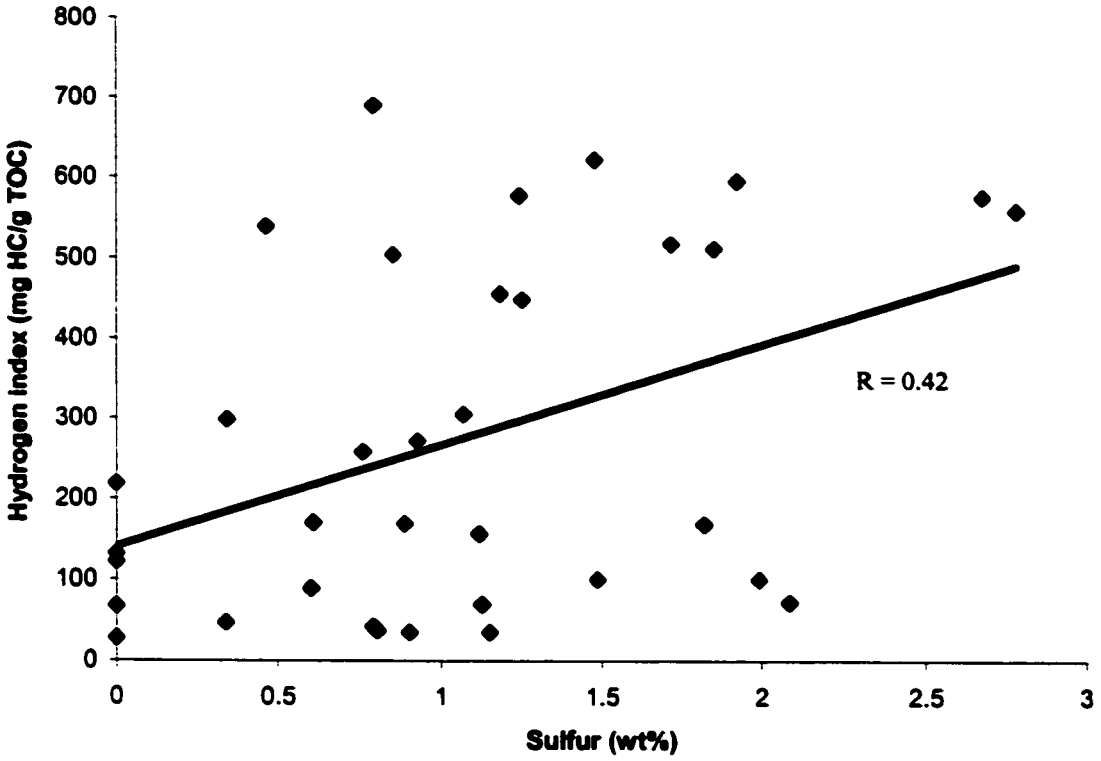

Fig 6.6 Plot of Sulfur and Hydrogen Index

10 mg HC/g rock has fair, good and very good generative potential, respectively. In Figure 6.5, samples from wells 4, 8 and 9 have relatively high TOC values, but their S_2 values seldom exceed 2.5. This maybe due to release of oil from the samples in these wells that have already become mature. Only one sample from well 9 has a S_2 value of 5.12 mg HC/g rock, which indicates a better oil potential. Therefore samples from wells 4, 8 and 9 have poor oil potential. Samples from wells 1 and 11 have S_2 values ranging

from 4.22 to 8.54 mg HC/g rock, indicating that they have good oil potential. Samples from wells 3, 10 and 12 have S_2 values greater than 10 mg HC/g rock and thus are predicted to have very good generative potential. The S_2 distribution for samples from well 5 is large, ranging from 0.11 to 55.75 mg HC/g rock. The low values are mainly found in lime mudstone facies, which also correlates with low TOC values. Most of the samples from well 5 have S_2 values of greater than 5 mg HC/g rock and could be thought to have good to very good oil potential.

Generally two trends of data distribution are found in Fig 6.5. With increased TOC, The S_2 values of samples from wells 4, 7, 8, 9 and 13 donot change much. However, an obvious increase of S_2 values with increased TOC was found for samples from wells 1, 3, 5, 10, 11 and 12. Both groups have good linear relationships with r values of 0.75 and 0.99, respectively. This may indicated that although the organic compositions of these two group are different, different wells have similar organic composition within each group (Langford and Valleron, 1990).

6.4 Sulphate Reduction

During the Duvernay time, average $\delta^{34}S$ values of seawater sulphate range from 20.5‰ at - 375 Ma to 27.6‰ at - 365 Ma. From the most depleted sulphur isotopic values, the fractionation factors for bacterial sulfate reduction were estimated to be 50.4‰ at -375 Ma and 40.6‰ at -365 Ma (Strauss, 1999).

The sulphate reduction process in the Duvernay Formation is thought to be dominantly bacterial. This is concluded from the relatively large $\Delta\ \delta^{34}S$ values ranging

from 25‰ to 50‰. As mentioned before, framboidal pyrite is always considered to be a syngenetic or early diagenetic component resulting from BSR. Coarse cubic pyrite, as well as saddle dolomite, are usually considered as indicators of TSR (Machel et al., 1995). However, coarse cubic pyrite is volumetrically minor in the Duvernay Formation. Thus this kind of pyrite can be regarded to be the result of either BSR or TSR in a deep burial environment.

Compared to the fractionation factor of 50.4‰ and 40.6‰ for Duvernay time noted above, most of $\Delta\ \delta^{34}S$ values obtained in this study are markedly lower. This may indicate that the Duvernay Formation was deposited in a partially closed environment. The lowest value of 12.7‰ is found in one black shale sample from well 1, which infers a fairly closed environment. The $\Delta\ \delta^{34}S$ values of samples is neither facies controlled nor locally controlled. The black shale facies shows a broad range of $\Delta\ \delta^{34}S$ values from 12.7‰ to 47.8‰, indicating a broad range from a rather closed environment to a very open environment.

6.5 Depositional Environment

Several lines of evidence can be used to infer the depositional environment of the Duvernay Formation and they will be discussed below.

1. TOC/S ratios

As introduced in Chapter V, the depositional environment can be inferred from the TOC/S ratios (Figs 5.16 and 5.17), but wide scatter is apparent in the data. This may be

caused by different depositional conditions in the different areas (e.g. sedimentation rate, depth of water column, and fluctuating degrees of bottom-water oxygenation) (Leventhal, 1987; Al-Aasm et al., 1996). As mentioned in Chapter V, several factors control the formation of pyrite and affect TOC/S ratios, namely: (1) metabolized organic matter, (2) dissolved sulphate and (3) reactive iron (Raiswell and Berner, 1985).

Figure 6.6 shows the relationship between hydrogen index and sulphur. Samples with HI values > 200 indicate that sufficient labile organic matter was available to promote BSR. However, a poor correlation ($r = 0.42$) between pyrite sulphur and HI is observed. A similar relationship between HI and sulphur was observed in a study of fine-grained lacustrine sediments in New Brunswick by Chowdhury and Noble (1996). They suggested that the poor correlation may indicate that organic matter content or its reactivity was not limited by pyrite formation.

From the sulphur isotopic results, the Duvernay Formation was formed under a partially closed to open environment. In a partially closed environment, all sulphate will be consumed and a higher TOC/S value will be obtained.

Most of the shales of the Duvernay Formation are calcareous, with carbonates accounting for 16 to 95% of the rocks. Generally, carbonate sediments contain little iron. Thus, apart from dissolved sulphate, the availability of reactive iron becomes another limiting factor in the formation of pyrite.

Figure 5.17 shows the relationship between sulphur and TOC between different facies. The relatively depleted sulphur isotopic values of the Duvernay samples prove that the sulphur is mainly in pyrite. The three black lines show the range of TOC/S = 2.8 $\pm$ 0.8 for modern normal marine environments (Berner, 1982). The red dashed line

represents normal marine environments during the Duvernay time. Obviously, most of the values are above the red line of Upper Devonian normal marine environment, indicating that these samples were formed in an anoxic environment. Only two black shale samples from well 12 show values below this line. The sulphur isotopic results show that the location of well 12 is located in a slightly closed environment. Considering the two limiting factors, dissolved sulphate and reactive iron, the pyrite formation in this area may be limited. So that the high TOC/S values are found and, therefore, these values should not be attributed to a normal marine environment.

2. Lack of Bioturbation

One of the most conclusive and readily available pieces of evidence for anoxic conditions for shales and mudstones in Duvernay Formation is the absence of benthic organisms and burrows during sedimentation. The lack of bioturbation leads to the preservation of original laminations or sharp horizontal microbedding planes. Wavy laminations in wells 10 and 11 are probably produced by the differential compaction of organic matter around silt/carbonate aggregates (Wignall, 1994). Undisturbed millimeter laminations in most of the wells reflect the absence of any infauna.

3. Organic Facies

As mentioned in Chapter I, Chow et al. (1995) indicated that maceral planktonic assemblages reflect a shared hydrodynamic control between near-surface water agitation and bottom-water oxygenation. As illustrated in Figure 6.8, organic facies A, B and C represent a sequence from the most basinward organic facies to the reef margin. For the

samples of this study, amorphous organic matter and thin-walled Prasinophyte are dominant and no acritarchs were found. This assemblage is referred to as organic facies A (Chow et al., 1995) and indicates the most basinward anoxic environment.

4. Size distribution of framboidal pyrite

Wilkin et al. (1996) proposed that, where secondary pyrite growth is limited, the size distribution of framboids is indicative of the formation conditions: framboids found in sediments underlying euxinic water columns are smaller than those in sediments underlying oxic or dysoxic water columns. From modern sediments in an euxinic environment and a combined oxic and dysoxic environment, the average mean framboid diameters are 5.0 ± 1.7 μm and 7.7 ± 4.1 μm, respectively. Furthermore, they found that the size distributions in modern sediments are comparable with those in ancient sedimentary rocks because framboid size is preserved through diagenesis and lithification. The diameters of the framboidal pyrites in the Duvernay Formation are small, with most of them < 5 μm. This may indicate that they were formed in an euxinic environment.

6.6 Depositional model

Sediments of the Woodbend Group comprise a single major cycle of deposition composed of a lower transgressive and an upper regressive portion (Stoakes, 1992). The Woodbend megasequence was initiated by a gradual lowering of sea level which led to the basinward progradation of lowermost Cooking Lake sediments over the Beaverhill

Lake and Mildred Member shales. After this short regressive episode, sea level began to rise incrementally. The repeated episodic relative rise of sea level, each in the order of 20 m, resulted in a maximum marine inundation by the Upper Devonian sea into the WCSB and established the maximum bathymetric relief (Stoakes and Wendte, 1987). The initially rapid rates of sea-level rise resulted in the backstepping of carbonate platform for the Cooking Lake Formation and lower Leduc Formation. Only a minor amount of sediment was added to basinal areas over most of the western Alberta Basin during the transgressive phase.

The regressive phase of the Woodbend megasequence comprises the partial infilling of the basin, largely from east to west, by prograding shales and thin carbonate platform units of the Duvernay and Ireton formations. These regressive units were deposited during intermittent rises in sea level. However, the overall slower rate of sea-level rise, accompanied by the delivery of fine terrigenous sediment into the basin, caused the deeper-water areas to be progressively filled and the reef growth to be finally terminated. Leduc reef growth and basin-filling took place at the same time. The source of the shale is considered to be the Ellesmerian Fold Belt in the Canadian Arctic Archipelago (Stoakes, 1979).

Basin-fill successions in the Woodbend Group comprise two major lithologies: carbonate-rich and shale-rich types. The former is from an intrabasinal source. It is composed of fine-grained carbonate produced through the biological and physical erosion of shallow-water carbonates within and around the basin edge that are reworked in the basin. The shale-rich type represents an extrabasinal source composed of fine-grained

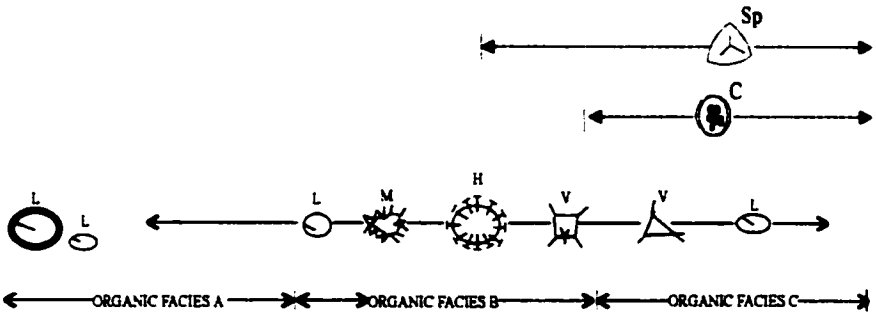

BASIN	SLOPE			LIMESTONE PLATFORM
	TOE	MIDDLE FORESLOPE	UPPER FORESLOPE	
- Black Shale - Laminated Mudstone - Laminated Dolomitic Mudstone	- Carbonate - Rich mudstone - Grey Shale - Grey Mudstone	- Brecciated Wackestone and Packstone - Bioturbated Calcreous Shale	- Nodular Limestone - Packstone	- Bioturbated Mudstone - Fossiliferous Packstone Sea level
AEROBIC	0 - 45 m			
DYSAEROBIC	45 - 100 m			
ANAEROBIC	>100 m			

RANGE OF SAMPLES IN THIS STUDY

Figure 6.7 Depositional model for the Duvernay Formation (modified from Stoakes, 1980; Dorning, 1987; Chow et al., 1995). Organic facies is based on recorded maceral abundance and position relative to the reef margin. Maceral key: C - coccoikal alginite, H - Hystrichosphaeridium-like acritarchs, L- Leiosphaeridia alginite, M - Micrhystridium-like acritarch, V - Veryachium-like acritarch, Sp - terrestrial sporinites.

clay-shale produced through erosion of distant terrains and brought into the basin by oceanic circulation.

Figure 6.7 shows the depositional model for the Duvernay Formation, which is modified from Stoakes (1980) and Chow et al. (1995). Lithofacies on the limestone platform are bioturbated mudstone and fossiliferous packstone. Abundant normal marine calcareous fauna indicate residence in the photic zone. The upper foreslope is characterized by nodular limestones and packstones that contain fewer faunal elements. On the middle sloping portion of the profile, fine-grained sediments and the absence of current structures suggest deposition below the level of persistent wave action. The dominant lithofacies are brecciated wackestones and packstones, and calcareous shales (Stoakes, 1980; Adam, 2000).

The main lithofacies discussed in this study appear on the toe of the slope and in the basinal portions of the profile. Inhospitable deep-water conditions are suggested by fine laminations, a lack of current structures, and the dark organic-rich nature of the rocks. The sediments are very fine-grained and contain only a sparse, mainly pelagic, fauna. Carbonate-rich mudstone (both lime mudstone and dolomitic mudstone), grey shale and grey mudstone are the dominant lithofacies on the toe of the slope. In the basin, the main lithofacies include laminated mudstone, black shale and laminated dolomitic mudstone.

In the Duvernay Formation, interlaminations and interbeds of different lithofacies are very common. Even in the same lithofacies, the different contents of organic matter can cause the samples to show interbeds of dark color and light color. The explanation of the phenomenon is difficult and two possibilities are discussed next.

Repeated episodic sea-level rise seems to be the most probable cause of the interbeds. Chow et al. (1995) concluded that the primary control on organic matter accumulation in the Duvernay Formation was preservation initiated by bottom-water anoxia. Episodic sea-level rises periodically changed the oxygenating conditions of the bottom water, resulting in black shale interbeds formed in anoxic environments and limestone interbeds formed in more aerobic environments. A greater amount of fossils in the limestone facies and than in the black shales provide evidence to support this interpretation. In Figures 5.4 and 5.5, TOC contents of lime mudstone and black shale from well 5 gradually increase with increasing depth; TOC contents of lime mudstone from well 8 gradually decrease with the increasing depth. These results may indicate gradual small changes of the redox environment caused by the episodic sea level rise. The relatively low TOC content for lime mudstones, dolomitic mudstones, grey shales and grey mudstones may indicate that they were formed in a more oxic conditions than the black shales and laminated mudstones. More evidence comes from the laminated dolomitic mudstones. In this facies, its organic-rich parts and organic-poor parts are interbedded yet the lithofacies does not change. Although no general trend is found in the TOC distribution with depth (Fig 5.6), the different TOC values reflect the thickness of organic-rich laminations in different samples: *ie* the thicker the organic-rich laminations, the higher the TOC values. An anoxic environment favours the preservation of organic matter so that the interbeds could result from periodically changing reduction-oxidation conditions.

Another possible cause for the formations of interbeds could be sporadic shelf bottom currents. In the interbedded black shale/dolomitic mudstones in wells 5 and 8,

very thin laminations (0.2 to 1 mm) of dolomitic mudstones are interbedded with relatively thick black shale laminations (1 mm to 2 cm). The scattered TOC distribution for the samples of this facies is probably caused by the varying thickness of the dolomitic mudstone interbeds. Other than wells 5 and 8, dolomitic mudstone is found only in well 7 where it dominates. Compared to the well-sorted dolomitic mudstones in well 7, the thin laminations composed of dolomitic mudstones in wells 5 and 8 are usually poor sorted. This suggests that dolomitic mudstones in wells 5 and 8 were redeposited by shelf bottom currents caused by sporadic storms.

CHAPTER VII

CONCLUSIONS

The following conclusions are based on detailed core examinations combined with petrographic and geochemical analysis of samples obtained from the Duvernay Formation, central Alberta.

(1) Lithofacies identified in the Duvernay Formation are: black shale, laminated mudstone, lime mudstone, dolomitic mudstone, laminated dolomitic mudstone, grey shale, grey mudstone, wackestone, packstone and nodular limestone.

(2) There are several types of calcite cement demonstrating five separate diagenetic events: mosaic calcite cement, sparry calcite cement and bladed/prismatic calcite cement. Non-ferroan calcite cement of all these three types is of early diagenetic origin, whereas ferroan mosaic and bladed calcite cement is of intermediate to deep burial origin. The ferroan calcite cement was probably precipitated in a ^{12}C, ^{16}O and iron enriched fluid.

(3) Physical compaction occurred after the sediments were cemented by sparry calcite.

(4) Dolomitization is the main diagenetic process in the Duvernay Formation and affects all the lithofacies. There are three types of dolomite: matrix dolomite (which is subdivided into three generations), saddle dolomite and vein-associated dolomite. Matrix dolomite is the earliest formed dolomite. It postdates non-ferroan sparry calcite and mosaic calcite cement. The ferroan Type II matrix

dolomite represents an intermediate to deep burial diagenetic event. Vein-associated dolomite postdates saddle dolomite. Both of them are uncommon in shales and mudstones, and represent a deep burial diagenetic event.

(5) High quartz content was observed in samples from some wells in north and northwest. This indicates that the terrestrial material was probably derived from the area to the northwest or north.

(6) TOC content ranges from 0.09 to 0.13 wt% for grey shales, 0.14 to 0.18 wt% for dolomitic mudstones, 0.09 to 1.64 wt% for lime mudstones, 0.32 to 2.05 wt% for limestones, 1.06 to 9.83 wt% for black shales and 0.43 to 4.58 wt% for laminated dolomitic mudstones. Because the TOC values were obtained from whole rock samples instead of individual laminites, higher TOC values could be expected from the organic-rich laminites.

(7) Pyrite occurred as framboidal pyrite, pyrite spheres, and cubic, pyritohedral and octahedral pyrite crystals. Framboidal pyrite has a syngenetic or early diagenetic origin and results from bacterial sulphate reduction. Fine-grained pyrite crystals probably represent a later diagenetic event and resulted from bacterial sulphate reduction. Coarse-grained pyrite crystals are not common and are probably the result of deep-burial bacterial sulphate reduction or thermal sulphate reduction.

(8) Sulphur isotopic results indicate that the sediments of the Duvernay Formation were deposited in a partially closed to open environment.

(9) Most of the samples from the area to the north have Type II kerogen. Most of the samples from the area to the south have mixed Type II and III kerogen or highly oxidized Type II kerogen. Type II kerogen has a marine origin, while Type III

kerogen indicates a terrestrial origin. The degrees of maturity increase from northeast to southwest, or from immature to overmature, respectively. The oil generation potential decreases from northeast to southwest.

(10) Organic carbon isotopic results do not comply with the rule of "terrestrial-lighter-than-marine" as is found in modern environments. There is at least a 6‰ shift to lighter values for marine organic matter in the Duvernay Formation from that formed for modern marine organic matter. The higher atmospheric pCO_2 level during Devonian time and / or using "recycled" CO_2 derived from the decomposition of organic matter by marine organisms is probably responsible for this large difference.

(11) The TOC/S ratios, organic facies, size distribution of framboidal pyrite and lack of bioturbation all indicate that the Duvernay shales and mudstones were deposited in an anoxic environment.

(12) In the presented depositonal model, the laminated mudstone, black shale and laminated dolomitic mudstone were deposited at the basinal portion of the profile, whereas the carbonate-rich mudstones, grey shale and grey mudstone were deposited on the toe of the slope. Interbedded black shale and limestone, as well as the interbedded organic-rich and organic-poor laminite in laminated dolomitic mudstone were probably the result of repeated episodic sea-level rise. Interbedded black shale/dolomitic mudstones probably resulted from redeposition by shelf bottom currents caused by sporadic storms.

REFERENCES

Adam, J., 2000, Lithofacies and geochemistry of carbonate in the late Devonian Duvernay Formation of central Alberta. Unpublished B.Sc. thesis, University of Windsor, 66pp.

Al-Aasm, I.S., Taylor, B.E., and South, B., 1990, Stable isotopes analysis of multiple carbonate samples using selective acid extraction. Chemical Geology (Isotope Geoscience Section), Vol. 80, p. 119-125.

Al-Aasm, I.S., Morad, S., Durocher, S. and Muir, I., 1996, Sedimentology, C-S-Fe relationships and stable isotopic compositions in Devonian black mudrocks, Mackenzie Mountains, Northwest Territories, Canada. Sedimentary Geology, Vol. 106, p. 279-298.

Allen, J.R. and Matthews, R.K., 1977, Carbon and oxygen isotopes as diagenetic and stratigraphic tools: Surface and subsurface data, Barbados, West Indies. Geology, Vol. 5, p. 16-20.

Anderson, T.F. and Arthur, M.A., 1983, Stable isotopes of oxygen and carbon and their application to sedimentologic and paleoenvironmental problems. In: Stable Isotopes in Sedimentary Geology. Society of Economic Paleontologists and Mineralogists, Short Course No. 10, p 1- 1 to 1-151.

Andrichuk, J.M.,1958, Cooking Lake and Duvernay (Late Devonian) sedimentation in Edmonton area of central Alberta, Canada. Bulletin of the American association of petroleum Geologists, Vol. 42, No. 9, p 2189-2222.

Andrichuk, J.M., 1961, Stratigraphic evidence for tectonic and current control of upper Devonian reef sedimentation, Duhamel area, Alberta, Canada. Bulletin of the American Association of Petroleum Geologists, Vol. 45, No. 5, p. 612-632.

Aravena, R., Warner, B.G., MacDonald, G.M. and Hanf, K.I., 1992, Carbon isotope composition of lake sediments in relation to lake productivity and radiocarbon dating. Quaternary Research. Vol. 37, p. 333-345.

Arthur, J.M., Tyson, R.V., Thomson, J. and Mattey, D., 1992, Early diagenesis fo marine organic matter: Alteration of the carbon isotopic composition. Marine Geology, Vol. 105, p. 51-61.

Arthur, M.A. and Sageman, B.B., 1994, Marine black shales: depositional mechanisms and environments of ancient deposits. Annual Reviews of Earth and Planetary Science. Vol. 22 p. 499-551.

Barghoorn, E.S., Knoll, A.H., Dembicki, H. and Meinschein, W.G., 1977, Variations in stable carbon isotopes in organic matter from the Gunflint Iron Formation. Geochimica et Cosmochimica Acta.Vol. 41, p. 425-430.

Bein, A., Almogi-Labin, A. and Sass, E., 1990, Sulphur sinks and organic carbon relationships in Cretaceous organic-rich carbonates, implications for evaluations of oxygen-poor depositional environments. American Journal of Science. Vol. 290, p. 882-911.

Berner, R.A., 1982, Burial of organic carbon and pyrite sulphur in the modern ocean: its geochemical and environmental significance. American Journal of Science. Vol 282, p. 451-473.

Berner, R.A., and Raiswell, R.,1983, Burial of organic carbon and pyrite sulphur in sediments over Phanerozoic time: a new theory. Geochimica et Cosmochimica Acta.Vol. 47, p. 855-862.

Berner, R.A., 1984, Sedimentary pyrite formation: An update. Geochimica et Cosmochimica Acta. Vol. 48, P. 605-615.

Berner, R. A., 1994, GEOCARB II: A revised model of atmospheric CO_2 over Phanerozoic time. American Journal of Science, Vol. 294, p. 56-91.

Bissada, K.K., 1982, Geochemical constraints on petroleum generation and migration – a review. Proc 2nd ASCOPE Conf, Manila, Oct, 1981, p. 69-87.

Boggs Jr., S., 1992, Petrology of Sedimentary Rocks. Macmillan Publishing Co., New York, 707pp.

Bore, P.L. de, 1980, Carbon isotope composition; an indicator of the paleoenvironment of black shale deposition. International Geological Congress, Abstracts- Congres Geologique international, Resumes. 26, Vol. 1 p. 222.

Breger, I.A., 1961, Kerogen. In: McGraw Hill Encyclopedia of Science and Technology. New York: McGraw Hill, 1961.

Campbell, F.A. and Oliver, T.A., 1968, Mineralogic and chemical composition of Ireton and Duvernay Formations, central Alberta. Bulletin of Canadian Petroleum Geology, Vol. 16, No. 1, p. 40-63.

Canfield, D.E. and Teske, A., 1996, Late Proterozoic rise in atmospheric oxygen concentration inferred from phylogenetic and sulphur-isotope studies. Nature, Vol.382, p.127-132.

Choquette, P.W. and James, N.P.,1987, Diagenesis in Limestones – 3. The deep burial environment. Geoscience Canada, 14: p 3-35.

Chow, N., Wendte, J., and Stasiuk, L.D., 1995, Productivity versus preservation control on two organic—rich carbonate facies in the Devonian of Alberta: sedimentological and organic petrological evidence. Bulletin of Canadian Petroleum Geology, Vol. 43, No.4, p. 433-460.

Chowdhury, A.H. and Noble, J.P.A., 1996, Organic carbon and pyrite sulphur relationships as evidences of bottom water conditions of sedimentation, Albert Formation fine-grained lacustrine sediments, New Brunseick, Canada. Marine and Petroleum Geology, Vol. 13, p. 79-90.

Cioppa, M.T. and Symons, D.T.A., 2001. Timing of hydrocarbon generation and migration; paleomagnetic and rock magnetic anlaysis of the Devonian Duvernay Formation, Alberta, Canada. Journal of Geochemical Exploration, Vol. 69-70, p. 387-390.

Claypool, G.E., Holser, W.T., Kaplan, I.R., Sakai, H. and Zak, I., 1980, The age curves of sulphur

and oxygen isotopes in marine sulphate and their mutual interpretation. Chemical Geology, Vol. 28, p. 199-260.

Compton, J.S., 1988, Degree of supersaturation and precipitation of organogenic dolomite. Geology, Vol. 16, p. 318-321.

Craig, H., 1953, The geochemistry of the stable carbon isotopes. Geochimica et Cosmochimica Acta, Vol. 3, p.53-92.

Creaney, S. and Allan, J., 1990, Hydrocarbon generation and migration in the Western Canada Sedimentary Basin. In Classical Petroleum Provinces, ed. By Brooks, J., p189-202. Geological Society of London. Special publication No. 50. Blackwell Scientific.

Cronin, J.R. and Morris, R.J., 1982, The occurrence of high molecular weight humic material from recent organic-rich sediment from the Naminianshelf. Estuarine Coastal Shelf Sci., Vol. 15, p. 17-27.

Cutler, D.W.G., 1983, Stratigraphy and sedimentology of the Upper Devonian Grosmont Formation, northern Alberta. Bulletin of Canadian Petroleum Geology, Vol. 31, p. 282-325.

Dean, W.E., Arthur, M.A. and Claypool, G.E., 1986, Depletion of ^{13}C in Cretaceous marine organic matter: source, diagenetic, or environmental signal? Marine Geology, Vol. 70, p. 119-157.

Degens, E.T., Okada, H., Honjo, S. and Hathaway, J.C., 1972, Microcrystalline sphalerite in resin globules suspended in Lake Kivu, East Africa. Mineralium Deposita. Vol. 7, p. 1-12.

Denies P., 1980, The isotopic composition of reduced carbon. In: Handbook of Environmental Isotope Geochemistry. Vol. 1 (ed. P. Fritz and J.C. Fontes), pp. 329-406. Elsevier.

Deroo, G., Powell, T.G., Tissot, B. and McCrossen, R.G., 1977, The origin and migration of petroleum in the Western Canada Sedimentary Basin, Alberta: A geochemical and thermal maturation study. Bulletin of the Geological Society of Canada 262. 136pp.

Deuser, W.G. and Degens E.T., 1967, Carbon isotope fractionation in the system CO_2 (gas)-CO_2 (aqueous)-HCO_3^- (aqueous). Nature, Vol. 215, p. 1033-1035.

Deuser, W.G., 1970, Isotope evidence for diminishing supply of available carbon during diatom bloom in the Black Sea. Natrue, Vol. 225, p. 1069-1071.

Dickson, J.A., 1965, Carbonte identification and genesis as revealed by staining. Journal of Sedimentary Petrology, Vol. 27, p. 107-118.

Dorning, K.J., 1987, The organic palaeontology of Palaeozoic carbonate environments. In: Micropalaeontology of Carbonate Environments. M.B. Hart (ed.). Ellis Horword, Chichester, p. 256-265.

Dunham, R.J., 1962, Classification of carbonate rocks. In: W.E. Ham (ed.), Classification of Carbonate Rocks, A Symposium. American Association of Petroleum Geologists, Memoir 1, p. 108-121.

Embry, A.F. and Klovan, J.E., 1971, A late Devonian reef tract on northeastern Banks Island, N.W.T. Bulletin of Canadian Petroleum Geology, Vol. 19, p. 730-781.

Espirtalie, J., Deroo, Cr., and Marquis, F., 1985, Rock-Eval pyrolysis and its applications. Report Institut Francais du Petrole. No. 33878, 72pp.

Espitalie, J., Laporte, J.L., Madec, M., Marquis, F., Leplat, p., Paulet, J., and Boutefeu, A., 1977, Methode rapide de caracterisation des roches meres, de leur potentiel petrolier et de leur degre d'evolution. Revue de l'Institut Francais du Petrole, Vol. 32, p. 23-42.

Folk, R.L., 1965, Some aspects of recrystallization in ancient limestones. In: L.C. Pray and R.C. Murray (eds.), Dolomitization and Limestone Diagenesis. Soc. Econ. Paleontologists and Mineralogists Special Publication, 13, p. 14-18.

Fontugne, M., Descolax-Gros, C. and Debilly, G., 1991, The dynamics of CO_2 fixation in the Southern Ocean as indicated by carboxylase activities and organic carbon isotopic ratios. Marine Chemistry, Vol. 35, p. 371-380.

Friedman, G.M. and Chakraborty, C., 1997, Stable isotopes in marine carbonates: their implicationfor the paleoenvironment with special reference to the Proterozoic Vindhyan carbonate (Central India). Journal Geological Society of India, Vol. 50, p.131-159.

Friedman, G.M. and Schultz, D.J., 1994, Precipitation of Vaterite ($CaCO_3$) during oil field drilling. Mineralogical Magazine. Vol. 58, p. 401-408.

Fry, B., Cox, J., Gest, H. and Hayes J.M., 1986, Discrimination between ^{34}S and ^{32}S during bacterial metabolism of inorganic sulphur compounds. Journal of Bacteriology. Vol. 165, p. 328-330.

Fry, B., Ruf, W., Gest, H. and Hayes J.M., 1988, Sulphur isotope effects associated with oxidation of sulphide by O_2 in aqueous solution. Chemical Geology, Vol. 73, p. 205-210.

Hannam, J.A., Andrews, J.E. and Bottrell, S.H., 1996, Carbon and sulphur geochemistry and clay mineralogy of the west Runton freshwater bed. Bulletin. Geological Society of America. Vol 45, p. 29-51.

Harrison, A.G. and Thode, H.G., 1957, The kinetic isotope effect in the chemical reduction of sulphate. Transactions, Faraday Symposia of the chemical Society. Vol. 53, p. 1-4.

Hendry, J.P., 1993, Calcite cementation during bacterial manganese, iron and sulphate reduction in Jurassic shallow marine carbonates. Sedimentology, Vol. 40, p. 87-106.

Hoefs, J., 1987, Stable Isotope Geochemistry. Springer, Berlin, 241pp.

Hurley, N.F. and Clohmann, K.C., 1989, Diagenesis of Devonian reefal carbonates in the Oscar Range, Canning basin, Western Australia. Journal of Sedimentary Petrology. Vol. 59, No.1, p. 127-146.

Husain, S.A., 1968, Sulphur isotope exchange reactions. Ph. D. Dissertation, University of Alberta, Edmonton, Alberta. 216pp.

Husain, S.A. and Krouse, H.R., 1978, Sulphur isotope effects during the reaction of sulphate with hydrogen sulphide. In: Stable isotopes in the earth sciences (ed. Robinson B,W.), Department of Scientific and Industrial Research Bulletin 220. p. 207-210.

Irwin, H., Curtis, C. and Coleman, N., 1977, Isotopic evidence for source of diagenetic carbonates formed during burial of organic rich sediments. Nature, Vol. 69, p. 209-213.

James, N.P. and Choquette, P.W., 1984, Diagenesis 9. Limestones – The meteoric environment. Geoscience Canada, Vol. 11, p161-194.

Jasper, J.P. and Hayes, J.M., 1994, Recognition of paleoceanic pCO_2 levels from carbon isotopic compositions of sedimentary biogenic components. In: Carbon cycling in the glacial ocean: Constraints on the ocean's rolein global change. R. Zahn, M. Kaminski, L.D. Labeyrie and T.F. Pedersen (eds.). Heidelberg, Germany, Springer, p. 323-342.

Jeffrey, J.D. and Donald A. Y., 1985, Enhanced carbonate petrography using fluorescence microscopy. Journal of Sedimentary Petrology, Vol. 55, No. 6, p 795-804.

Joachimski, M.M., 1997, Comparison of organic and inorganic carbon isotope patterns across the Frasnian-Famennian boundary. Palaeogeography, Palaeoclimatology, Palaeoecology, Vol. 132, p. 133-145.

Kajiwara, Y., Kaiho, K. and Ohkouchi, N., 1997, An invitation to the sulphur isotope study of marine sediments; implications and constraints of the exogenic sulphur cycle. Annual Report of the Institute of Geoscience, University of Tsukuba. 23. p. 69-74.

Kiyosu, Y., 1980, Chemical reduction and sulphur isotope effects of sulphate by organic matter under hydrothermal conditions. Chemical Geology, Vol. 30, p.47-56.

Kiyosu, Y. and Krouse H.R., 1990, The role of organic acid in the abiogenic reduction of sulphate and the sulphur isotope effect . Geochemical Journal. Vol. 24, p. 21-27.

Lafargue, E., Marquis, F. and Pillot, D., Rock-Eval 6 applications in hydrocarbon exploration, production, and soil contamination studies, Revue de L'Institut Francais du Petrole, Vol. 53, No. 4, p. 421-437.

Land, L.S., 1980, The isotopic and trace element geochemistry of dolomite: the stage of the art. In: D.H. Zenger, J.B. Dunham and R.L. Ethreington (eds.), Concepts and Models of Dolomitization. Society of Economic Paleotologists and Mineralogists, Special Publication. No. 28, p. 87-110.

Langford, F.F. and Valleron, M.M.B., 1990, Interpreting Rock-Eval pyrolysis data using graphs of pyrolizable hydrocarbons vs. total organic carbon. The American Association of Petrleum Geologists Bulletin, Vol. 74, p. 799-804.

Lewan, M.D., 1986, Stable carbon isotopes of amorphous kerogens from Phanerozoic sedimentary rocks. Geochimica et Cosmochimica Acta, Vol. 50, p. 1583-1591.

Leventhal, J.S., 1983, An interpretation of carbon and sulphur relationships in Black Sea sediments as indicators of environment of deposition. Geochimica et Cosmochimica Acta, Vol. 47, p. 133-137.

Leventhal , J.S., 1987, Carbon and Sulphur relationships in Devonian shales from the Appalachian basins as indicator of environment of deposition. American Journal of Science. Vol. 287, p. 33-49.

Li, M., Yao, H., Stasiuk, L.D., and Fowler, M.G., 1997, Effect of maturity and petroleum expulsion on pyrrolic nitrogen compound yields and distributions in Duvernay Formation petroleum source rocks in central Alberta, Canada. Organic Geochemistry, Vol. 26, No. 11-12, p 731-744.

Link, T.A., 1950, Theory of transgressive and regressive reef (Bioherm) development and origin of oil. Bulletin of the American Association of Petroleum Geologist, Vol. 3 p. 263-94.

Love, L.G. and Amstutz, G.G., 1966, Review of microscopic pyrite. Fortschritte der Mineralogie, Vol 43, p. 273-309.

Machel, H.G., Krouse, H.R. and Sassen, R., 1995, Products and distinguishing criteria of bacterial and thermochemical sulphate reduction. Applied Geochemistry. Vol. 10, p. 373-389.

Machel, H.G., 1989, Relationships between sulphate reduction and oxidation of organic compounds to carbonate diagenesis, hydrocarbon accumulations, salt domes, and metal sulphide deposits. Carbonates and Evaporites, Vol. 4, p. 137-151.

Machel, H.G., 1987, Saddle dolomite as a by-product of chemical compaction and thermochemical sulphate reduction. Geology, Vol. 15, p. 936-940.

Machel, H.G., 1986, Limestone diagenesis of the Upper Devonian NiskuFormation in the subsurface of central Alberta. Canadian Journal of Earth Sciences, Vol. 23, p. 1804-1822.

Mazzullo, S.J., 2000, Organogenic dolomitization in peritidal to deep-sea sediments. Journal of Sedimentary Research, Vol. 70, p. 10-23.

McArthur, J.M., Tyson, R.V., Thomson, J. and Mattey, D., 1992, Early diaenesis of organic matter: Alteration of the carbon isotopic composition. Marine Geology, Vol. 105, p.51-61.

McCrossan, R.G., 1961, Resistivity mapping and petrophysical study of Upper Devonian inter-reef calcareous shales of central Alberta, Canada. Bulletin of the American Association of Petroleum Geologists, Vol. 45, No. 4. p 441-470.

McKenzie, J.A., 1985, Carbon isotopes and productivity in the lacustrine and marine environment. In: Chemical Processes in Lakes (Edited by Stumm M.), p. 99-118, Wiley, New York.

Minister, T., Nathan, Y. and Raveh, A., 1992, Carbon and sulphur relationships in marine Senonian organic-rich, iron-poor sediments from Israel – a case study. Chemical Geology. Vol. 97, p. 151-161.

Nakai, N. and Jensen, M.L., 1964, The kinetic isotope effect in the bacterial reduction and ocidation of sulphur. Geochimica et Cosmochimica Acta, Vol 28, p. 1893-1912.

Newland, J.B., 1954, Interpretation of Alberta reefs based on experience in Texas and Alberta. Journal of the Alberta Society of Petroleum Geologists, Vol. 2, P. 1-6.

Ohmoto, H., Kaiser, C.J. and Geer, K.A., 1990, Systematics of sulphur isotopes in recent marine sediments and ancient sediment-hosted basemetal deposits: University of Western Australia. Geology Department and University Extension Publication 23. p.70-120.

Orr, W.L., 1977, Geologic and geochemical controls on the distribution of hydrogen sulphide in natural gas. In: Advances in Organic Geochemistry (ed. R.Campos and J.Coni). Enadisma, p. 571-597.

Painter, M.G.M., Golding, S.D., Hannan, K.W. and Neudert, M.K., 1999, Sedimentologic, petrographic, and sulphur isotope constraints on fine-grained pyriteFormation at Mount Isa Mine and Environs, northwest Queensland, Australia. Economic Geology, Vol. 94, p. 883-912.

Park, R. and Epstein, S., 1960, Carbon isotope fractionation during photosynthesis. Geochimica et Cosmochimica Acta, Vol. 21, p. 110-126.

Patzkowsky, M.E., Slupik, L.M., Arthur, M.A., Pancost, R.D. and Freeman, K.G., 1997, Late Middle Ordovician environmental change and extinction: harbinger of the Late Ordovician or continuation of Cambrian patterns? Geology, Vol. 25, No. 10, p. 911-914.

Peters, K.E., Sweeney, R.E. and Kaplan, I.R., 1978, Correlation of carbon and nitrogen stable isotopes in sedimentary organic matter. Limnology and Oceanography, Vol. 23, p. 598-604.

Peters, K.E., 1986, Guidelines for evaluating petroleum source rock using programmed pyrolysis. The American Association of Petroleum Geologists Bulletin. Vol. 70, p. 318-329.

Piggot, N. and Lines, M.D.,1991, A case study of migration from the West Canada Basin.In Petroleum Migration, eds. W.A. England and A.J. Fleet, p 207-225. Geological Society Special Publication, No. 59.

Podruski, J.A., Barclay, J.E., Hamblin, A.P., Lee, P.J., Osadetz, K.G., Procter, R.M. and Taylor, G.C., 1988. Conventional Oil Resources of Western Canada. Part I.Resource Endowment. Geological Survey of Canada Paper 87-26,149pp

Porter, J. W., Price, R.A. and McCrossan, R.G., 1982. The Western Canada Sedimentary Basin. Philosophical Transactions of the Royal Society of London, A305, p.169-192.

Raiswell, R. and Berner, R.A., 1987, Organic carbon losses during burial and thermal maturation of normal marine shales. Geology, Vol. 15, p, 853-856.

Raiswell, R. and Berner, R.A., 1986, Pyrite and organic matter in Phanerozoic normal marine shales. Geochimica et Cosmochimica Acta, Vol 50, p. 1967-1976.

Raiswell, R. and Berner, R.A., 1985, PyriteFormation in euxinic sediments and semi-euxinic sediments. American Journal Science, Vol 285, p. 710-724.

Rau, G.H., Sweeney, R.E. and Kaplan, I.R., 1982, Plankton 13C: 12C ratio changes with latitude: differences between northern and southern oceans. Deep-Sea Res., 29, 1935-1939.

Rau, G.H., Takahashi, T. and Des Marais, D.J., 1989, Latitudinal variations in plankton $\delta^{13}C$: implications for CO_2 and productivity in past oceans. Nature, Vol. 341, p. 516-518.

Rau, G.H., Froelich, P.N., Takahashi T. and Des Marais D.J., 1991, Does sedimentary organic $\delta^{13}C$ record variations in Quaternary ocean [CO_2 (aq)]? Paleoceanography. Vol. 6, p. 335-347.

Rees, C.E., 1973, A steady-state model for sulphur isotope fractionation in bacterial reduction processes. Geochimica et Cosmochimica Acta, Vol 37, p.1141-1162.

Sackett, W.M. and Thompson, R.R., 1963, Isotopic organic carbon composition of recent continental derived clastic sediments of eastern gulf coast, gulf of Mexico. Bulletin of the American Association of Petroleum Geologists, Vol. 47, No. 3, p. 525-531.

Sasaki, A., Arikawa, Y., and Folinsbee, R.E., 1979, Kiba reagent method of sulphur extraction applied to isotope work. Bulletin, Geological Survey Japan, Vol. 30. p. 241-245.

Sass, E., Bein, A. and Algomi-labin, A., 1991, Oxygen-isotope composition of diagenetic calcite in organic rocks: evidence for ^{18}O depletion in marine anaerobic porewater. Geology, Vol. 19, p. 839-842.

Schwarcz, H.P. and Burnie, S.W., 1973, Influence of Sedimentary Environments on Sulphur Isotope Ratios in Clastic Rocks: a review. Mineralium Deposita, Vol. 8, p. 264-277.

Shinn, E.A. and Robbin, D.M., 1983, Mehcanical and chemical compaction in fine-grained shallow water limestones. Journal of Sedimentary Petrology, Vol. 53, p. 595-618.

Stanton, Jr.R.J., 1963, Upper Devonian calcispheres from Redwater and south Sturgeon Lake reefs, Alberta, Canada. Bulletin of Canadian Petroleum Geology, Vol. 11, No. 4, p 410-418.

Staplin, F.L., 1961, Reef-controlled distribution of Devonian microplankton in Alberta. Palaeontology, Vol. 4, Part 3, p. 392-424, pls. 48-51.

Stoakes, F.A., 1979, Sea level control of carbonate deposition during progradational basin-filling: The Upper Devonian Duvernay and IretonFormations of Alberta, Canada : Unpublished Ph.D. thesis, University of Calgary, Calgary, Alberta, 346pp.

Stoakes, F.A., 1980; Nature and control of shale basin fill and its effect on reef growth and termination: Upper Devonian Duvernay and IretonFormations of Alberta, Canada. Bulletin of Canadian Petroleum Geology, Vol 28, p. 345-410.

Stoakes, F.A.and Creaney, S., 1984, Sedimentology of a carbonate source rock: The Duvernay Formation of central Alberta. In: Carbonates in subsurface and outcrL. Eliuk (ed.). Proceedings of the 1984 Canadian Society of Petroleum GeologiCore Conference, Calgary, p.132-147.

Stoakes, F.A. and Creaney, S., 1985, Sedimentology of a carbonate source rock: the Duvernay Formation of Alberta, Canada. In: Rocky Mountain Carbonate Reservoirs a Core Workshop. M.W. Longman, K.W. Shanley, R.F. Lindsay, D.E. Eby (eds.). Society of Economic Paleontologists and Mineralogists, Core Workshop No.7, p.343-374.

Stoakes, F.A. and Wendte, J.C., 1987, The Woodbend Group. In: Krause, F.F. and Burrowes, O.G.(Eds.), Devonian Lithofacies and Reservoir Styles in Alberta. 13th Canadian Society of Petroleum Geologists Core Conference and Display and Second International Symposium on

the Devonian System, Canadian Society of Petroleum Geologists. p.153-172.

Stoakes, F.A., 1992, Woodbend megasequence. In: Devonian-Early Mississippian Carbonates of the Western Canada Sedimentary Basin: a Sequence-Stratigraphic Framework. J.C. Wendte, F.A. Stoakes and C.V. Campbnell (authors). Society for Sedimentary Geology, Short Course No. 28. p.183-206.

Strauss, H., 1999, Geological evolution from isotope proxy signals – sulphur. Chemical Geology, Vol. 161, p. 89-101.

Switzer, S.B., Holland, W.G., Christie, D.S., Graf, G.C., Hedinger, A.S., McAuley, R.J., Wierzbicki, R.A. and Packard, J.J., 1994, Devonian Woodbend-Winterburn strata of the Western Canada Sedimentary Basin. In: Geological Atlas of the Western Canada Sedimentary Basin. G.D. Mossop and I. Shetsen (comps.). Canadian Society of Petroleum Geologists and the Alberta Research Council, p.165-202.

Tan, F.C., and Vilks, G., 1987, Organic carbon isotope ratios and paleoenvironmental implications for Holocene sediments in Lake Melville, southeastern Labrador. Canadia Journal of Earth Sciences, Vol. 24, p. 1994-2003.

Thode, H.G. and Monster, J., 1965, Sulphur isotope geochemistry fo petroleum evaporites, and ancient seas; in Fluids in subsurface environments. American Association of Petroleum Geologist Memoir, Vol. 4, p. 367-377.

Thode, H.G., MacNamara, J. and Flemimg, W.H., 1953, Sulphur isotope fractionation in nature and geological and biological time scales. Geochimica et Cosmochimica Acta, Vol. 3, p.235-243.

Tissot, B.P. and Welte, D.H., 1984, Petroleum Formation and Occurrence. Second Revised and Enlarged Edition. Springer-Verlag, Berlin Heidelberg New York Tokyo, 699pp.

Tucker, M.E., 1996, Sedimentary Rocks in the Field. John Wiley & Sons Ltd., Chichester, 153pp.

Tucker, M.E. and Wright, V.P., 1990, Carbonate Sedimentology. Blackwell Scientific Publictions, Oxford, 482pp.

Waples, D.W., 1984, A reappraisal of anoxia and organic richness, with emphasis on the Cretaceous North-Atlantic. In: Graciansky, P.-C. de Poag, C.W. et al. Init. Rep. Of the Deep Sea Drill. Proj. 80, Washington D.C. (US Government Printing Office). P. 999-1018.

Wenger, L.M., Baker, D.R., Chung M. and McCulloh, T.H., 1987, Environmental control of carbon isotope variations in Pennsylvanian black-shale sequences, Midcontinent, U.S.A.. Organic Geochemistry, Vol. 13, p. 765-771.

Westgate, L.M. and Anderson, T.F., 1982, Extraction of various forms o sulphur from coal and shale for stable sulphur isotope analysis. Analytical Chemistry. Vol. 54, p. 2136-2139.

Wickman, F.E., 1952, Variations in the relative abundance of the carbon isotopes in plants. Geochimica et Cosmochimica Acta, Vol. 2, p 243-254.

Wignall, P.B., 1994, Black Shales. Clarendon Press. Oxford. 127pp.

Wilkin, R.T., Barnes, H.L. and Brantley, S.L., 1996, The size distribution of framboidal pyrite in modern sediments: An indicator of redox conditions. Geochimica et Cosmochimica Acta, Vol. 60, p. 3897-3912.

APPENDIX I

WELL LOCATIONS FOR STUDY

1. 7-1-41-3w5
2. 16-6-48-24w4
3. 6-17-59-17w4
4. 4-22-45-5w5
5. 16-18-52-5w5
6. 6-14-35-28w4
7. 3-1-52-11w5
8. 2-6-47-4w5
9. 6-14-37-7w5
10. 14-18-54-25w4
11. 5-19-54-25w4
12. 11-26-58-23w4
13. 16-35-59-15w4

APPENDIX II

CORE DESCRIPTIONS

Well #1: 7-1-41-3w5

Depth (m)	Facies	Descriptions
2789.00	Limestone	
2789.18	Black shale	Black, thin laminations, matrix dolomite I.
2789.66	Limestone	Dissolution seams, pervasive dolomite, pseudomorphic dolomite
2800.48	Black shale	Black, parallel laminations, fractures, mechanical compaction, matrix dolomite.
2801.59	Limestone	
2802.60	Black shale	Black, parallel laminations, cementation, matrix dolomite I, saddle dolomite, pyrite, brachiopods, amorphous OM.
2806.92	Limestone	Pervasive dolomite, dissolution seams.
2809.28	Black shale	Black, wavy laminations, cementation, matrix dolomite I, pyrite, small calcite vein, bivalves, gastropods, tentaculites, amorphous OM.
2809.75	Limestone	
2810.65	Black shale	Black, laminated, fractures.
2813.40-2819.68	Limestone	Fine matrix dolomite, large anhydrite vein, calcite veins.

Well #2: 16-6-48-24w4

Depth (m)	Facies	Descriptions
1877.77-1884.91	Limestone	Calcite cementation, matrix dolomite, dissolution seam-associated dolomite, saddle dolomite.
1886.43-1886.46	Sandstone	Fine matrix dolomite

Well #3: 6-17-59-17w4

Depth (m)	Facies	Descriptions
1007.12	Limestone	Calcite cementation, geopetal fabric, pyrite.
1008.48	Laminated mudstone	Dark grey, parallel to little wavy laminations, physical compaction, matrix dolomite I, pyrite,

		cementation, bivalves, ostracods, tentaculites calcareous spheres, amorphous OM, thin-walled Prasinophyte alginates.
1009.36	Grey shale	Light grey, matrix dolomite.
1009.96-1010.78	Limestone	Pyrite nodules, calcite cementation.

Well #4: 4-22-45-5w5

Depth (m)	Facies	Descriptions
2883.41	Black shale	Dark grey to black, parallel laminations, physical compaction, cementation (non-ferroan and ferroan), calcareous spheres, amorphous OM.
2884.78	Mudstone	Dark grey to black, massive, cementation (non ferroan and ferroan), nodules, matrix dolomite I, saddle dolomite, fractures, tentaculites, amorphous OM.
2888.894	Black shale	Black, wavy laminations.

Well #5: 16-18-52-5w5

Depth (m)	Facies	Descriptions
2333.75	Black shale	Black, parallel laminations, cubic pyrite crystals, amorphous OM.
2334.31	Interbedded Black shale/Dolomitic mudstone	Black interbedded with grey, pyrite, wavy laminations, physical compaction, cementation (non-ferroan and ferroan), matrix dolomite I and II, dissolution, amorphous OM.
2335.13	Black shale	Black, parallel laminations.
2336.60	Interbedded Black shale/Dolomitic mudstone	Black interbedded with grey, pyrite, slightly wavy laminations, cementation (non-ferroan and ferroan), matrix dolomite I and II, brachiopods, ostracods, calcareous spheres, amorphous OM, Tasmanites.
2340.65	Mudstone	Brownish grey to brownish black, massive, pyrite, cementation (non-ferroan and ferroan), matrix dolomite I, fractures, ostacods, tentaculites, calcareous spheres, amorphous OM, little thin-walled Prasinophyte alginates.
2345.14	Limestone	Matrix dolomite, calcite cementation.
2346.51-2346.75	Mudstone	Light brown, massive, very fine matrix dolomite.

Well #6: 6-14-35-28w4

Depth (m)	Facies	Descriptions
2611.32-2653.11	Limestone	Matrix dolomite, pseudomorphic dolomite, saddle dolomite, pervasive dolomite, calcite cementation, pyrite, dissolution seams, anhydrite nodules, silicification, geopetal fabric, stylolites.

Well #7: 3-1-52-11w5

Depth (m)	Facies	Descriptions
2636.596-2925.775	Dolomitic Mudstone	Grey to dark grey, massive, cementation (ferroan and non-ferroan), matrix dolomite II, brachiopods.

Well #8: 2-6-47-4w5

Depth (m)	Facies	Descriptions
2633.22	Mudstone	Dark grey, massive, cementation (non-ferroan and ferroan), matrix dolomite I, pyrite, brachiopods, ostracods, tentaculites, amorphous OM.
2635.098	Black shale	Dark grey to black, slightly wavy laminations.
2636.977	Interbedded Black shale/Dolomitic mudstone	Dark grey to black, parallel to wavy laminations, matrix dolomite I and II, pyrite, bivalve, ostracods, tentaculites, amorphous OM.
2639.72	Mudstone	Dark grey, massive, cementation (non-ferroan and ferroan), matrix dolomite I, saddle dolomite, pyrite, fractures, amorphous OM.
2644.877	Interbedded Black shale/Dolomitic mudstone	Black, parallel laminations, matrix dolomite II, pyrite, amorphous OM.
2647.569	Black shale	Black, laminated.
2648.255-2648.407	Limestone	Dark grey.

Well #9: 6-14-37-7w5

Depth (m)	Facies	Descriptions
3640.00	Limestone	
3641.28	Black shale	Black, parallel laminations.
3641.62	Limestone	
3642.00	Laminated mudstone	Black, wavy laminations, cementation, matrix dolomite I, saddle dolomite, vein associated dolomite, physical compaction, pyrite crystals,

		fractures, ostracods, tentaculites.
3643.72	Black shale	Black, wavy laminations, cementation, matrix dolomite I, physical compaction, pyrite, bivalve, ostracods, calcareous spheres.
3644.54	Limestone	
3645.32	Black shale	Black, parallel laminations.
3646.75	Limestone	
3647.64	Laminated mudstone	Black, slightly wavy laminations, cementation, pyrite, bivalves, calcareous spheres.
3649.10	Limestone	
3649.68	Black shales	Black, parallel laminations, cementation, fractures, pyrite, matrix dolomite I, calcareous spheres.
3649.90-3657.00	Nodular limestone	Anhydrite nodules, calcite cementation, pervasive dolomite, saddle dolomite, physical compaction, silicification.

Well #10: 14-18-54-25w4

Depth (m)	Facies	Descriptions
1620.926	Laminated mudstone	Black, wavy laminations, cementation, physical compaction, matrix dolomite I, pyrite, ostracods, tentaculites, calcareous spheres, amorphous OM, thin and thick-walled Prasinophyte alginates.
1622.425-1628.775	Laminated dolomitic mudstone	Black laminated with grey, very wavy laminations, matrix dolomite III, cementation, pyrite crystals, gastropods, amorphous OM, thin and thick-walled Prasinophyte alginates.

Well #11: 5-19-54-25w4

Depth (m)	Facies	Descriptions
1624.838	Laminated dolomitic mudstone	Black laminated with grey, pyrite, parallel to wavy laminations, physical compaction, fine matrix dolomite III, amorphous OM, thin and thick-walled Prasinophyte alginates.
1625.676	Limestone	Fine matrix dolomite, anhydrite veins, saddle dolomite.
1626.108-1631.417	Laminated dolomitic mudstone	Black laminated with grey, wavy laminations, physical compaction, matrix dolomite III, pyrite, amorphous OM, little thin-walled Prasinophyte alginates.

Well #12: 11-26-58-23w4

Depth (m)	Facies	Descriptions
1280.59	Black shale	Black, parallel laminations, geopetal fabric, brachiopods.
1283.818	Limestone	Pyrite nodules, calcite cementation.
1284.53	Laminated mudstone	Black, slightly wavy laminations, cementation (non-ferroan and ferroan), physical compaction, matrix dolomite I, pyrite crystals, geopetal fabric (pelecypods), bivalves, ostrapods, tentaculites, calcareous spheres, amorphous OM.
1285.342	Limestone	Pervasive dolomite, saddle dolomite, calcite cementation.
1286.358-1288.644	Black shale	Black, wavy laminations, physical compaction, cementation, little matrix dolomite, bivalves, calcispheres, amorphous OM, thin and thick-walled Prasinophyte alginates.

Well #13: 16-35-59-15w4

Depth (m)	Facies	Descriptions
891.1844	Grey shale	Light grey, fine matrix dolomite, argillaceous, pyrite crystals, little thin-walled Prasinophyte alginates.
894.1308-896.7724	Grey mudstone	Light grey, fine matrix dolomite, argillaceous, pyrite crystals, little thin-walled Prasinophyte alginates, dolomite cementation.

APPENDIX III

Mineralogical components of samples (X-ray diffraction results)

Well number	Depths (m)	Facies	wt.% Total Carbonate	Quartz (%)	Calcite (%)	Dolomite (%)	Feldspars (%)	Mica (%)	Chlorite-Kaolinite(%)	Fe-Ti oxides(%)
1	2801.1	Limestone	41	15	50	15	10	5	0	5
4	2884.1	Black shale	42	35	50	5	0	5	0	5
5	2336.0	Black shale	16	55	15	6	8	5	5	6
8	2647.6	Black shale	15	55	15	10	5	5	5	5
9	3641.3	Black shale	95	5	80	<5	<5	<5	<5	<5
9	3645.3	Black shale	48	25	55	5	5	5	0	5
9	3647.6	Laminated mudstone	45	30	45	10	5	5	0	5
5	2340.1	Interbedded shale/mudstone	25	55	20	10	<5	<5	<5	<5
8	2639.3	Interbedded shale/mudstone	17	55	20	5	5	5	10	5
10	1624.7	Laminated dolomitic mudstone	31	50	5	40	<5	<5	0	<5
11	1626.4	Laminated dolomitic mudstone	18	60	5	20	5	5	0	5
13	891.2	Grey shale	41	15	50	15	10	5	0	5

APPENDIX IV

Rock-eval pyrolysis results

Well number	Facies	Depth (m)	TOC (wt%)	T_{max} (°C)	HI(mg HC / g TOC)	OI (mg CO_2 / g TOC)	S_1 (mg/g)	S_2 (mg/g)	S_3 (mg/g)	PI ($S_1/(S_1+S_2)$)
1	BS	2802.60	2.09	445	258	12	0.89	5.36	0.33	0.142
	BS	2804.51	1.68	441	271	17	0.65	4.52	0.39	0.126
	BS	2809.28	1.39	440	305	20	0.35	4.22	0.38	0.077
2	LS	1879.29	0.11	438	218	339	0.07	0.24	0.49	0.226
	LS	1886.35	0.18	375	28	141	0.10	0.05	0.31	0.667
3	LS	1008.08	1.79	423	539	66	0.31	9.62	1.42	0.031
	LM	1008.95	3.61	415	577	46	0.90	20.79	1.96	0.041
	LS	1009.96	4.37	418	595	36	0.94	25.99	1.79	0.035
4	BS	2883.68	1.06	423	35	50	0.36	0.36	0.65	0.500
	BS	2884.02	1.58	465	38	20	0.87	0.61	0.33	0.588
	BS	2884.12	1.28	430	37	48	0.45	0.46	0.72	0.495
	BS	2884.37	1.34	430	35	38	0.41	0.46	0.67	0.471
	BS	2888.89	0.15	420	47	297	0.05	0.07	0.55	0.417
5	BS	2333.50	2.89	437	445	13	2.00	12.88	0.38	0.134
	BS	2333.55	2.46	435	499	23	1.68	12.28	0.59	0.120
	BS	2333.70	6.18	435	620	6	4.70	38.34	0.40	0.109
	BS	2333.80	3.7	433	468	9	3.11	17.35	0.35	0.152
	ISM	2334.50	4.19	436	439	8	3.60	18.43	0.37	0.163
	ISM	2335.07	5.73	439	376	10	3.78	21.55	0.61	0.149
	BS	2335.10	5.17	437	467	6	3.63	24.18	0.33	0.131
	BS	2335.40	5.98	435	463	7	4.32	27.73	0.42	0.135
	BS	2335.99	9.36	432	508	11	4.90	47.57	1.05	0.093
	BS	2336.00	8.6	434	630	5	6.49	54.24	0.51	0.107
	BS	2336.30	7.45	434	514	7	5.00	38.36	0.53	0.115
	BS	2336.40	2.47	438	410	14	3.14	10.14	0.35	0.236
	ISM	2336.90	2.8	444	314	31	3.13	8.80	0.88	0.262
	ISM	2337.20	1.96	437	377	19	1.51	7.40	0.39	0.169
	ISM	2337.21	2.91	439	484	32	1.68	14.09	0.94	0.107
	ISM	2338.00	1.25	436	239	51	0.58	2.99	0.64	0.162
	ISM	2338.29	9.61	429	558	8	5.19	53.55	0.77	0.088

Rock-eval pyrolysis results (continued)

Well number	Facies	Depth (m)	TOC (wt%)	T_{max} (°C)	HI(mg HC / g TOC)	OI (mg CO_2 / g TOC)	S_1 (mg/g)	S_2 (mg/g)	S_3 (mg/g)	PI ($S_1/(S_1+S_2)$)
5	ISM	2338.30	1.28	437	261	33	0.86	3.35	0.43	0.204
	ISM	2338.40	9.72	434	539	5	7.19	52.43	0.58	0.121
	ISM	2339.00	9.83	434	567	5	7.22	55.75	0.55	0.115
	ISM	2339.60	3.09	436	404	15	3.13	12.51	0.48	0.200
	ISM	2339.64	4.31	438	494	20	3.18	21.33	0.88	0.130
	ISM	2339.65	5.86	429	512	10	3.49	29.95	0.68	0.104
	ISM	2340.10	4.55	434	451	11	3.20	20.56	0.52	0.135
	LMS	2340.30	0.36	438	161	97	0.28	0.58	0.35	0.326
	LMS	2341.20	0.32	438	137	103	0.14	0.44	0.33	0.241
	LMS	2341.80	0.35	439	157	88	0.15	0.55	0.31	0.214
	LMS	2342.40	0.53	436	162	88	0.19	0.86	0.47	0.181
	LMS	2343.50	0.55	439	167	52	0.20	0.92	0.29	0.179
	LMS	2343.91	1.1	439	363	77	0.66	4.00	0.85	0.142
	LMS	2344.20	0.88	437	202	40	0.37	1.78	0.36	0.172
	LMS	2344.83	1.35	439	356	72	0.78	4.81	0.98	0.140
	LMS	2345.00	1.64	437	285	30	1.10	4.68	0.50	0.190
	LS	2345.40	0.32	434	125	100	0.78	0.40	0.32	0.661
	LS	2346.20	0.99	438	28	42	0.50	0.28	0.42	0.641
	LMS	2346.51	0.09	434	122	617	0.03	0.11	0.74	0.214
	LMS	2346.70	0.35	437	71	111	0.35	0.25	0.39	0.583
6	LS	2614.88	2.05	456	144	17	0.70	2.97	0.35	0.191
	LS	2616.81	0.22	442	132	79	0.19	0.29	0.21	0.396
	LS	2617.90	0.09	447	89	156	0.05	0.08	0.17	0.385
	LS	2643.65	0.21	442	233	148	0.07	0.49	0.41	0.125
7	DM	2636.59	0.18	442	67	226	0.02	0.12	0.53	0.143
	DM	2644.11	0.16	439	63	164	0.02	0.10	0.36	0.167
	DM	2649.85	0.14	449	79	237	0.01	0.11	0.45	0.083
8	BS	2635.09	0.13	449	100	133	0.09	0.13	0.23	0.409
	BS	2636.10	1.02	443	43	24	0.53	0.44	0.25	0.546
	BS	2636.80	3.08	462	46	8	1.18	1.43	0.25	0.452
	ISM	2637.60	4.36	473	50	4	1.94	2.22	0.20	0.466

Rock-eval pyrolysis results (continued)

Well number	Facies	Depth (m)	TOC (wt%)	T_{max} (°C)	HI(mg HC / g TOC)	OI (mg CO_2 / g TOC)	S_1 (mg/g)	S_2 (mg/g)	S_3 (mg/g)	PI ($S_1/(S_1+S_2)$)
8	ISM	2638.30	2.16	457	39	10	0.93	0.85	0.22	0.522
	ISM	2639.10	3.57	474	50	5	1.69	1.81	0.18	0.483
	LMS	2639.90	4.04	469	48	6	1.67	1.94	0.26	0.463
	LMS	2640.18	1.62	472	37	19	0.69	0.60	0.31	0.535
	LMS	2640.60	5.02	469	51	4	2.20	2.60	0.25	0.458
	LMS	2642.20	2.17	455	37	11	1.02	0.82	0.24	0.554
	LMS	2642.90	1.85	455	41	12	0.79	0.76	0.23	0.510
	LMS	2643.70	1.13	450	43	23	0.59	0.49	0.26	0.546
	LMS	2644.40	1.45	451	44	20	0.69	0.64	0.29	0.519
	LMS	2644.64	0.86	463	100	41	0.45	0.84	0.47	0.349
	ISM	2645.20	1.63	451	42	19	0.76	0.70	0.32	0.521
	ISM	2645.40	3.92	466	31	16	2.15	1.23	0.66	0.636
	ISM	2646.10	3.41	470	46	7	1.63	1.58	0.25	0.508
	ISM	2646.70	3.57	471	43	8	1.60	1.56	0.30	0.506
	ISM	2647.50	3.84	465	39	9	1.71	1.53	0.36	0.528
	BS	2647.56	3.58	468	72	11	1.40	2.51	0.44	0.358
	LS	2648.30	4.11	463	43	9	1.67	1.77	0.40	0.485
9	BS	3641.28	3.17	482	168	16	2.06	5.12	0.54	0.287
	BS	3643.72	1.25	467	42	21	0.33	0.51	0.34	0.393
	BS	3649.68	3.23	478	69	8	1.06	2.15	0.32	0.330
10	LDM	1623.18	2.03	430	504	23	0.67	10.21	0.55	0.062
	LDM	1625.09	0.43	431	298	65	0.18	1.27	0.36	0.124
	LDM	1627.53	3.89	428	511	10	1.62	19.86	0.40	0.075
	LDM	1628.49	4.58	428	517	13	2.43	23.65	0.67	0.093
11	LDM	1626.18	1.77	432	441	23	0.55	7.79	0.53	0.066
	LDM	1628.01	1.91	429	448	15	0.96	8.54	0.36	0.101
	LDM	1630.85	1.61	432	455	21	1.13	7.31	0.42	0.134
12	BS	1280.59	9.42	417	575	15	3.05	54.17	1.28	0.053
	LM	1284.73	4.67	425	689	10	2.03	32.14	0.52	0.059
	BS	1287.01	8.66	423	621	9	3.09	53.71	0.87	0.054
13	GS	891.18	0.13	420	169	861	0.03	0.21	1.50	0.125
		891.84	0.09	422	156	917	0.02	0.14	1.12	0.125
		892.25	0.10	427	170	654	0.03	0.17	0.86	0.150

APPENDIX V

Elemental analysis results

Well Number	Sample Number	Facies	Depth (m)	TOC (wt%)	Sulfur (wt%)	TOC/S Ratio	Carbon (wt%)	Inorganic carbon (wt%)
1	011801	BS	2802.60	-	0.95	-	6.75	-
	011902	BS	2803.63	2.09	0.76	2.75	5.45	4.69
	0120A	BS	2804.51	1.68	0.93	1.81	7.66	6.73
	0107A	BS	2809.28	1.39	1.07	1.30	9.07	8.00
2	020301	LS	1879.30	0.11	0.00	-	10.62	10.62
	0206B	LS	1881.86	-	0.00	-	11.83	-
	020801	LS	1886.36	0.18	0.00		6.88	6.88
3	030301	LS	1008.08	1.79	0.47	3.85	9.28	8.81
	0304A	LM	1009.00	3.61	1.24	2.90	9.22	7.98
	0305A	GS	1009.36	-	1.16	-	6.44	-
	030602	LS	1009.96	4.37	1.93	2.27	8.77	6.84
	0307B	LS	1010.78	-	4.03	-	16.65	-
4	040101	BS	2883.69	1.06	1.15	0.92	3.68	2.53
	0402A	BS	2884.12	1.28	0.80	1.59	5.38	4.58
	040303	BS	2884.37	1.34	0.90	1.48	5.78	4.88
	0406A	LMS	2885.87	-	0.00	-	11.10	-
	0408B	LMS	2887.88	-	0.48	-	10.30	-
	0410B	BS	2888.89	0.15	0.34	0.44	8.81	8.47
5	0500A	BS	2333.75	-	1.98	-	9.62	-
	050503	ISM	2338.29	9.61	2.78	3.46	13.63	10.85
	050701	ISM	2339.65	5.86	-	-	-	-
	0508A	ISM	2340.13	-	1.63	-	6.26	-
	0513A	LMS	2346.51	0.09	0.00	-	10.15	10.15
6	060601	LS	2616.81	0.22	0.00	-	12.06	12.06
	0606A	LS	2617.90	0.09	0.60	0.15	11.90	11.30
	0608E	LS	2643.65	0.21	-	-	-	-
7	0700A	DM	2636.60	0.18	0.00		6.54	6.54
	0707B	DM	2644.11	0.16	-	-	-	-
	0707D	DM	2646.25	-	0.56	-	5.67	-
	0708B	DM	2649.85	0.14	-	-	-	-
8	0802B	BS	2635.10	0.13	1.99	0.07	2.69	0.70

Elemental analysis results (continued)

Well Number	Sample Number	Facies	Depth (m)	TOC (wt%)	Sulfur (wt%)	TOC/S Ratio	Carbon (wt%)	Inorganic carbon (wt%)
8	0802E	ISM	2636.98	-	1.19	-	6.62	-
	0805A	ISM	2639.31	-	3.09	-	7.51	-
	081001	LMS	2644.65	0.86	1.49	0.58	4.69	3.21
	0811B	ISM	2645.39	-	2.01	-	7.58	-
	0814A	ISM	2646.27	-	2.97	-	8.14	-
	0814B	BS	2647.57	3.58	2.09	1.72	7.38	5.29
9	0901A	BS	3641.28	3.17	1.82	1.74	13.87	12.05
	0904A	BS	3643.72	1.25	0.79	1.58	11.78	10.99
	0905A	BS	3645.32	-	1.08	-	12.55	-
	0907A	LM	3647.64	-	1.12	-	10.25	-
	0909A	BS	3649.68	3.23	1.13	2.87	9.59	8.47
10	100303	LDM	1623.19	2.03	0.85	2.38	7.09	6.23
	1004B	LDM	1624.69	-	0.45	-	6.26	-
	100602	LDM	1625.09	0.43	0.34	1.25	7.67	7.33
	100802	LDM	1626.39	-	0.40	-	6.06	-
	101001	LDM	1627.53	3.89	1.85	2.10	6.74	4.88
	101103	LDM	1627.93	-	1.54	-	7.51	-
	1011A	LDM	1628.50	4.58	1.72	2.66	6.71	4.99
11	1101A	LDM	1625.27	-	0.66	-	9.60	-
	110302	LDM	1626.18	1.77	-	-	-	-
	110502	LDM	1626.59	-	1.26	-	5.92	-
	110602	LDM	1627.63	-	0.57	-	6.92	-
	110703	LDM	1628.01	1.91	1.25	1.53	6.27	5.02
	111101	LDM	1630.38	-	0.89	-	6.50	-
	1112A	LDM	1630.86	1.61	1.18	1.36	7.33	-
12	120003	BS	1280.59	9.42	2.67	3.52	17.61	14.94
	120302	LM	1284.73	4.67	0.79	5.89	14.17	13.38
	1205C	BS	1286.36	-	1.44	-	14.60	-
	1207A	BS	1287.02	8.66	1.48	5.86	15.27	13.79
	1210A	BS	1288.39	-	1.66	-	15.20	-
13	1300A	GS	891.18	0.13	0.89	0.15	3.52	2.63
	1300B	GS	891.84	0.09	1.12	0.08	6.66	5.54
	130101	GS	892.25	0.10	0.61	0.16	7.88	7.27

APPENDIX VI

Inorganic carbon and oxygen isotopic results

Well Number	Sample Number	Facies	Depth (m)	$\delta^{18}O$ (VPDB‰) (calcite)	$\delta^{13}C$(VPDB‰) (calcite)	$\delta^{18}O$(VPDB‰) (dolomite)	$\delta^{13}C$(VPDB‰) (dolomite)
1	011801	BS	2802.60	-6.30	2.45	-7.49	2.68
	0120A	BS	2804.51	-6.00	2.79	-7.06	2.86
	0107A	BS	2809.28	-6.10	3.47	-6.55	3.21
2	020301	LS	1879.30	-	-	-6.95	3.85
	0206B	LS	1881.86	-4.84	-12.50	-1.25	-1.37
3	0305A	GS	1009.36	-5.21	0.47	-6.11	0.15
4	040101	BS	2883.69	-11.73	-2.13	-7.92	-0.47
	0408B	LMS	2887.88	-7.67	-0.08	-	-
5	0500A	BS	2333.75	-6.50	-0.36	-9.66	-0.95
	050503	ISM	2338.29	-9.06	-0.91	-8.25	-0.07
	0508A	ISM	2340.13	-6.29	0.20	-6.35	-0.02
6	060601	LS	2616.81	-5.99	1.83	-6.97	1.78
	0606A	LS	2617.90	-6.32	1.68	-6.00	1.57
7	0700A	DM	2636.60	-	-	-4.37	2.60
	0707D	DM	2646.25	-5.87	3.71	-10.39	0.23
8	0802E	ISM	2636.98	-8.76	-0.08	-7.42	-0.67
	0805A	ISM	2639.31	-7.72	0.34	-6.79	0.23
	0811B	ISM	2645.39	-7.34	-0.48	-8.32	-0.50
	0814A	ISM	2646.27	-7.54	0.19	-7.86	-0.02
9	0901A	BS	3641.28	-6.97	1.09	-7.91	1.12
	0904A	BS	3643.72	-6.01	1.52	-9.67	0.68
	0905A	BS	3645.32	-6.24	-	-6.93	0.34
	0907A	LM	3647.64	-7.42	1.99	-7.29	2.27
	0909A	BS	3649.68	-7.40	1.93	-6.78	2.24
10	100303	LDM	1623.19	-4.50	-0.57	-5.38	-0.42
	1004B	LDM	1624.69	-6.06	-0.75	-4.58	-0.60
	100802	LDM	1626.39	-4.08	-0.08	-5.15	0.01
	101103	LDM	1627.96	-	-	-5.13	0.31
11	1101A	LDM	1625.27	-6.88	-0.63	-6.27	0.15
	110502	LDM	1626.59	-5.65	-0.85	-5.29	-0.37

Inorganic carbon and oxygen isotopic results (continued)

Well Number	Sample Number	Facies	Depth (m)	$\delta^{18}O$ (VPDB‰) (calcite)	$\delta^{13}C$(VPDB‰) (calcite)	$\delta^{18}O$(VPDB‰) (dolomite)	$\delta^{13}C$(VPDB‰) (dolomite)
11	110602	LDM	1627.63	-4.04	-0.50	-5.39	-0.46
	110703	LDM	1628.01	-4.87	-0.48	-5.50	-0.49
	111101	LDM	1630.38	-5.41	0.02	-6.20	0.27
12	120003	BS	1280.59	-6.25	3.22	-	-
	120302	LM	1284.73	-5.71	0.83	15.52	-0.28
	1205C	BS	1286.36	-6.41	0.31	-	-
	1210A	BS	1288.39	-6.01	0.04	-6.79	0.77
13	1300A	GS	891.18	-5.22	2.98	-	-
	130101	GS	892.25	-4.86	3.06	-5.48	2.51

APPENDIX VII

Organic carbon isotopic results

Well Number	Sample Number	Facies	Depth (m)	$\delta^{13}C_{org}$ (VPDB‰)
1	011801	BS	2802.60	-29.88
	0120A	BS	2804.51	-29.50
	0107A	BS	2809.28	-27.85
2	0206B	LS	1881.86	-26.68
	020801	LS	1886.36	-29.87
3	0305A	GS	1009.36	-29.68
4	040101	BS	2883.69	-30.91
	0408B	LMS	2887.88	-30.54
5	0500A	BS	2333.75	-29.13
	050503	ISM	2338.29	-29.68
	0508A	ISM	2340.13	-29.99
6	060601	LS	2616.81	-11.40
	0606A	LS	2617.90	-29.47
7	0700A	DM	2636.60	-26.71
	0707D	DM	2646.25	-26.49
8	0802E	ISM	2636.98	-29.91
	0805A	ISM	2639.31	-29.32
	0811B	ISM	2645.39	-28.72
	0814A	ISM	2646.27	-29.14
9	0901A	BS	3641.28	-30.53
	0904A	BS	3643.72	-29.80
	0905A	BS	3645.32	-30.16
	0907A	LM	3647.64	-29.73
	0909A	BS	3649.68	-28.08
10	100303	LDM	1623.19	-30.81
	1004B	LDM	1624.69	-30.91
	100802	LDM	1626.39	-30.45
	101103	LDM	1627.96	-30.66
11	1101A	LDM	1625.27	-32.54
	110502	LDM	1626.59	-30.99
	110602	LDM	1627.63	-30.93
	110703	LDM	1628.01	-30.82
	111101	LDM	1630.38	-30.94
12	120003	BS	1280.59	-27.96
	120302	LM	1284.73	-29.96
	1205C	BS	1286.36	-30.29
	1210A	BS	1288.39	-29.99
13	130101	GS	892.25	-27.66

APPENDIX VIII

Sulfur isotopic results

Well Number	Sample Number	Facies	Depth (m)	$\delta^{34}S$ (CDT ‰)	$\Delta(\delta^{34}S_{sulfate} - \delta^{34}S_{sulfide}$, CDT ‰)
1	012001	Black shale	2804.08	12.30	12.70
3	0307B	Wackestone	1010.78	-5.00	30.00
4	040101	Black shale	2883.69	-14.30	39.30
5	0501B	Black shale	2336.02	-6.30	31.30
	050701	Interbedded black shale/dolomitic mudstone	2339.65	1.60	23.40
8	0802B	Black shale	2635.10	-22.80	47.80
	081001	Lime mudstone	2644.65	-15.10	40.10
	0814B	Black shale	2647.57	-4.20	29.20
9	0901A	Black shale	3641.28	-13.00	38.00
	0905A	Black shale	3645.32	-0.80	25.80
	0909A	Black shale	3649.68	0.20	24.80
10	101001	Laminated dolomitic mudstone	1627.53	-5.30	30.30
11	110302	Laminated dolomitic mudstone	1626.18	-7.70	32.70
	1112A	Laminated dolomitic mudstone	1630.86	-5.10	30.10
12	120003	Black shale	1280.59	-8.70	33.70

VITA AUCTORIS

NAME: Jing Gao

PLACE OF BIRTH: Beijing, China

YEAR OF BIRTH: 1969

EDUCATION: Beijing University, Beijing, China

1987 –1991, B.Sc.

Univeristy of Windsor, Windsor, Ontario, Canada

1999-2001, M.Sc.